Institut National de la Recherche Scientifique, Energie, Materiaux, et Telecommunications
(INRS-EMT)

EXPLORING THE EFFECTS OF ENERGY MEDIATING MIDDLE SHELLS ON CLASSICAL $LiYbF_4$ UPCONVERTING NANOPARTICLES

Par

Arohan Dutta

Mémoire ou thèse présenté(e) pour l'obtention du grade de
Maître ès Sciences (M.Sc.)
en sciences de l'énergie et matériaux

Jury d'évaluation

Président du jury et examinateur interne	Emanuele Orgiu INRS-EMT
Examinateur externe	Niko Hildebrandt Department of Engineering Physics McMaster University
Examinateur interne	Emanuele Orgiu
Directeur de recherche	Fiorenzo Vetrone

REMERCIEMENTS

I would like to first start by thanking my parents. They have been my biggest supporters throughout this journey. They have provided me levels of love and encouragement that no other people in this world can even hope to achieve. To have them as my parents is a great blessing, which I thank my lucky stars for everyday.

I would next like to thank my second biggest supporter, Professor Fiorenzo Vetrone. Professor Vetrone has guided me through the toughest of times with the utmost unyielding zeal - always calming me down whenever I was stressed or telling me not to worry over the most trivial matters. He has supported every decision of mine, especially when I wanted to attend conferences, and has given me ideas, thoughts, and advice whenever I hit a roadblock. Only because of the grace and good fortune of Professor Fiorenzo backing me, was I able to complete this task.

I would also like to take a moment and thank everyone at INRS, the administration and registrar, who were prompt in their responses and emails whenever I was doubtful of anything regarding my registration. And I would like to thank INRS for giving me the opportunity to conduct my research and experiments in such a prestigious institute.

In addition, my lab mates, whether they were temporary or permanent, need a shout-out as well. Starting all the way back in September 2020, during the height of the COVID-19 pandemic, when I was at INRS for a Co-op, when Artiom and Cheng Ting both helped me learn my way around the lab. It was because of the things they taught me all the way back then that I am where I am today. I would also like to thank my current lab mate as well, Miao, who has been there to help me conduct experiments whenever I have been ill, stressed, or too busy to do so. All the lab mates who came as exchange students over the course of the past 2 years, please also take my warmest wishes - my most memorable times in the lab were when all of you would share your stories and experiences with me while we did experiments.

I would also like to thank all my friends, wherever they are in the world. Without them being by my side to alleviate the stresses, which of course came in undertaking such a task, I would not have been able to finish writing my thesis.

And lastly, to my maternal grandparents and grandaunt: I know that you have been watching me from the stars and adorning me with your kindness and tenderness. I know that you have been by my side throughout this journey, and for that words, cannot explain how thankful I am to you. Love, Raaj.

RÉSUMÉ

La capacité des nanoparticules à conversion ascendante (UCNP) à convertir la lumière infrarouge proche (NIR) à faible énergie en lumière ultraviolette (UV) et/ou visible à haute énergie en a fait des candidats intéressants pour une utilisation en théranostique. En raison de leur large spectre d'émission et de leur petite taille, les UCNP peuvent être utilisées à la fois pour la thérapie, comme l'administration de médicaments, la thérapie photodynamique ou la thérapie photothermique, et pour le diagnostic, comme la biodétection et la bioimagerie. Les UCNP typiques fonctionnent avec des paires d'ions traditionnelles telles que Ytterbium-Erbium ou Ytterbium-Thulium afin d'émettre une lumière UV, bleue ou verte. La longueur d'onde d'excitation pour déclencher le processus de conversion ascendante est de 980 nm. Cependant, la lumière de 980 nm est également absorbable par l'eau, ce qui signifie que dans les conditions in vivo, une partie, voire la majorité, de l'énergie fournie par cette longueur d'onde est absorbée par l'eau entourant le tissu. Il est donc essentiel de créer des UCNP de petite taille et de grande luminosité afin de garantir que même lorsqu'une petite quantité de la longueur d'onde d'excitation atteint les UCNP dans les applications en tissus profonds, ils sont toujours capables d'émettre efficacement. L'une de ces méthodes explorées dans cette thèse est l'utilisation d'une couche intermédiaire de migration d’énergie pour assurer le transfert d'énergie entre les ions sensibilisateurs et activateurs.

Mots-clés : Upconversion; UCNPs; Lanthanoïdes; Terres rares; Théranostique; Biomédical; Thérapie photodynamique; Traitement du Cancer

ABSTRACT

The ability of Upconverting Nanoparticles (UCNPs) to convert low energy, Near Infrared (NIR) light, into high energy, ultraviolet (UV) and/or visible light have made them attractive candidates for use in theranostics. Due to their broad emission spectra and smallness in size, UCNPs can be used for both therapy, such as drug delivery, photodynamic therapy, or photothermal therapy, and diagnostics such as biosensing and bioimaging. Typical UCNPs work with traditional ion pairs such as Ytterbium-Erbium or Ytterbium-Thulium in order to emit UV, blue, or green light. The excitation wavelength in order to trigger the upconversion process is 980 nm. However, 980 nm light is also water absorbable meaning that in vivo settings, some, if not majority, of the energy provided by this wavelength is absorbed by water surrounding the tissue. Therefore creating small, and bright UCNPs is crucial in order to ensure that even when only a small amount of the excitation wavelength reaches the UCNPs in deep tissue applications, they are still able to emit efficiently. One such method explored in this thesis is the utilisation of an energy migrating middle shell, to mediate the energy transfer between the sensitising and activating ions.

Keywords : Upconversion; UCNP; Lanthanoids; Rare-Earth; Theranostics; Biomedical; Photodynamic Therapy; Cancer Treatment

EXPLORER LES EFFETS DES COQUILLES MOYENNES DE MÉDIATION ÉNERGÉTIQUE SUR LES NANOPARTICULES DE CONVERSION ASCENDANTE CLASSIQUES $LiYBF_4$

SOMMAIRE RÉCAPITULATIF

La conversion ascendante est le processus dans lequel plusieurs photons de faible énergie sont absorbés séquentiellement pour émettre un photon de plus haute énergie. Cela produit une lumière d'une longueur d'onde plus courte et d'une énergie plus élevée que la lumière d'excitation, comme la conversion de la lumière proche infrarouge (NIR) en lumière visible ou ultraviolette (UV).

Le décalage de Stokes se produit lorsque le photon émis a une énergie inférieure à celle des photons absorbés, ce qui est un phénomène courant en spectroscopie de fluorescence et Raman. Il se produit en raison de relaxations vibrationnelles ou de pertes d'énergie dans l'environnement environnant. En revanche, le décalage anti-Stokes se produit lors de la conversion ascendante, où le photon émis a une énergie plus élevée que celui absorbé. Ce gain d'énergie supplémentaire peut provenir de mécanismes tels que la dissipation thermique ou l'annihilation triplet-triplet.

Alors que les molécules organiques peuvent se convertir en ascendant, cet article met en évidence les nanoparticules inorganiques qui utilisent des lanthanoïdes, qui se sont avérées excellentes dans ce domaine. La recherche sur les lanthanoïdes est essentielle pour améliorer leur efficacité de conversion ascendante.

L'absorption à deux photons et la génération de la seconde harmonique impliquent également l'émission de photons de plus haute énergie, mais leurs mécanismes diffèrent de la conversion ascendante. La conversion ascendante peut se produire par le biais de divers mécanismes, et aujourd'hui, cinq ont été identifiés : l'absorption à l'état excité (ESA), l'avalanche de photons (PA), la conversion ascendante par transfert d'énergie (ETU), la conversion ascendante par médiation migrée d'énergie (EMU) et la conversion ascendante coopérative (CU). Ces mécanismes fonctionnent dans des matériaux comme les macrostructures à base de lanthanides qui contiennent des ions capables de conversion ascendante.

L'ESA, le mécanisme de définition de la conversion ascendante, est un processus en plusieurs étapes dans lequel les photons sont absorbés séquentiellement pour exciter un ion de l'état fondamental à un état excité. Au départ, un photon excite un ion de l'état fondamental à un état intermédiaire, et d'autres photons l'excitent à des niveaux d'énergie plus élevés. Les phonons

peuvent aider à ces absorptions. Il est important de noter que l'ESA est un processus à ion unique, ce qui signifie que la concentration d'ions de conversion ascendante dans le matériau n'affecte pas les taux de pompage. De plus, dans l'ESA, il existe deux puissances laser distinctes qui fonctionnent ensemble afin d'exciter un ion à son état excité le plus élevé.

La relaxation croisée fait référence aux interactions ion-ion dans les cristaux de conversion ascendante, où l'énergie est transférée entre deux ions. Dans ce processus, l'ion 2 transfère une partie de son énergie excitée à l'ion 1, en particulier lorsque l'état excité de l'ion 2 interagit avec l'état fondamental de l'ion 1. Le processus dépend de la concentration de dopant dans les cristaux, et des niveaux de dopage élevés peuvent conduire à une photoluminescence plus faible en raison de l'extinction de la concentration. Cependant, la relaxation croisée peut toujours être utilisée intentionnellement pour contrôler la sortie de couleur ou améliorer la conversion ascendante par avalanche de photons. Les ions impliqués peuvent être du même type, et pas nécessairement des ions de conversion ascendante différents.

L'avalanche de photons (PA) est un processus complexe impliquant trois étapes clés : la transmission, l'émission et le temps de montée, avec un seuil de pompage critique lié à l'intensité de la puissance de pompage. Dans un système à quatre énergies (E0, E1, E2 et E), le processus commence par un électron absorbant l'énergie d'une longueur d'onde d'excitation. Cette énergie peut ne pas correspondre parfaitement aux états intermédiaires comme E2, mais la relaxation croisée permet à l'électron de se déplacer vers E2. Un transfert d'énergie se produit entre l'électron E2 et un autre dans l'état fondamental (E0), formant ainsi deux électrons dans l'état E1. Sous l'effet d'un rayonnement continu, l'un de ces électrons gagne de l'énergie et entre dans l'état excité supérieur, interagissant avec les électrons dans l'état fondamental pour produire davantage d'électrons dans l'état E1. Lorsque le rayonnement entre en résonance avec la transition de E1 à E, le processus se répète, formant une boucle de rétroaction.

L'ETU est un mécanisme efficace dans les lanthanides, impliquant deux ou plusieurs ions lanthanides dopés dans un réseau cristallin pour réaliser une conversion ascendante. Il fonctionne indépendamment de la puissance de pompage et se produit lorsque les ions sensibilisateur et activateur sont suffisamment proches dans le réseau, permettant le transfert d'énergie du sensibilisateur à l'activateur. Ce transfert peut également se produire par des processus non radiatifs assistés par phonons s'il existe une inadéquation énergétique entre le sensibilisateur et l'activateur. La conception de ces matériaux nécessite des concentrations de dopage prudentes, bien qu'une ETU efficace puisse toujours se produire avec un seul ion lanthanide agissant à la fois comme donneur et comme récepteur.

Les nanoparticules à conversion ascendante (UCNPs) sont des nanoparticules capables de conversion ascendante, dans la mesure où elles absorbent les photons infrarouges (IR) et émettent des photons visibles ou UV, en fonction de dopants comme Tm3+ et Er3+. Les UCNP offrent une compréhension plus détaillée de la conversion ascendante par rapport aux cristaux massifs en raison de leurs diverses applications. Le processus de conversion ascendante nécessite des états métastables qui permettent l'absorption séquentielle des photons, facilitée par les structures électroniques complexes des lanthanides, qui capitalisent sur leurs orbitales 4f.

Lorsqu'elles sont dopées dans un réseau hôte nanocristallin, ces orbitales 4f se divisent pour former des états intermédiaires essentiels à la conversion ascendante. La nature non liante des orbitales 4f, associée au blindage des coquilles 5s et 5p, entraîne un faible couplage au réseau environnant, ce qui conduit à de longues durées de vie des états excités et à des caractéristiques optiques nettes.

Les UCNP présentent des effets liés à la surface et à la taille, contrairement aux cristaux massifs, qui peuvent influencer leurs performances. Les problèmes proviennent de la dissipation d'énergie par relaxation radiative et non radiative, où les transitions radiatives impliquent l'absorption ou l'émission de photons, tandis que les transitions non radiatives impliquent un transfert ou une dissipation d'énergie. La densité d'états des phonons joue un rôle crucial dans le transfert d'énergie, car les phonons peuvent aider les électrons excités à atteindre des états intermédiaires. Cependant, les effets concurrents de la relaxation non radiative et de l'assistance des phonons affectent l'efficacité du transfert d'énergie et la durée de vie des états excités dans les UCNP.

La structure et la composition chimique des UCNP ont un impact significatif sur leur efficacité de conversion ascendante. Le choix du réseau hôte est crucial pour déterminer les caractéristiques spectrales, car il assure la conduction et le transfert d'énergie entre les ions. Les facteurs clés dans la sélection d'un réseau hôte comprennent une faible énergie des phonons, une stabilité chimique élevée et une faible symétrie du réseau. Une faible énergie de phonons minimise l'extinction non radiative des phonons, tandis qu'une stabilité chimique élevée garantit que les ions lanthanides restent non liants et que les UCNP restent neutres et non réactifs.

La règle de sélection de Laporte suggère que les UCNP avec des réseaux à faible symétrie, tels que les cristaux tétraédriques, présentent des spectres d'émission plus brillants en raison de transitions électroniques moins restrictives. Au départ, les oxydes étaient utilisés pour leur stabilité, mais leurs énergies de phonons élevées entraînaient une faible luminosité. Les ions halogènes comme le chlore et le brome offrent de faibles énergies de phonons mais sont

chimiquement instables. Les ions fluorure (F-) offrent un meilleur équilibre entre stabilité et faible énergie de phonons, ce qui les rend idéaux pour la synthèse d'UCNP, avec des cations courants comme le lithium et le sodium, qui se lient facilement avec F- et correspondent à la taille des ions lanthanides.

Le choix des paires d'ions appropriées est également essentiel, car les différences de niveau d'énergie entre les états fondamental, intermédiaire et excité des ions activateurs doivent s'aligner pour faciliter un transfert d'énergie fluide et minimiser les pertes non radiatives. L'ion Ytterbium (Yb^{3+}) est un sensibilisateur courant en raison de sa grande section efficace d'absorption pour la lumière NIR et de ses niveaux d'énergie compatibles avec les ions activateurs comme Er^{3+} et Tm^{3+}, permettant un transfert d'énergie efficace. La concentration des ions est importante, car des concentrations élevées peuvent entraîner une relaxation croisée et une émission plus faible.

Le diagramme de Dieke, développé dans les années 1950 et 1960, répertorie les niveaux d'énergie des lanthanides et permet d'identifier les paires de sensibilisateurs et d'activateurs appropriés pour la conversion ascendante. Le diagramme illustre également la division des niveaux d'énergie et les symboles de termes qui leur sont associés, qui sont importants pour comprendre les transitions énergétiques et sélectionner des paires d'ions pour une conversion ascendante efficace.

Les UCNP sont extrêmement polyvalentes et malléables, ce qui les rend adaptées à de nombreux domaines, des semi-conducteurs à l'ingénierie biomédicale, en raison de leur stabilité chimique, de leur petite taille et de leur facilité de modification post-synthèse. Cependant, lors de leur synthèse, les UCNP sont initialement coiffées de ligands organiques, ce qui les rend dispersibles uniquement dans des solvants organiques. Pour les applications biomédicales, les UCNP doivent être rendues dispersibles dans l'eau grâce à un processus d'échange de ligands, en remplaçant les ligands hydrophobes par des ligands hydrophiles comme le polyéthylène glycol (PEG) ou l'acide polyacrylique (PAA).

Ce processus d'échange, bien qu'essentiel, est difficile et peut provoquer l'agrégation des particules, entraînant une perte de leurs spectres d'émission intenses. Malgré les efforts déployés avec des réactifs comme l'acide chlorhydrique (HCl) et le tétrafluoroborate de nitrosonium ($NOBF_4$), l'agrégation reste un problème et une préparation incorrecte peut introduire des résidus toxiques, les rendant impropres à l'utilisation biomédicale.

Néanmoins, la capacité de modifier les surfaces des UCNP pour générer une lumière localisée à haute énergie et obtenir des émissions réglables les rend attrayantes pour des applications biomédicales telles que la libération de médicaments, la bioimagerie, la biodétection et la

détection de température, où elles exploitent le phénomène unique de conversion ascendante pour interagir avec les fonctions complexes du corps humain.

L'essor des nanotechnologies a ouvert la voie à de nouvelles méthodes non invasives et précises pour traiter les maladies, mais il a également suscité des inquiétudes concernant la sécurité, la synthèse de médicaments et les risques potentiels pour la santé humaine, les animaux et l'environnement. Ces inquiétudes ont conduit à la nécessité d'analyses et de réglementations toxicologiques, même pour les UCNP, qui sont largement considérées comme sûres pour une utilisation biomédicale. Les principaux défis à relever avant que les UCNP puissent être appliquées dans les essais cliniques comprennent la synthèse reproductible, le contrôle de la taille et de la forme, la chimie de surface biocompatible, la détection in vivo et les applications théranostiques.

La théranostique, une technique de médecine personnalisée, combine des fonctions diagnostiques et thérapeutiques, comme en médecine nucléaire, dans laquelle des agents comme l'iode 131 ont été utilisés pour le cancer de la thyroïde. Cependant, la théranostique est confrontée à des défis, notamment en matière de sécurité, d'efficacité, de coût et de ciblage précis. Les UCNP sont prometteuses en théranostique en raison de leur biocompatibilité, de leurs larges spectres d'émission et de leur capacité à être activées avec de simples lasers, réduisant ainsi les coûts et le besoin d'équipements spécialisés. Cependant, leur synthèse reste coûteuse en raison du prix élevé des terres rares utilisées.

Le développement de nouvelles méthodes de synthèse ascendante pour les nanomatériaux dopés aux lanthanides a permis la production d'UCNP bien définies avec des tailles ajustables, ce qui les rend de plus en plus utilisées en nanotechnologie et en biomédecine. Leur capacité à imiter la taille des systèmes biologiques naturels, tels que les cellules et les protéines, améliore leur biocompatibilité et réduit la probabilité de provoquer une réponse immunitaire indésirable.

Un facteur clé de leur efficacité, en particulier dans le traitement du cancer, est leur capacité à tirer parti de l'effet de perméabilité et de rétention améliorées (EPR), où les nanoparticules sont plus susceptibles de s'accumuler dans les tumeurs solides que dans les tissus normaux. Le contrôle de la taille des UCNP est crucial pour cibler les cellules cancéreuses, et des études récentes ont montré des résultats prometteurs dans l'utilisation des UCNP Yb-Er à base de sodium pour traiter le cancer du foie.

Contrairement aux marqueurs fluorescents traditionnels, qui peuvent endommager les tissus avec une lumière à haute énergie, les UCNP fonctionnent dans la région spectrale NIR, évitant les effets nocifs et réduisant la diffusion de la lumière. Cela les rend idéales pour des applications comme la nanothermométrie cellulaire. De plus, les UCNP peuvent émettre de la

lumière sur différentes longueurs d'onde en fonction de leur composition en dopants, ce qui permet des propriétés d'émission sur mesure. Par exemple, les UCNP émettant de la lumière UV peuvent être utilisées pour les thérapies des tissus profonds, offrant l'énergie nécessaire aux réactions photochimiques.

Pour optimiser les UCNP pour les applications biomédicales, des paramètres de conception spécifiques doivent être pris en compte. La paire Yb-Er est couramment utilisée car lorsqu'elle est irradiée par une lumière de 980 nm, l'ion Er^{3+} émet une lumière verte (520-550 nm), ce qui est utile pour des applications telles que le photoclivage de polymères pour libérer des médicaments ou déclencher des réactions photochimiques. Cependant, bien que la lumière verte soit plus énergétique que la lumière IR, NIR ou rouge, elle accomplit souvent sa tâche lentement dans les applications de libération de médicaments. Cela est dû au fait que l'intensité de la lumière émise est considérablement réduite in vivo en raison de l'eau environnante, qui absorbe la lumière de 980 nm, ce qui entraîne une perte d'énergie globale.

L'absorption de l'eau provoque un effet d'extinction, où une grande partie de la lumière est absorbée par les molécules d'eau au lieu des UCNP, réduisant l'intensité de la lumière émise dans les environnements biologiques par rapport aux conditions de laboratoire. Malgré cela, les UCNP doivent rester dispersibles dans l'eau pour des applications biologiques efficaces, ce qui en fait un élément clé à prendre en compte lors de leur conception pour une utilisation dans les tissus vivants.

Pour améliorer l'efficacité de la libération de médicaments à l'aide des UCNP, il est essentiel de les rendre plus brillantes, car les faibles intensités d'émission limitent souvent les taux de libération de médicaments. Les UCNP plus brillantes émettront des intensités plus élevées lorsqu'elles seront irradiées, ce qui améliorera leur efficacité. Les UCNP doivent également être petites pour garantir qu'elles adhèrent à l'effet EPR, ce qui leur permet de cibler efficacement les tumeurs. Les particules plus petites sont également moins susceptibles de provoquer des réponses immunitaires et ont des demi-vies sanguines plus longues, ce qui les rend plus efficaces lorsqu'elles sont administrées par voie intraveineuse.

En ce qui concerne la longueur d’onde d’excitation, la lumière de 808 nm est préférée à la lumière de 980 nm en raison de sa pénétration tissulaire plus profonde. Bien que la lumière de 808 nm excite l’ion Nd^{3+}, qui a une efficacité quantique élevée, elle entraîne une luminescence de conversion ascendante plus faible en raison du transfert d’énergie en retour. Par conséquent, l’ion Ytterbium est choisi comme sensibilisateur, avec Tm^{3+} comme activateur, car il émet des UV et de la lumière bleue. La lumière bleue est plus énergétique que la lumière verte, et la lumière UV peut être utilisée localement pour induire la production d’espèces réactives de

l’oxygène (ROS), qui peuvent aider à détruire les tissus cancéreux sans endommager les tissus sains environnants.

En s’appuyant sur les recherches développées dans l’article de Ting Cheng et al. comme base, la particule d’intérêt est devenue LiYbF4(0,5%Tm^{3+}). Alors que les UCNP à base de sodium sont souvent utilisées dans des applications biomédicales, les nanoparticules de conversion ascendante à base de LiYF4 (UCNP) sont également efficaces pour générer des pics d'émission nets et intenses, en particulier dans la gamme UV/bleu, et parfois préférées à leurs homologues sodiques. L'étude présente une méthode pour ajuster la taille de ces UCNP, qui étaient auparavant trop grandes (80 nm) pour les applications d'internalisation cellulaire. Elle aborde également la question de l'amélioration des intensités de conversion ascendante en modifiant la taille des noyaux, ce qui permettrait davantage de modifications de surface et de décorticage.

L'article se concentre sur les UCNP $LiYF_4$(Yb^{3+}, Tm^{3+}), qui, bien que capables d'émettre dans la gamme UV, émettent toujours principalement de la lumière NIR. Les auteurs ont cherché à augmenter l'émission UV de ces particules. En ajustant la méthode de synthèse, en particulier les ratios d'oléylamine (OM) et d'acide oléique (OA), la taille des UCNP a été contrôlée, allant de 5 à 90 nm. L’étude a également révélé que les UCNP de moins de 10 nm émettaient davantage de lumière NIR et étaient instables, ce qui les rendait difficiles à modifier. Pour surmonter ce problème, l’étude a introduit une nouvelle technique pour créer des noyaux UCNP stables d’environ 10 nm, adaptés au décorticage et à d’autres modifications de surface.

La première synthèse de noyaux a été introduite dans l’article de Ting Cheng et al. et a révolutionné la synthèse des UCNP à base de lithium. Après plusieurs itérations d’expériences et d’essais, les auteurs ont découvert qu’en ayant un rapport OA et OM de 1:1, les deux agissant comme ligands de coordination dans le processus de nucléation, cela induisait la production de nanoparticules extrêmement petites, d’environ 5 nm de diamètre. Ces nanoparticules ne convenaient cependant pas à toute sorte de modification post-synthèse, comme le décorticage, et étaient très faiblement émettrices. Afin de surmonter ce problème, Ting Cheng et al ont créé une procédure de stabilisation dans laquelle ces UCNP super petits nouvellement formés ont été cultivés jusqu'à une taille d'environ 8 à 10 nm de diamètre en présence du plus stable des deux ligands de coordination, OA. Ces noyaux stables et toujours extrêmement petits sont devenus d'un grand intérêt car, une fois entourés d'une coque inerte, ils émettaient beaucoup dans la gamme UV et bleue, c'est-à-dire avec des énergies capables de provoquer la destruction cellulaire.

La luminosité des UCNP peut théoriquement être améliorée en ajustant les concentrations de dopants, car des niveaux plus élevés de sensibilisateur et d'activateur augmentent la collecte de

lumière et le transfert vers les ions activateurs. Cependant, des niveaux de dopage élevés peuvent provoquer une extinction de concentration et une relaxation croisée préjudiciable entre les ions voisins. Une façon de surmonter ce problème est d'utiliser une excitation à forte irradiance, bien qu'elle puisse avoir des effets nocifs sur les tissus humains. Pour éviter les pertes d'énergie dues à la relaxation croisée, des UCNP multicouches avec des coques migrant l'énergie sont utilisées. Ces coquilles améliorent la luminescence de conversion ascendante, en particulier dans les gammes verte, bleue et UV, et peuvent également permettre la commutation de couleur d'émission à l'aide d'un seul ion lanthanide.

La conception d'UCNP dans le but d'augmenter leurs émissions nécessite de comprendre leurs fonctions optiques et leurs applications. En plus d'une coquille externe passive pour empêcher l'extinction de surface, au moins une ou plusieurs coquilles intermédiaires sont nécessaires pour manipuler la dynamique de conversion ascendante. Trois types de structures multicouches cœur-coquille (MLCS) ont été étudiés à ce jour : premièrement, deux couches luminescentes sont séparées par une couche inerte pour empêcher les interactions indésirables entre les ions actifs au laser. Cette structure est réglable en couleur et émet des couleurs différentes en fonction de la longueur d'onde d'excitation. Deuxièmement, les couches actives sont reliées par un réseau migratoire d'énergie qui manipule les intensités luminescentes. Et enfin, troisièmement, une région luminescente est confinée entre deux couches (actives ou inactives) pour améliorer les spectres d'émission de conversion ascendante en réduisant la migration d'énergie nocive entre les ions sensibilisateurs.

Avec la recherche cosmopolite menée autour de l'utilisation des UCNP à plusieurs coques pour améliorer leurs fonctions, une UCNP à plusieurs coques avec $LiYF_4(Yb^{3+}, Tm^{3+})$ comme noyau a été synthétisée et étudiée. Un article, publié en 2020, par Bin Zhou et al, a fait état d'une augmentation de 100 fois de l'intensité des UCNP Yb-Er à base de sodium avec une coque intermédiaire médiatrice d'énergie, employant essentiellement la science de la troisième structure MLCS. La question de savoir si une telle augmentation serait possible dans les UCNP déjà fortement émettrices d'UV et de bleu rapportées par Ting Cheng et al, est devenue la base de cette thèse. Et ainsi, la première particule proposée est devenue $LiYbF_4(0,5\%Tm^{3+})$@LiYF4(20%Yb^{3+})@$LiYbF_4$. L'idée était d'avoir une coque intermédiaire médiatrice d'énergie dopée avec un petit pourcentage du sensibilisateur et une coque externe absorbant complètement la lumière.

Les trois premières itérations de ce MLCS UCNP ont échoué dans sa fonction. Elles ont été préparées avec un protocole modifié de celui publié par Ting Cheng et al, mais étaient toujours d'une taille acceptable. Les noyaux mesuraient environ 10 nm et les particules à double coque mesuraient entre 24 et 25 nm avec une épaisseur de coque moyenne d'environ 4 nm. Avec ces

paramètres, on a émis l'hypothèse que la particule avait augmenté les intensités du spectre Yb-Tm caractéristique. Cependant, tous les pics étaient éteints et étaient complètement incomparables aux spectres d'émission classiques. Cela ne veut pas dire qu'ils n'ont pas augmenté leur intensité - bien que les pics aient été sévèrement éteints et à peine plus intenses que les pics de fond, les spectres ont montré de légères déviations dans la gamme rouge qui indiquaient qu'une certaine forme de lumière rouge était toujours émise, et donc que ces particules étaient en train de monter en intensité.

Le problème ici résidait dans le fait que ces itérations manquaient de toute sorte de protection contre le solvant. Cela a été rectifié en remplaçant la coque externe absorbant complètement la lumière par une coque $LiYF_4$ inerte. En substance, cela ne changerait pas la fonction de l'UCNP. Qu'il y ait ou non une coque Yb complètement dopée sur la surface la plus externe n'a pas d'importance car sur le bord extérieur de la nanoparticule, la quantité de lumière disponible sera toujours de 100%. En fait, l'ajout de cette coque passivante devrait en théorie augmenter les intensités des spectres d'émission non convertis. Et c'est ce qu'ils ont fait.

La nouvelle particule $LiYbF_4(0.5\%Tm^{3+})@LiYF_4(20\%Yb^{3+})@LiYF_4$ a en fait augmenté l'intensité du pic UV d'au moins le double, 2,19 pour être exact. Les intensités de tous les autres pics ont également augmenté de manière drastique. Cette augmentation n'était en aucun cas proche d'un facteur 100, mais elle était néanmoins visuellement et quantitativement significative. Une fois la preuve de concept prouvée, deux autres particules ont été fabriquées de manière similaire avec des ajustements de la concentration de dopage de la couche intermédiaire qui ont été ajustés à 10% et 25%. Des expériences spectrales menées sur ces nouvelles particules ont révélé que l'abaissement de la concentration de Yb dans la couche intermédiaire à 10 % atténuait en fait les pics à des valeurs inférieures au pic classique, à l'exception du pic rouge qui était toujours plus fort que son homologue classique. Cependant, l'augmentation de la concentration de dopage de seulement 5 % a considérablement amélioré le pic UV, tandis que la valeur du pic bleu est restée quelque peu la même. Cela indique qu'il peut y avoir des pourcentages de dopage de Yb dans la couche intermédiaire supérieurs à 20-25 %, ce qui entraînerait une augmentation plus importante des intensités de conversion ascendante.

Avec ces informations en tête, de nombreuses expériences futures peuvent encore être menées. Tout d'abord, il faut modifier les concentrations de dopage pour obtenir des changements plus observables qu'une simple augmentation de 5%. Avec un petit changement de concentration, les valeurs d'intensité maximale augmentent, ce qui signifie qu'à des valeurs plus élevées, elles peuvent augmenter davantage. Ainsi, l'optimisation de la concentration de dopage de la couche intermédiaire est quelque chose qui doit être testé : avoir une concentration de 10%, 20%, 40%, 50% et 70% de Yb^{3+} peut montrer à quel point le pourcentage

de dopage commence à stagner ou à éteindre les pics. À ce propos, l'épaisseur de la couche intermédiaire est restée (quelque peu) constante entre toutes les itérations, mais comme l'ont rapporté Bin Zhou et al., et d'autres personnes menant des expériences sur les UCNP MLCS, l'épaisseur de la couche joue également un rôle crucial dans la manipulation des intensités.

À l'avenir, en plus de simplement optimiser les valeurs de concentration de dopage du Yb^{3+}, l'épaisseur de la couche intermédiaire doit également être modifiée pour déterminer son épaisseur optimale. Il s'agit d'une expérience facilement ajustable puisque, avec la synthèse par injection à chaud, l'épaisseur de la couche intermédiaire peut être manipulée de différentes manières, notamment le taux d'injection, ainsi que le rapport cœur-couche. L'épaisseur de la couche externe n'a pas autant d'importance, puisque l'existence de la couche inerte ne sert qu'à empêcher la trempe à la surface, donc tant qu'elle est suffisamment épaisse pour arrêter les pertes d'énergie vers les solvants à la surface, elle peut rester à une valeur constante. D'après des expériences et des articles précédents, cette valeur varie entre 5 et 8 nm.

Enfin, et le plus important : ces UCNP ont été fabriqués dans le but de les appliquer à la recherche biomédicale, principalement dans le traitement du cancer. Le but de les rendre super brillants était de s'assurer que même avec un peu de lumière d'excitation, ils soient toujours capables de se convertir suffisamment efficacement pour produire suffisamment d'énergie pour remplir leurs fonctions, qu'il s'agisse de créer des espèces ROS, de photo-cliver ou de déclencher des réactions photochimiques. Cela est dû au fait que la lumière de 980 nm, la longueur d'onde d'excitation, est absorbée par l'eau entourant le tissu, et donc la majeure partie n'excite pas réellement les UCNP. Après avoir optimisé l'épaisseur de la coque et la concentration de dopage de la coque intermédiaire, l'expérience finale doit consister à dépouiller les UCNP de leurs ligands organiques à la surface et à les rendre dispersibles dans l'eau. Ensuite, les spectres doivent être mesurés de la même manière, c'est-à-dire dispersés dans 1 ml d'eau plutôt que d'hexane, afin de déterminer dans quelle mesure ils sont éteints. Cela donnera un résultat holistique et précis de leur performance réelle in vivo. À ce stade, ce projet peut être conclu.

Étant donné que ces nanoparticules étaient déjà assez brillantes par nature et se situaient dans la gamme de l'effet EPR, si les expériences dans l'eau révèlent qu'elles restent plus brillantes que leurs homologues classiques, elles peuvent alors être utilisées directement pour le traitement du cancer. L'objectif de cette thèse était de tirer parti de la méthode de synthèse FN développée par Ting Cheng et al., pour créer des UCNP plus petites et encore plus brillantes afin de laisser beaucoup d'espace pour les modifications de surface. Cela a été réalisé, et ce faisant, comme les particules ne dépassaient pas 25 nm de diamètre, il restait plus de 50 à 70

nm pour travailler en termes de conjugaison de la surface de ces particules avec des molécules biologiques pour les traitements biologiques.

Cependant, tout cela étant dit, il ne fait aucun doute que l'insertion d'une coque intermédiaire appropriée augmente les intensités globales de la particule classique $LiYbF_4(0,5\%Tm^{3+})@LiYF_4$, ce qui était l'objectif principal de cette thèse. Ce faisant, il y a un pas en avant dans l'utilisation d'une telle particule pour le traitement des tumeurs cancéreuses. Non seulement ces particules sont brillantes, mais leurs tailles et d'autres paramètres, tels que les concentrations de dopage, sont facilement modifiables pour s'adapter aux besoins de leur fonction.

TABLE DES MATIÈRES

LISTE DES FIGURES

LISTE DES TABLEAUX

LISTE DES ÉQUATIONS

N/A

LISTE DES ABRÉVIATIONS

Upconverting Nanoparticle(s) - UCNP(s)

Ultraviolet - UV

Infrared - IR

Near Infrared - NIR

Excited State Absorption - ESA

Photon Avalanche - PA

Energy Transfer Upconversion - ETU

Energy Migrated-Mediated Upconversion - EMU

Cooperative Upconversion - CU

Polyethylene Glycol - PEG

Polyacrylic Acid - PAA

Enhanced Permeability and Retention Effect - EPR Effect

Single Photon Emission Computed Tomography - SPECT

Reactive Oxygen Species - ROS

Photodynamic Therapy - PDT

Photothermal Therapy - PPT

E. coli Nissle - EcN

Oleic Acid - OA

Octadecene - ODE

Oleylamine - OM

OM-Lanthanoid - OM-Lan

OA-Lanthanoid - OA-Lan

First Nuclei - FN

Multi-Layer-Core-Shell - MLCS

Interfacial Energy Transfer - IET

Reaction Solution - React Sol’n

Precursor Solution - Precursor Sol’n

Transmission Electron Microscope - TEM

X-ray Diffraction - XRD

1. INTRODUCTION

The ability of Upconverting Nanoparticles (UCNPs) to convert low energy, Near Infrared (NIR) light, into high energy, Ultraviolet (UV) and/or visible light have made them attractive candidates for use in theranostics. Due to their broad emission spectra, UCNPs can be used for both therapy, such as drug delivery, photodynamic therapy, or photothermal therapy, and diagnostics such as biosensing and bioimaging. Their applications are most prevalent when used for the treatment of tumours and other diseases that are considered to be in 'deep tissue'. Drugs, and drug carriers often rely on high energies to trigger their photochemical or photocleaveable reactions making UV, blue, and green light an attractive photo trigger. However, UV and visible light lack the penetration depth to reach drug carriers situated in deep tissue, and to irradiate human tissue with UV light is deleterious and detrimental. NIR light, while having the penetration depth generally lacks the energy to trigger these photochemical reactions. With UCNPs we can couple the setbacks and benefits of each type of light and generate a way to create UV and visible light in-situ, localised, at the site of interest.

1.1. Upconversion

Upconversion or photon upconversion, is the phenomenon which occurs due to the sequential absorption of two of more photons to emit one photon of higher energy; in theory, this means that the emitted light is of a shorter wavelength and of higher energy than the excitation light. The conversion of near infrared (NIR) light into visible or ultraviolet (UV) light is an example of upconversion (Edinburgh Instruments, 2021).

The name given to the type of emission in which there is a shift in position between the maxima of the excited and emitted spectra is the Stokes shift. When a photon is absorbed by an atom or molecule, it enters an excited state and gains energy - to compensate for this new energy gain, the atom or molecule often releases a photon in order to relax back to it's so called 'ground state'. When the emitted photon is of a lower energy than the absorbed photon, a Stokes Shift occurs. This is the most common case in nature, and its mechanisms are applied in fluorescence microscopy or Raman spectroscopy (Ghasemi et al., 2023). When shone on with UV light, certain minerals and marine organisms glow, making them fluorescent in nature. The UV photons have higher energy than the visible light photons humans perceive when observing these objects.

In a Stokes shift, the reason why the emitted photon is of lower energy than the absorbed one is because of vibrational relaxations or dissipations in the material, or energy dispersions into the

solvent and/or surrounding fluid(s). In the case of upconversion where the emitted photon is of higher energy than the absorbed one, an anti-stokes shift occurs. This extra energy gained by the emitted photon can be attributed to a variety of different mechanisms including but not limited to, the dissipation of thermal phonons in the crystal lattice or triplet-triplet annihilation to name a few (Auzel, 2004).

While organic molecules can achieve upconversion by themselves, this paper will focus on the synthesis and characterisation of inorganic nanoparticles using the f-block elements, the lanthanoids (Auzel, 2004). Repeatedly over the course of the past 10-15 years several papers and literature reviews have expressed and proven that the lanthanoids excel at upconversion. Novel research into this burgeoning field requires the understanding of these curious and mysterious lanthanoids in order to effectively engineer them to efficiently perform to their highest capabilities, upconversion.

1.2. Upconversion Mechanisms

While two-photon absorption and second harmonic generation are also processes in which the emitted photon is of higher energy than the absorbed photon, they have distinguishably different mechanisms to that of Upconversion.

Either a singular or multiple mechanism(s) can work hand-in-hand to achieve upconversion. There have been five mechanisms in total that have been identified till date: Excited State Absorption (ESA), Photon Avalanche (PA), Energy Transfer Upconversion (ETU), Energy Migrated-Mediation Upconversion (EMU), and Cooperative Upconversion (CU). These mechanisms can be observed in different Upconverting materials such as bulk materials or nanoparticles as long as they contain elemental ions which are capable of Upconverting, like the lanthanoids (Dubey et al., 2022).

ESA is the mechanism of upconversion, which gave the word its definition. It is a multistep process in which photons are absorbed sequentially from the ground state to an intermediate state after which they then finally populate the excited state from which upconversion occurs (Chen et al., 2012). Figure 1.1 below shows a simple schematic of this process. Photons in the ground state 1 when excited with a wavelength, ϕ_1, which's energy is resonant with the transition from ground state 1 to excited state 2, will absorb the energy and populate that state 2. Any incoming photons resonant with the next energy gap, state 2 to state 3, can excite the already-excited Photons populating state 2 to populate state 3 (Nomura et al., 2022). Phonons, which are the collective excitation of condensed matter which quantises the vibrations within the elastic structure of crystals (Joubert, 1999), may assist in these absorptions to the higher states. It is

crucial to note that ESA is a single ion process, which means that the pumping rates, denoted by R_1 and R_2 in the figure below do not depend on the upconverting ion concentrations in the host material.

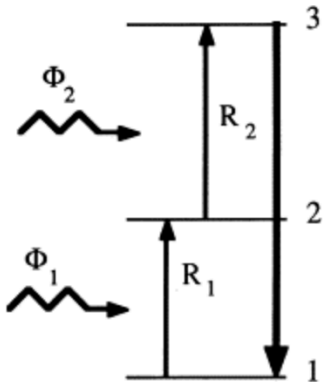

Fig 1.1: Excited State Absorption (ESA).
A diagram showing ESA, denoted by the absorption of two photons of two separate wavelengths denoted by ϕ_1 and ϕ_2 (from Nomura et al., 2022).

Note that there are two separate pump powers required to fully excite the ion to its highest excited state, ϕ_1 and ϕ_2. This means that unless the transitions between states 1 and 2, and 2 and 3, have the same energy, two pump lasers, each corresponding to the resonant energies of the two states gaps would be needed to achieve upconversion in such an ion. Under continuous wavelength excitation, the anti-stokes fluorescence is almost proportional to the product of ϕ_1 and ϕ_2.

Cross-Relaxation is a term used to describe the ion-ion interactions which may occur in Upconverting crystals. In Figure 1.2, below, it is the energy transfer which occurs between ion 1 and ion 2 when ion 2 transfers a part of its excited energy to ion 1, mainly when E2 of ion 1 + G (ground state) of ion 2 transfers to E1 of ion 1 + E1 of ion 2. This process is highly reliant on the dopant concentration of the crystals and usually high doping concentration of upconverting ions within a crystal lattice results in weaker photoluminescence intensities due to concentration quenching. However, it can still be used intentionally to tune the colour output of the material or to develop efficient photon avalanche upconversion. The ions may be of the same type, and need not necessarily be two different upconverting ions (Chen et al., 2014).

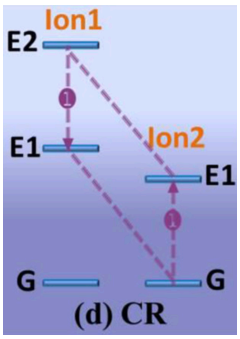

Fig 1.2: Cross-Relaxation (CR) Schematic.
Diagram of CR taken (from Chen et al., 2014).

Photon Avalanche is a more complex process characterised by three distinct steps: transmission, emission, and rise time on a pump power intensity with a critical pump threshold. In a four energy system (Figure 1.3 below), where E_0 is the ground state, E_1 and E_2 are the intermediate states, and E is the upper excited states, the first step, as it is the case with most mechanisms, is the absorption of energy by an electron when irritated with an excitation wavelength. In PA, this energy is not perfectly resonant with any of the intermediate states - the energy may be higher than E_2, in which case, through cross relaxation the electron manages to go down to the E_2 state. Then, an energy transfer occurs between the E_2 electron and another electron in the ground state, E_0, leading to the formation of two electrons in the E_1 state (the E_2 electron releasing energy and dropping down, and the E_0 electron gaining energy and rising up). Under continuous wavelength radiation, ω, one of these electrons gain energy to enter the upper excited state, at which point it interacts with electrons in the ground state to create three more electrons in the E_1 state. And since the radiation provided is resonant with the transition from E_1 to E, the process loops (Chen et al., 2012; Nomura et al., 2022; Skripka et al., 2023).

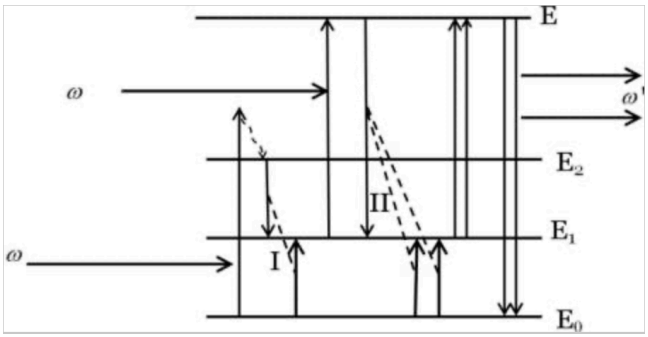

Figure 1.3: Four Energy system demonstrating the mechanism of Photon Avalanche (PA).
A diagram demonstrating a singular excitation wavelength leads to a cascading number of photons being excited to the same state(s) and releasing energy by returning to the ground state taken (from Dubey et al., 2022).

Given the avalanching nature of the PA mechanism, the number of electrons which populate E begins to rise drastically, and their consequent relaxation back to their ground state, E_0, causes them to release high energy photons. While this may seem highly beneficial in creating these high frequency, short wavelength photons, weak ground state absorption, and high laser pump power thresholds leads to limited maximum output of materials that capitalise off the PA mechanism (Chen et al., 2014).

Energy Transfer (ET) mechanisms studied and understood in lanthanoids until the mid 1960s were of the type where only the sensitiser, or light sensing ion, was in an excited state, while it's pair, the activator, or light emitting ion, remained in its ground state. Then once the sensitiser had accumulated enough energy, it would transfer its energy to an activator, leading to fluorescence. It was not until 1966, that there was a proposition which explained the possibility that when an activator enters its excited state, an ESA of the activator into an even higher excited state may occur, or there might be another type of energy transfer which occurs where both the sensitiser and the activator are in their excited state(s) before the energy transfer occurs. If these were cases, it may lead to fluorescence at wavelengths smaller than the excitation wavelength(s) (Nomura et al., 2022). These types of energy transfers are part of the ETU mechanism.

ETU, the most favoured and most efficient mechanism catalogued till date of the lanthanoids, enlists the usage of two or more lanthanoids doped into a crystal lattice to achieve upconversion. It is independent of the pump power. When both the sensitiser and the activator ions are close enough together in a crystal lattice and their excited energies are nearly equal, the energy accumulated by the sensitiser can be transferred to the activator, exciting it to its excited state (Chen et al., 2012). If there is an energy mismatch in the energy levels between the sensitiser and activator, phonon assisted non-radiative transfer can occur. Since, unlike ETA, ETU relies

on the closeness of lanthanoid ions to each other, designing such materials requires careful consideration of the doping concentrations of these ions within a host lattice. However, efficient ETU can still occur in single-lanthanoid doped ions as well, in which the sensitiser acts as both the donating and receiving ion (Chen et.al, 2014). Figure 1.4 below illustrates all different types of possible ETU mechanisms which can occur when two different ions are doped into the same crystal lattice.

Figure 1.4a) is the traditional ET mechanism where only the sensitiser is excited and transfers its energy to the activator after which ESA occurs in the activator. This requires two separate laser excitation wavelengths as denoted by, ϕ_1 and ϕ_2. In successive energy transfer (Figure 1.4b)), only the electrons of the sensitiser are excited by the incident radiation, after which the activator is promoted to its first excited state 2 by a first ET, and then to state 3 by another ET from the sensitiser. Figure 1.4c) illustrates Cross Relaxation upconversion which usually occurs between identical ions. If multiple sensitisers are excited by the excitation wavelength, and they all transfer their energies to the activators, then cooperative sensation occurs, as is demonstrated in Figure 1.4d). Finally, Figure 1.4e) describes the case where an emission occurs due to a single process of one photon from two excited and interacting ions.

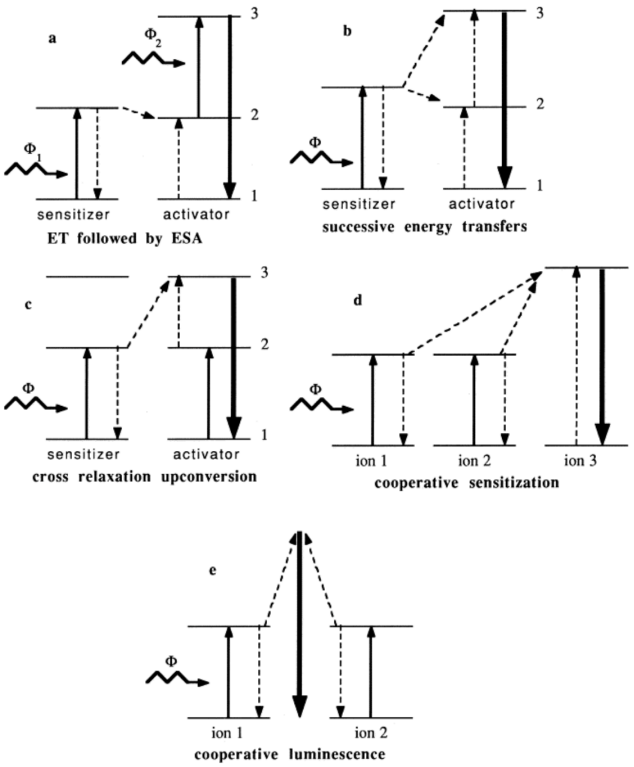

Figure 1.4: Common Energy Transfer Upconversion Mechanisms (ETU).
ETU Diagrams taken (from Nomura et al., 2022).

In recent years there has been research focused on the creation of upconverting materials that utilise their macro structure as a means of an upconversion mechanism. This research started due to the understanding that certain lanthanoids are not able to upconvert as efficiently as the others. The Thulium ion and the Erbium ion are examples of two lanthanoid ions which have the ability to upconvert extremely efficiently given their long lasting intermediate states which act as energy reservoirs. However, the Terbium or Europium ions, for example, lack the prevalent intermediate states present in the aforementioned ions, and thus a new mechanism must be developed in order to assist them in their upconversion. The name given to the upconversion mechanism employed particularly for upconverting ions which are generally considered inefficient, is Energy Migrated-Mediation Upconversion or EMU.

For EMU to occur, four different categories of ions must first be identified: sensitisers, accumulators, migrators, and activators. Sensitising and activating ions are the same as the ones defined in the previous mechanisms. The accumulator ion, as the name suggests is the ion responsible for first absorbing the energy sensitised by the sensitiser, and then entering an excited state. The migrator ion draws out the energy from the high energy states of the accumulator ion and passes it on to the activator, in order to achieve upconversion.

Given the flowing nature of the EMU process the spatial distribution of ions, particular the accumulator ions and the activator ions, is important in order to finely control the energy exchange interactions. Thus, most upconverting materials which employ the EMU technique are often in the form of core and shell nanoparticles. This separation of the the sensitiser and accumulators from the activator is an important factor to consider in order to eliminate the detrimental quenching that can occur due to cross relaxation (Cheng et al., 2024; Su et al. 2012).

EMU however needs not necessarily only be used to elevate the optical properties of ‘weaker’ ions such as Tb^{3+} or Eu^{3+}. Instead, EMU can also be employed for the already bright ions, such as Tm^{3+}, in order to make materials which use these ions, even brighter. This will be the main focus of this paper: EMU, ETA, and ETU, working hand-in-hand in order to create bright nanoparticles.

1.3. Upconverting Nanoparticles

Upconverting Nanoparticles (UCNPs) are, as the name suggests, nanoparticles with the ability to upconvert. While upconversion was initially studied through bulk crystals and optical fibres, the development of UCNPs allowed for a more sophisticated and deeper understanding of the upconversion process given the different ways in which UCNPs could be applied more so than

their macro crystal counterparts. Depending on the dopants, and their concentrations, UCNPs generally absorb photons in the infrared (IR) region and emit photons in the visible or UV region - this is especially prevalent in ion dopants such as Tm^{3+} and Er^{3+} (Haase et al., 2012).

As identified in the previous section, photon upconversion requires the existence of metastable states to facilitate the sequential absorption of photons - ie, excited electrons need to remain in their intermediate states long enough for another electron to become excited. The lanthanoids have been identified to possess these germane metastable states due to their complex electronic structures by virtue of their 4f orbitals. When doped into a suitable nano crystalline host lattice, these 4f orbitals split further in the presence of the crystal field to create a series of states with similar energies. These ladder-like, long-lasting intermediate states are the key to upconversion. Furthermore, with the 4f shell existing close to the ionic nucleus, and the 5s and 5p shells providing shielding from the exterior crystal field, the 4f shell is non-bonding. Thus, the coupling of electronic excited states to the surrounding lattice is weak, leading to long excited state lifetimes and sharp optical line shapes (Bünzli et al., 2011).

Within these nanoparticles, depending on its structure and the dopants, any or all of the aforementioned physical mechanisms described in chapter 1.2 may take place. In relation to their bulk crystal counterparts, in which the same mechanisms take place, UCNPs have considerable surface and size-related effects which have been shown to have important consequences. Since the 4f electrons are sufficiently localised, quantum confinement, which addresses an issue with regards to the smallness in size of nanoparticles compared to the electronic wavelength (Neikov et al., 2019) is not an issue. Instead, issues arise due to the energy dissipation that may occur within the crystal or between the ions, namely radiative and non-radiative relaxation. Radiative transitions are either the absorption or emission of a photon, while non-radiative transitions arises through different mechanisms through which energy is either transferred between the ions and molecules, or is dissipated from the molecules to its surroundings.

In order to consider energy losses and/or gains during the migrations and energy transfers between the ions, phonon density of states becomes an important factor. Phonons can also sometimes play a major part in assisting the excited electrons to reach the intermediate states by bringing the f orbitals in range so that energy transfer can occur. Since non-radiative relaxation decreases the lifetime of the excited states, and phonon-assistances increase the probability of energy transfers these effects compete with each other when considering the size of UCNPs (Liu, 2015; Xu et al., 2021).

1.4. Chemistry and Crystal Structure of UCNPs

The structure and chemical composition of UCNPs directly influence their ability and efficiency to upconvert as can be understood from the previous chapter. Apart from choosing the appropriate sensitiser and activator ion duo, the host lattice plays a crucial part in determining the spectral characteristics of UCNPs. In essence, the host lattice provides the framework through which energy conduction can be mediated and transferred between all relevant ion species. Three key factors must be considered when choosing an appropriate host lattice: low phonon energy, high chemical stability, and low lattice symmetry. Depending on the UCNPs being prepared, low phonon energies are generally preferred even if phonon-assisted UC takes place, since non-radiative phonon energy quenching may still occur leading to low emission intensities. High chemical stability is a key factor not only due to the fact that the lanthanoid ions must remain non-bonding so that they can perform their function, but also because UCNPs are generally applied in fields where they must be neutral in nature and non-reactive.

The Laporte selection rule is a law which describes the intensities of the absorption spectra of atoms or molecules which are centrosymmetric in nature. It states that electronic transitions which conserve parity are forbidden. In essence this means that electronic transitions between like orbitals (s to s, p to p, d to d, and f to f) are forbidden and cannot occur in centrosymmetric atoms and/or molecules. A centrosymmetric point group is described a point group within a crystal which contains an inversion centre as one of its symmetry elements - for every (x, y, z) point in the unit cell, there is also exists a corresponding (-x, -y, -z) point. Benzene is an example of a molecule which is centrosymmetric in nature with its centre of symmetry being at its centre (Wang et al., 2022). Thus, UCNPs with lattices which have low symmetry often tend to be brighter than those which have higher symmetry. In fact, Tetrahedral crystals do not have the point groups which contain the inversion operation, and thus are naturally bright and have intense emission spectra and are attractive candidates for UCNP synthesis (Schläfer, 1969).

During the early stages of UCNP development and research, researchers discovered that choosing appropriate host lattices proved to be challenging, not only due to the considerations of symmetry and phonon energies but also due to the choice of cations and anions to use. Initially, oxides were used to conduct experiments with UCNPs due to their high chemical stability, however these particles, while upconverting, were not very bright due to the high phonon energies of the oxides. The halogen ions, halides, of the 17th group of the periodic table, such as the Chlorine and Bromine ions possess low phonon energies but are also hygroscopic in nature giving rise to chemically unstable UCNPs. For this reason, the Fluoride ion, F^- was chosen as a potential candidate, since it provided a somewhat decent balance between the two issues, owning both stability and low phonon energy. Their cationic counterparts need to be of

similar size to the laser active ions, ie. The lanthanoid dopants. Alkaline earth metals suit this particular need, and since they can also bond easily with the F^- ions, Lithium and Sodium became the main cations for UCNP synthesis (Wu et al., 2014; Wang et al., 2012). In essence, the host lattice for UCNPs these days are ionic compounds either: Sodium fluorides or Lithium fluorides, doped with the common laser active sensitisers and activators, Yb^{3+}, Tm^{3+}, Er^{3+}.

In fact, choosing appropriate ion pairs are also important. The energy level differences between the ground and intermediate, and the intermediate and excited states of the activator ions must be similar - this key factor facilities better absorption and energy transfer while minimising the detrimental effects of non-radiative energy losses. This is once again another reason why lanthanoids are such excellent candidates for upconverting ions, since they have multiple ladder-like energy levels providing a vast selection of intermediate states for electrons to excite to depending on the excitation wavelength and the energy differences in the levels of their sensitiser ion-pair.

One of the most common sensitiser ions used in the creation of UCNPs today is the Ytterbium ion due to its large absorption cross-section for incident NIR light and a corresponding single excited 4f state. Furthermore, the energy gap between the excited state and ground state of the Yb^{3+} ion matches well with the ladder-like gaps of the states of the activator ions allowing for smooth and easy energy transfers between the two ions types through resonant energy transfer. When doping multiple ions into a host lattice (ie, the sensitiser and the activator ions), concentration is a key factor to consider, as this determines the average distance between the activator and the sensitiser, and the activator to other activators - high concentrations may lead to cross-relaxation and thus weaker emission spectra (concentration quenching) (Zhou et al., 2014).

In the 1950s and 1960s, Dieke and his co-workers worked on cataloguing all the possible energy levels of all the lanthanoids into a concise and easy-to-read diagram. And in 1968, in a book issued posthumously after Dieke's passing, the diagram in Figure 1.5 below, known as 'Dieke's Diagram' was published. As can be discerned, the diagram contains a comprehensive and detailed illustration of the energy levels of all the lanthanoids including the energy between the levels as well as the J multiplets. The initial diagram was constructed using experiments based off of Chloride hosts. However, Bill Carnall carried out an important legacy work utilising the Fluoride hosts which are more stable and optically transparent. The close energy splitting of certain levels can also be observed in the diagram as well as the ground state - this is important when it comes to identifying proper sensitiser and activator ion pairs for Upconversion as described in the previous two paragraphs (Suzuki et al., 2023; Peijzel et al., 2005).

Furthermore, the diagram also details the term symbols associated with each energy level and its splitting, giving details for the spin, angular momentum, and orbital quantum numbers. When there are an odd number of electrons in the 4f shell, each multiplet with J splits into J + 1/2 crystal field levels in symmetries lower than cubic, which includes the tetragonal crystal structures of the Lithium or Sodium fluoride host lattices (Peijzel et al., 2005).

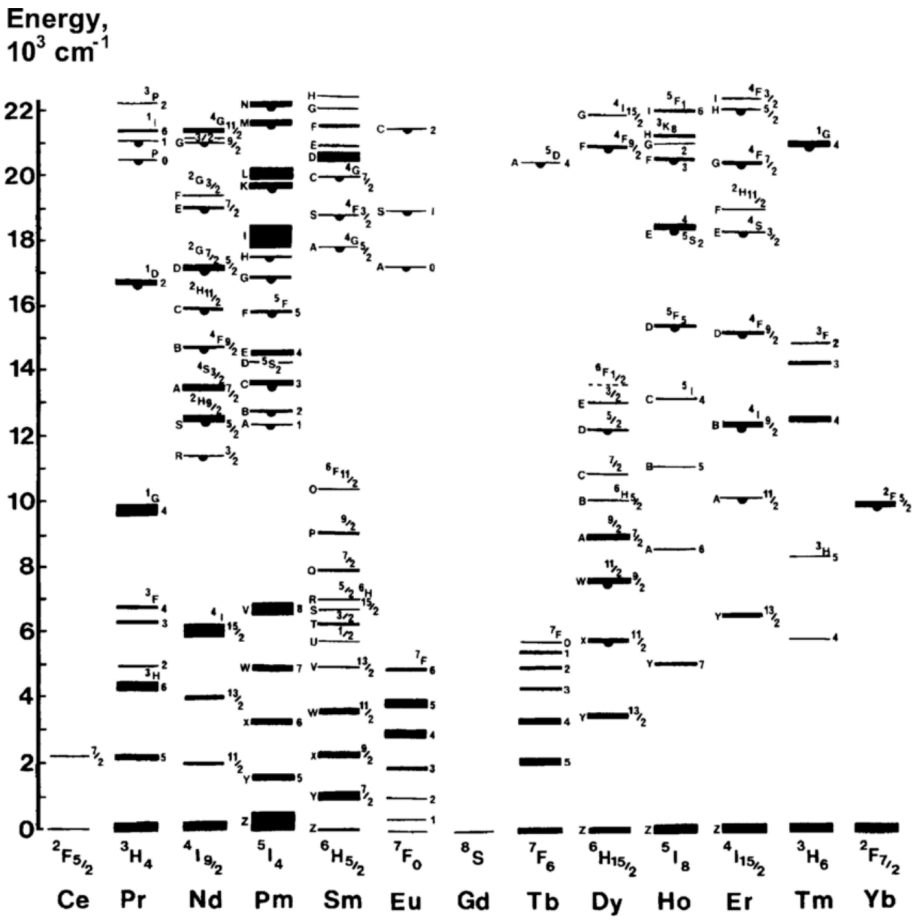

Figure 1.5: Dieke's Diagram.

Describes the $4f^n$ energy levels of trivalent lanthanoid ions. Dieke's Diagram taken (from Peijzel et al. 2005).

2. MOTIVATION

One of the benefits of UCNPs is their malleability in being used in a variety of different fields. Given their high chemical stability and their smallness in size, as well as their ease of post-synthesis modification, UCNPs can be tuned and engineered to be used in an eclectic selection of fields from the semiconductor industry to even biomedical engineering.

As will be seen later, the UCNPs prepared in literature, as well as those prepared in this report are made in organic solvents and surfactants leaving them capped in organic ligands. These ligands, during the synthesis process, aid in controlling the size of the nanoparticles, however afterwards leave them only dispersible in organic solvents such as hexane and toluene. While this may not be an immediate issue for analysis and basic applications, for applications in more refined fields, like the biomedical field, UCNPs require surface modifications which make them water-dispersible. The organic ligands are hydrophobic in nature and prevent this basic requirement. A ligand exchange synthesis or process is thus employed to replace these hydrophobic ligands with hydrophilic ones such as Polyethylene Glycol (PEG) or Polyacrylic Acid (PAA) which are usually multi-chelating to provide better stabilisation and binding.

However, usually after the ligand exchange, a process which in itself is tedious and needs to be optimised for every situation given the size, nature, and chemistry of the UCNPs, the particles tend to aggregate and thus lose their intense emission spectra. This is an issue which persists to this day even though several different reagents and acids such as Hydrochloric Acid (HCl) and Nitrosonium Tetrafluoroborate ($NOBF_4$) have been tried and tested. It is worth noting that using $NOBF_4$ makes the nanoparticles have a lower tendency to aggregate, but in my experience the aggregation is still high enough to cause issues with the intensities (Muhr et al., 2014). Furthermore, if not prepared properly after reacting with these reagents, the nanoparticles may contain residual and random Boron or HCl ions and atoms which make them cytotoxic and unable to be used for biomedical applications.

In either case, the ease of surface modifications of these nanoparticles, their ability to generate high energies localised around them, and their tuneable emissions, make them especially attractive for applications in the biomedical field. Drug release, bioimaging, biosensing, and temperature detection are just a few of several ways UCNPs can be applied, but are also the four most interesting ways, as they employ the simple yet pedantic phenomenon of Upconversion to the complex yet distinct functions of the human body.

2.1. Applications in the Biomedical Field

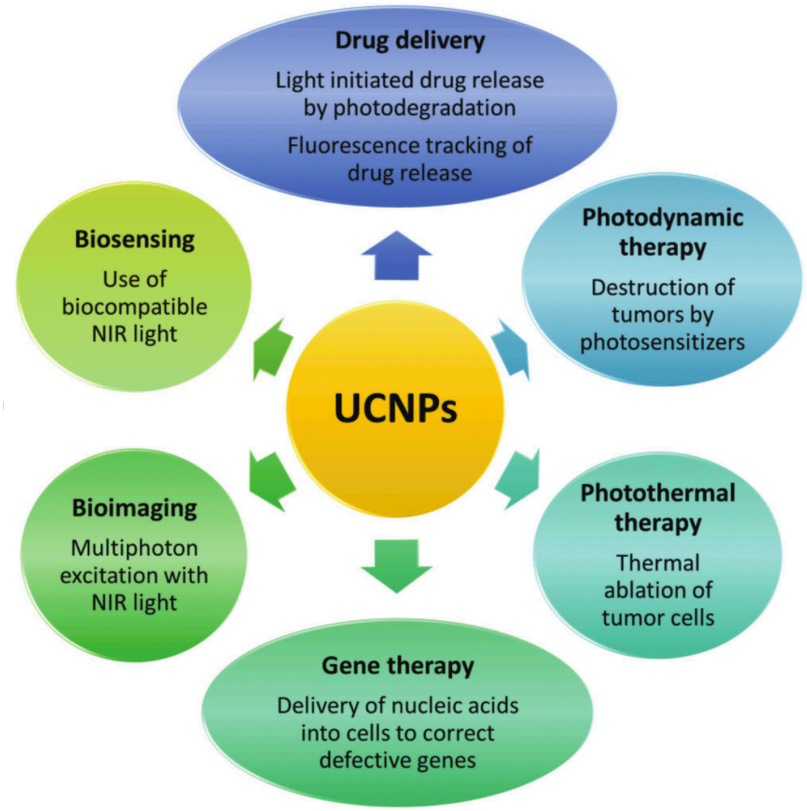

Fig 2.1: Potential applications of UNCPs in the Biomedical Field
Schematic of various Biomedical fields and applications with respect to UCNPs (from Oliveira et al., 2018)

With the discovery and rise in research of nanotechnology, researchers found potential ways to treat diseases which affect surrounding healthy tissues, non-invasively and with more precision. These nano materials however, gave rise to important concerns regarding safety in synthesis, as well as their potential adverse affects on human and animal health, and the environment. Thus, the sudden rise in interest in nanotechnology for biomedicine was accompanied by critical toxicological analyses and regulations. Even UCNPs face some of these issues. While they are mostly considered safe for biomedical use, other issues with UCNPs before application in clinical trials include 1) reproducible synthesis, 2) control over UCNP size and shape, 3) preparation of biocompatible surface chemistry, 4) instrumentation for activating and detecting the UCNPs in-vivo, and finally 5) theranostics (Oliveira et al., 2018).

In Personalised Medicine (or Precision Medicine), Theranostics is a technique which employs the usage of a particular type of object, medicine, drug, or technology which can provide both a diagnostic as well as a therapeutic result. This entire technique burgeoned from Nuclear

Medicine, which combines radionucleotide imaging (diagnostics) with radiation therapy (therapeutics) (Okamoto et al., 2021). For example, the iodine isotope 131 was one of the first used theranostic agents to study and treat thyroid cancer (Gomes Marin et al., 2020) - here it is worth noting that a great setback for theranostics are the regulatory and safety considerations. Maintaining the security of the target, the efficacy of these medicines, as well as the quality of these theranostic products are all of critical considerations. Cost-efficiency is also another issue to be addressed since these techniques tend to be costly in nature given the use of specialised equipment and advanced technologies. Furthermore precision and accurate targeting of sites of interest is another setback of this technique (Solnes et al., 2021). UCNPs however, while not yet perfect, are biocompatible, and a reliable source of both therapy and diagnostics given their wide emission spectra. Furthermore, simple lasers can be used to activate their properties rather than any high-tech equipment, alleviating the cost-factor and the need for a specialised workforce. However, synthesising them can be quite expensive as the prices of the rare earth oxides from which they are derived are costly.

2.2. Advantages of UCNPs for Biomedical Applications

A major advancement for the wider use of lanthanoid-doped nanomaterials in nanotechnology and biomedicine was the creation of novel bottom-up synthesis methods that produce well-defined UCNPs with tuneable sizes. This development led to their rapid adoption in bioassays and sparked global interest in utilising UCNPs for biomedical purposes. Several companies are now evaluating the potential of UCNPs as detection labels for their particular applications.

In fact, having sizes which can mimic the smallness in size of the human body's natural biological systems such as cells and proteins make UCNPs extremely beneficial when it comes to biomedical applications. In order to avoid invoking an adverse immune response, biomimetic materials are often employed to treat diseases - these materials are defined as "man-made synthetic materials that replicate the natural biological objects in our daily life" (Purkait et al., 2018). Since UCNP sizes can be controlled during synthesis to mimic the size of cells in the microbiota at their place of application, it lowers the chance of an inimical host response, furthermore adding to their high biocompatibility.

A controversial yet germane topic of discussion when regarding the size of nanoparticles in treating solid tumours is the enhanced permeability and retention (EPR) effect. This concept describes the abnormal uptake of macromolecular drugs and technologies, like nanoparticles, into solid tumours more so than they do in normal tissue. This phenomenon is attributed to the fact that in order for tumours to continue to grow efficiently, frequent angiogenesis, the physiological process which contributes to the formation of new blood vessels, must occur. This

leads to the unusually large intake of components in the blood and other vascular particles - according to many sources, if a nanoparticle is between a few nanometers in diameter to 100 nm in diameter, they satisfy this effect, and are more likely to target cancer cells than embed themselves into normal, healthy tissue. This is yet another reason why having great control over UNCP size is important for biological applications. Sodium based Yb-Er UCNPs to treat Hepatocellular Carcinoma using the EPR effect alongside other surface modifications showed great promise (Subhan et al., 2021; Wu, 2021).

Most organic fluorescent labels are activated by high energy light (visible and/or UV light), which also causes the activation or excitation of endogenous fluorophores native to the human body due to their broadband and overlapping spectra. However, UV light, the most energetic light in the spectrum with the shortest wavelength can cause damage to human tissue, and other cellular biomolecules like DNA and caused by photochemical reactions due to photoexcitation. UCNPs however operate in the NIR spectral region, between 650 - 1000 nm, and the 2nd and 3rd optical window as can be seen from Figure 2.2c) below. This 'window' is called the therapeutic window since wavelengths of light within this region do not cause any harmful effects to the aforementioned biological components. Since the light is not absorbed by these native components, light scattering is strongly reduced and leads to a higher signal-to-noise ratio in applications such as UCNP-based cellular nanothermometry (Oliveira et al., 2018; Jaque et al., 2014).

As mentioned previously, the Yb-Tm pair is capable of emitting UV, red, and IR light. A broad range of emission lines are not unique to this only pair, but simply changing the UCNP dopant compositions, their concentrations, and their structures can yield a variety of different emissions peaks, giving rise to their malleability and thus their function. UCNPs capable of UV emissions are attractive for usage in deep tissue therapies; While UV light lacks penetration depth and is toxic to human tissue but possess the energy necessary to trigger surface bound photosensitises or other photochemical reactions (such as the production of reactive oxygen species), NIR light has the penetration depth and is within the therapeutic window but not the energy - so with UCNPs, researchers are able to create localised and in-situ UV light needed for cancer therapy (Zhu et al., 2018).

2.3. Bioimaging

Since the same UCNP can emit both in the UV and blue, and the red and IR range, it can also be used for biological imaging which is the detection the frequency doubled light, ie, the longer wavelength, IR light. Due to their anti-stokes mechanism, UCNPs can use lower-energy light that is both less harmful to skin and other tissues for prolonged exposure and can also penetrate

deeply as compared to traditional bio labels. Figure 2.2 below is a demonstration of the benefit of utilising NIR light for both imaging and activation.

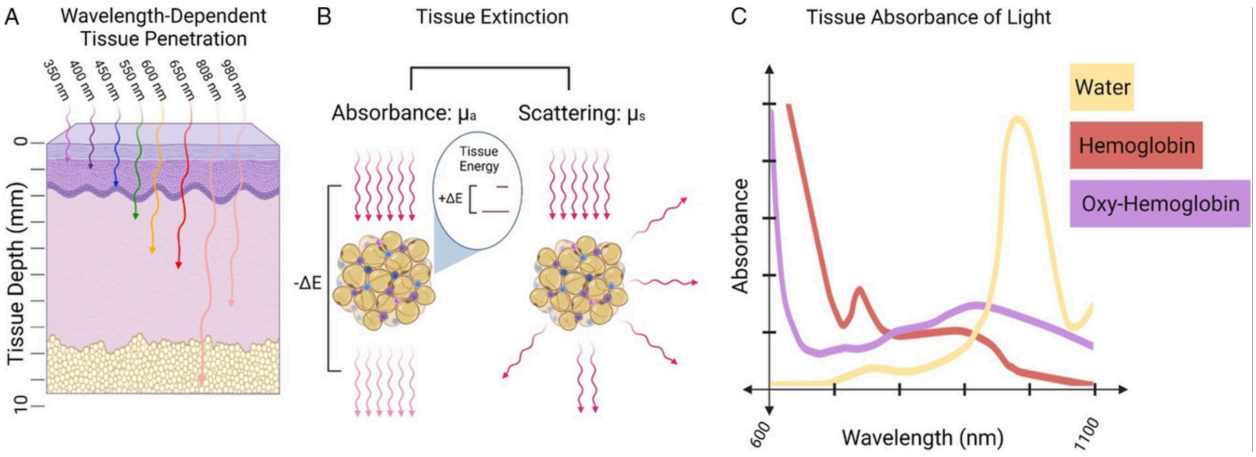

Fig 2.2: Interaction of different wavelengths of light, focusing on NIR light, and their interaction with skin tissue

Diagrams taken (from Mettenbrink et al., 2022).

In Figure 2.2a) it can be observed that the most common wavelengths of light needed to activate UCNPs which are 808 and 980 nm can penetrate up to 1 cm into skin tissue. The deep penetration of these higher wavelengths of light can be attributed to their lower absorbance coefficient (μa) and lower scattering coefficient (μb), and thus an overall lower extinction, which can be seen in Figure 2.2b). Absorbance occurs when energy is transferred to materials native to the human biological tissue, and scattering occurs when energy is reflected by these materials (Mettenbrink et al., 2022).

Significant developments have been made with UCNPs for usage in MRI, and X-ray computed tomography (X-ray CT) scans (Wang et al., 2011). For example, in 2018, Yb-Er based, $NaLuF_4$ was used as a spectral contrast agent to diagnose Osteosarcoma, and was more successful than the traditional, clinical contrast agent, iohexol (Jin et al., 2018). One of the strongest barriers to cross in nature is the blood-brain barrier, making imaging, and/or otherwise diagnosing brain diseases tricky. However, in January 2024, researchers managed to utilise upconverting nanoprobes, modified on the surface with Angiopep-2 to cross the blood brain barrier to assist in MRI scans of the brain (Han et al., 2024). Furthermore, by taking advantage of the interaction between the fluoride and lanthanoid ions, UCNPs have also seen use as imaging agents for single photon emission computed tomography (SPECT) in order to help image lymph nodes and also for staging cancer surgery. By adding receptors and other ligands on the surface of the UCNPs, researchers have also been able to image single cells by using

UCNPs as targeted fluorophores (Chen et al., 2015; Achatz et al., 2010). Since there is an ease of surface modification, the limit does not just stop at imaging cells, but also antibodies, as UCNPs can be conjugated to certain antibodies to treat different types of cancer (Cao et al., 2022).

2.4. Drug Release and Cancer Treatment

The most attractive of all the biological applications of UCNPs is their ability to release drugs in deep tissue due to their ability to create high energy UV and visible light in-situ. Most drug release systems require high energies to trigger their photochemical reactions, and thus higher energy light is more coveted than their lower energy counterparts which instead can be used for imaging purposes (Zhu et al., 2022).

The construction of UCNP drug release systems can be done in one of three ways: first, UCNPs can transport hydrophobic drugs, like doxorubicin (a contemporary drug used for chemotherapy) encapsulated within the hydrophobic pocket on the particle's surface; second, and more popularly, mesoporous silica bound to the surface of the UCNP can be used as a drug carrier; and third, a technique which is still in development as it requires more precise UCNP synthesising is by creating a hollow shell within the outer layer of the UCNP into which the drug can be loaded (Nomura et al., 2022). The therapy in which light of certain wavelengths activates any of the aforementioned process is more commonly know as Photodynamic Therapy (PDT), and is a very heavily researched and studied point of interest for modern-day cancer treatment.

PDT can be used through UCNPs effectively since these nanoparticles can be tuned and be manufactured for their specific applications. A very common and attractive area of interest using PDT is the localised production of Reactive Oxygen Species (ROS) to kill the cancer tissue. An excessive production of ROS can lead to both apoptosis (programmed cell death) and even necrosis (regular cell death) of cancer cells, making them an important chemical to understand - produced locally means that the ROS affects only the cancerous tumour and less so the surrounding healthy tissue. In order to effectively produce ROS in-situ, UV radiation must be present (Meijer et al. 2019; Wu et al. 2019; Jager et al., 2017), hence the application of the UCNPs. Due to the localised heating produced by the UCNPs as well as the wavelength of light used to trigger the response, photothermal therapy (PTT) is another type of treatment which can be used to kill malicious cells through heat. In 2019, a paper reported on using a Bismuth-Selenium compound conjugated with an Na-based, Yb-Er UCNP able to both image and destroy cancer cells when irradiated with 808 nm light (Zhao et al., 2019). More recently, in 2024, a UCNP system using cyanobacteria, a commonly used bacteria conjugate used alongside

UCNPs, also reported on successful treatment of Periodontitis with both PDT and PTT (Wang et al. 2024).

Features of solid tumours also include regions of hypoxia and immunosuppressive environments. Due to the lack of oxygen, certain anaerobic bacteria can thrive preferentially within those regions making them the perfect candidate for delivering anti-cancer drugs. One such bacteria, is E. Coli Nissle (EcN), a contemporary bacteria used in biomedical research for drug delivery applications - in 2022 a report commented on utilising EcN paired with Yb-Tm, Na based UCNPs and a blue-light-activatable plasmid to trigger an immune response at the cancer site by delivering a immunoactivator to the tumour (Xu et al., 2022).

Given the complex nature of the human body, as well as the different opportunities presented by tumour sites and other sites of interest, for as long as UCNPs remain pliant to surface and other chemical modifications, their unique ability to convert light can be used for a variety of different therapies. In fact, all current systems which rely of light emission to either combat, kill, or diagnose different diseases, I believe, can be replaced with UCNPs for more efficient results.

2.5. Biosensing

Since UCNPs are pliable to surface modification without hindering its function, they can be used in a variety of different biosensing applications as well. By attaching certain ligands, enzymes, and/or antibodies to the surface of the UCNPs, researchers can allow these particles to attach to certain biomolecules or organs via active targeting. This is the process by which surface modified nanoparticles are guided to specific cells, tissues, or organs by exploiting the unique features of the microbiota and/or pathological features of the target site (Inside Therapeutics, n.d.). Once at the place of interest, by irradiating the UCNPs with NIR light, researchers can monitor the function of the site of interest or even track the movement of cells.

In 2016, researchers reported on a successful demonstration in using UCNPs to accurately detect mRNA-related oligonucleotide markers in complex biological fluids. In fact, due to the very unique property of UCNPs to upconvert and provide a low photon count readout, it enabled them to reliably detect low quantities of small oligonucleotides in the femtomolar range. The experiments were carried out in human blood serum, and the detection of these analytes relevant to mRNA present in Alzheimer’s disease and prostate cancer makes this research paramount and important to not only help understand and perhaps detect and prepare for early-onset Alzheimers but also one of the most common cancers in the world (Veila et al., 2016).

Because with any sort of luminescence there is also a corresponding production of heat, UCNPs have also seen use as nanothermometers, being able to detect even the slightest internal

temperature changes. The positions of the emission versus the excitation bands, the intensity of the emission bands, excited state life times, and emission rise times are all features of UCNPs which are readily used to determine these slight temperature changes. Each lanthanoid has a unique luminescent fingerprint (which is another reason why UCNPs can be tuned to have different emissions depending on what they are needed for), as can be seen from Figure 2.3 below, however as the temperature rises, the sharp optical peaks tend to broaden and the intensities decrease due to higher lattice vibrations and the life time of radiative transitions shorten since non-radiative transitions become more probable. All of these factors can be used for temperature sensing. While the quantum yield of UCNPs is quite low compared to other luminescent probes, their sensitivity in detecting temperatures from between cryogenic to >1400 K is a very attractive advantage for many different applications beyond just biological ones (Far et al., 2023; Ryszczyńska et al., 2023)

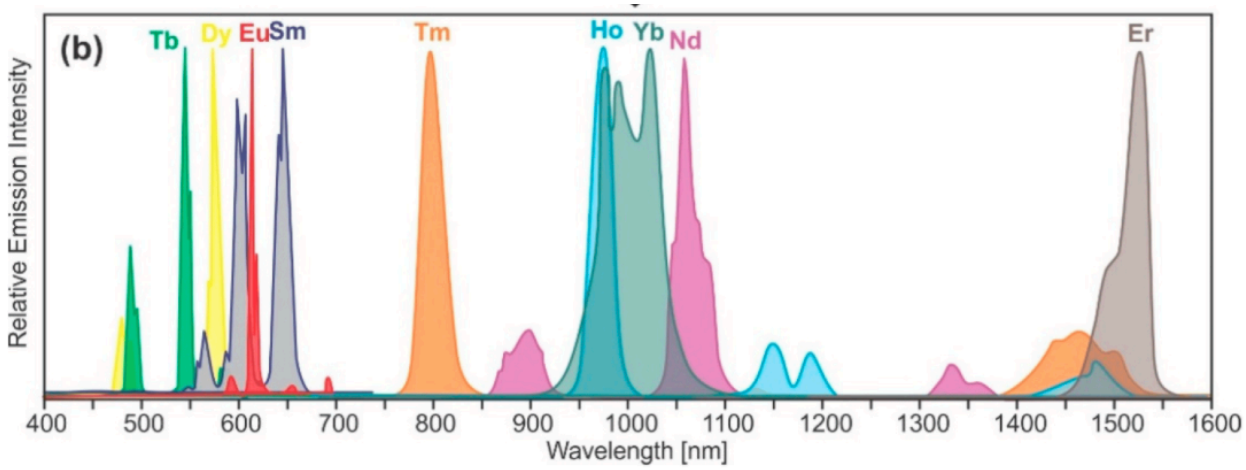

Fig 2.3: Emission Spectra of Different Lanthanoid Trivalent Ions between 400 nm and 1600 nm. Diagram taken (from Far et al., 2023).

2.6. Design Specifications

Keeping the mechanisms and the applications of these nanoparticles in mind, we can set some design parameters for these nanoparticles to perform their functions in the biomedical setting. Most researchers these days use the classical Yb-Er pair primarily because when irradiated with 980 nm light, in this system the Er^{3+} ion emits in the green range between ~ 520 nm - 550 nm, as can be seen from Figures 2.4 and 2.5 below. Green light though it manages to successfully perform its function, whether that is photocleaving polymers to release drugs or triggering photochemical reactions, and while it is more energetic than IR, NIR, or red light, is often slow when it comes to actually releasing these drugs. This is primarily because of one reason in that the overall intensity of the emitted light is significantly lower in an in-vivo setting than in a lab setting due to the amount of water surrounding the tissue. 980 nm light is water absorbable and

thus a significant portion of the light is absorbed by the hydroxyl groups in the water rather than the UCNPs (Arppe et al., 2015; Feng et al., 2021). This phenomena can be seen from the two graphs below from two separate papers studying the quenching effect of water on UCNP emission intensities. Although their intensities drop sharply, they need remain water dispersible for all biological applications.

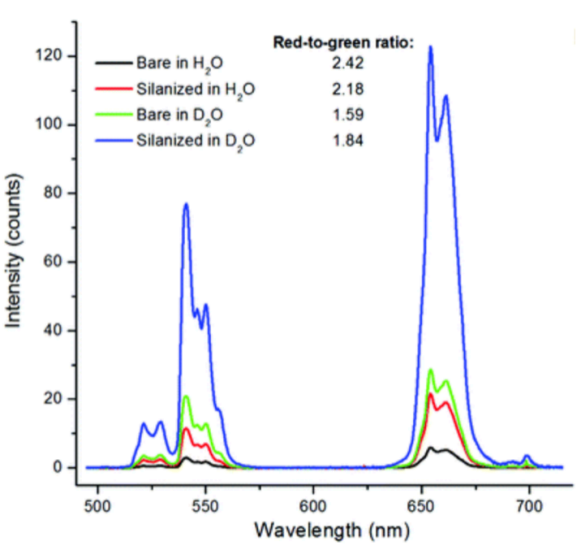

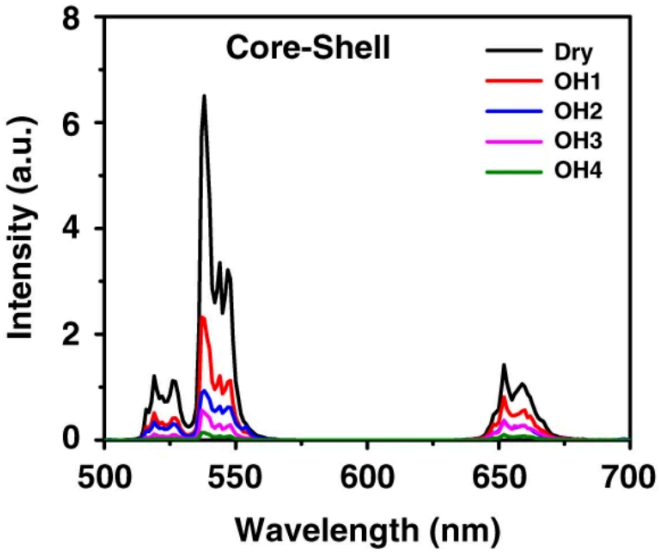

Figs 2.4 (left) and 2.5 (right): Er-based UCNPs Upconversion Emission performance in different solvents including regular water.
Spectral images and data taken (from Arppe et al., 2015; Feng et al., 2021).

Therefore, making brighter UCNPs will help aid in the efficiency of the drug release, as this is often the point of adversity when UCNPs are used for drug release purposes, the rate limiting step. If the UCNP is naturally brighter then when irradiated with the corresponding wavelength of light for its application, its overall emission intensities are higher than their classical counterparts (the ones implemented in studies today). The UCNPs also need to be small in order to obey the EPR effect mentioned previously. Their smallness may also avert the possible invocation of an adverse immune response. Furthermore, smaller nanoparticles have longer blood half-times due to reduced uptake by the reticuloendothelial system - this proves a benefit when UCNPs are delivered through intravenous injections at the target site (Zhang et al., 2017). Essentially this means that the UCNPs last longer in the blood plasma before being filtered out through the body's natural filtering system; the endocrine system and the liver.

From Figure 2.2 it would seem more beneficial to use 808 nm light rather than 980 nm light as the excitation wavelength given its deeper tissue penetration. 808 nm light excites the Nd^{3+} ion, which has a 70% quantum efficiency and a ten times larger absorption cross-section than the

Yb^{3+} ion. However, unlike the Ytterbium ion which has a singular energy level, the multiple energy levels of the Neodymium ion leads to an overall weak upconversion luminescence due to the energy back transfer from the activator to the 4Ij orbital of the Nd^{3+} ion [57]. For this reason, since we are trying to increase upconversion luminescence, I choose the Ytterbium ion as my sensitiser; as for my activator, I choose Tm^{3+} over Er^{3+} simply because the Yb-Tm ion pair emits in the UV and blue range while the Yb-Er pair emits in the green range, and blue light is more energetic than green light. Furthermore the detrimental effects of UV light on biological tissue can be averted and its destructive capabilities maximised due to the fact that the UV light would be produced in-situ, localised at the site of interest, which in this case would be a cancerous tumour. In addition, UV light has another benefit over green light in that it has the ability to induce the production of ROS which in itself can cause massive destruction to cancer tissue.

Thus, the design parameters for the UCNPs for applications in the biomedical field would be as follows:

- Small: between 20-25 nm in diameter. This leaves room for any surface modifications needed such as biological conjugation or water dispersibility.
- Water dispersible: All Lithium Fluoride and Sodium Fluoride based UCNPs can be modified to be water dispersible.
- Yb-Tm based: This ion pair emits in the region which I would like to see maximised, the UV-Blue region.
- Bright: The main point is to increase the brightness of the particle - whatever the outcome may be, it needs to be brighter than the classical/controlled particle which has been also been created and applied for research

3. RESULTS AND DISCUSSION

In 2018, Ting Cheng, Riccardo Marin, and Artiom Skripka had published a paper discussing the synthesis of super bright, and small $LiYbF_4$(Tm) UCNPs which served the basis and main inspiration of this thesis. This paper tackles the first design parameter identified in the previous chapter (Cheng et al., 2018).

As can be observed from the applications, Sodium based host matrices are the more common of the two (lithium being the other) employed in biomedicine today - however, $LiYF_4$ based UCNPs are also on par in generating efficient upconversion emissions, and sometimes even preferred over their Na counterparts when considering emissions in the UV/Blue range (Naccache et al., 2015). This paper was the first to explore and propose a way in which the size of these UCNPs could be tuned, since during the time of its publication Li-based UCNPs were 80 nm in size, which are too large for applications in which the UCNPs must be internalised by cells (Barua et al., 2014). Furthermore, since it is common to add shells to the nanoparticles for various different purposes, the primary one being to enhance the upconversion intensities; making smaller cores would aid in allowing for more leeway for surface modifications and shelling. The principal UV/Blue emitting UCNP at the time was $LiYF_4(Yb^{3+}, Tm^{3+})$, which basically mimicked the structure of it's kin, $NaYF_4(Yb^{3+}, Er^{3+})$, used in biomedical applications and green light emitting. Although the UV emission of this Lithium based UCNP was strong compared to all the other UCNPs being made at the time, the overall emission was still majorly comprised of NIR light (Hong et al., 2017). Thus this paper also touched on how to increase the UV emission of their classical $LiYF_4(Yb^{3+}, Tm^{3+})$ particle.

The sizes of the UCNPs were tuned by manipulation of the classical thermal decomposition method used to synthesise them. In this method, Oleic Acid (OA) is used as a coordinating ligand, and Octadecene (ODE) is used as a non-coordinating solvent. Together, they produce nanoparticles between 50 - 80 nm in size with very little control over the size and size distribution of the particles. However, Oleylamine (OM), another coordinating ligand can be used in conjunction with OA to assist in the nucleation of the UCNPs. By tuning the ratios between the OM and OA, this paper managed to successfully report on being able to control the size of the UCNPs they produced, which is, as mentioned previously, a very important factor to have control over when considering the synthesis of nanoparticles - with sizes ranging between 5 nm to 90 nm. Furthermore, the paper reported on the chemical stability and the subsequent upconversion emissions of these particles of various sizes. In fact, the UCNPs which were majorly composed of NIR light rather than UV light were those in the sub 10 nm range, which was reported earlier by A. Ra Hong et. Al from Korea University (Hong et al., 2017). Furthermore, those extremely

small 5-10nm UCNPs were very unstable leading to difficulties in growing shells or performing surface modifications. To make-up for these drawbacks, the paper also reported on a unique synthesis technique, the first of its kind, which aided in the generation of chemically stable UCNP cores of around 10 nm in diameter ready for shelling.

3.1. First Nuclei Synthesis

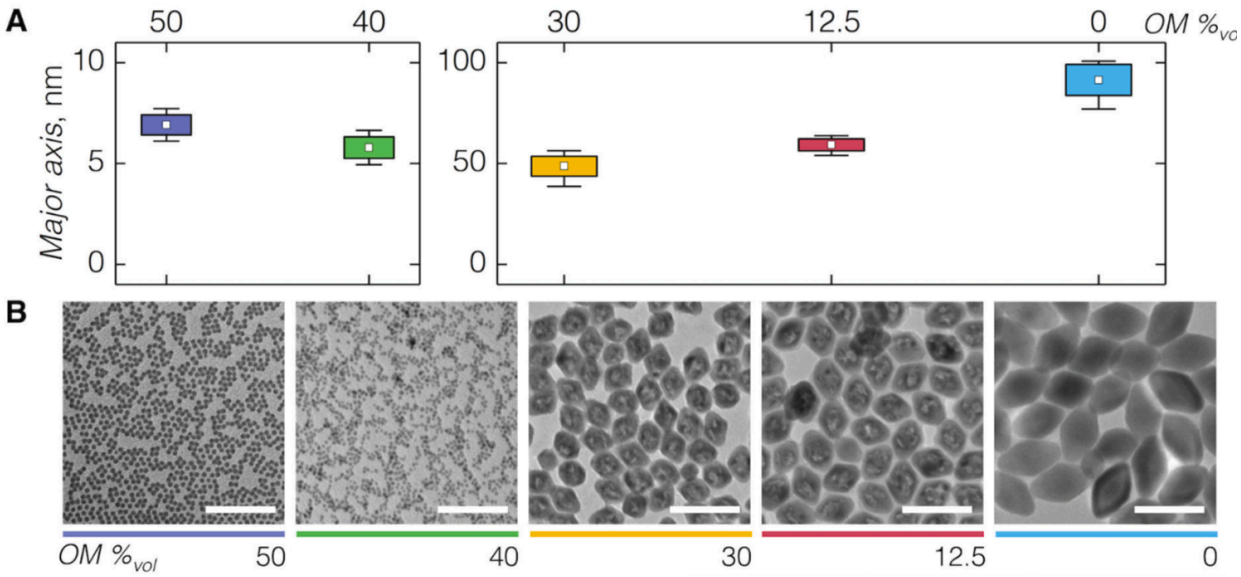

Fig 3.1: A) Size distribution of nanoparticles with respect to Volume % of OM and OA, B) Corresponding TEM images (from Cheng et al., 2018).

As can be seen from Figure 3.1, above, the size of the UCNPs, which in this case were $LiYF_4$(25% Yb^{3+}, 0.5% Tm^{3+}) can be finely tuned by mixing the appropriate volumes of OM and OA. When the volume of OM is 50% of the solution, ie the volume of the OM and OA are the same, the particles are the smallest, 5 nm. Using only OA as the coordinating ligand yields the largest particles which were 91 x 55 nm along their major and minor axes respectively. With volume percentages of OM at 12.5% and 30%, smaller particles which retained their bipyramidal morphology were obtained - however, once the volume % of the OM was 50%, the particles became nearly spherical in shape, given their extremely small size. With this information and supporting XRD data, the role of these two coordinating ligands was explored and explained in more depth: The OA's carboxylic group can be deprotonated leading to the formation metal-oleates, or in this case OA-Lathanoid (Referred to hence forth as OA-Lan) adduct molecules. In the case of OM, the Lanthanoid ions interact with the lone electron pair found on the primary amine group, however this same amine group can be protonated leading to fewer possible interactions with the positive metal ions due to electrostatic repulsion. This means that in theory the OM-Lanthanoid (OM-Lan) molecules are less stable than the OA-Lan molecules and thus

the OM-Lan adducts should decompose faster than the OA-Lan adducts. The paper states that these OM and OA adducts with the lanthanoid ions are a complex species in which ligands enter the coronation sphere of the metal cations alongside the trifluoroacetate anions which are found in the precursors, meaning that these adducts are more than just OA-Lan and OM-Lan. Overall, OM-Lan are nucleation favouring while OA-Lan are growth favouring acting as a reservoir of the precursors which are consumed slowly during the synthesis procedure. The unstable coordination of the OM with the metal-trifluoroacetates leads to faster nucleation and thus the formation of several, smaller nanoparticles as can be seen from the results. When the solution contains mostly OA, there is a continuous growth of UCNPs, however once OM is added to the mixture it halts said growth and allows for more nucleation. This synthesis method was thus given the name First Nuclei (FN) synthesis.

More importantly however was how these particles reacted to NIR, 980 nm irradiation. Upon irradiation, all the particles displayed the characteristic emission spectra of the Yb-Tm ion pair with a wide range of emission peaks from the UV to the NIR range, each corresponding to a specific energy transition process governed by the number of photons absorbed. For example, the 340 nm and 360 nm peaks require 5 or 4 photons to excite the Tm^{3+} ion respectively, while only 2 photons are needed for the peak at 790 nm. As can be observed from Figure 3.2 below, the size of the UCNPs synthesised also had an effect on the intensity of the emission peaks - the intensities decrease as the size of the UCNP decreases from 90 - 50 nm, and nanoparticles which were sub 10 nm barely demonstrated any upconversion luminescence due to high surface-to-volume ratio which prominent surface defects and subsequent ligand and solvent quenching. Though these newly formed particles using FN synthesis are small and thus attractive for cellular uptake and biomimicry, their weak emissions are unideal for usage as candidates in tumour therapy, thus further modifications are required to enhance their emission intensities.

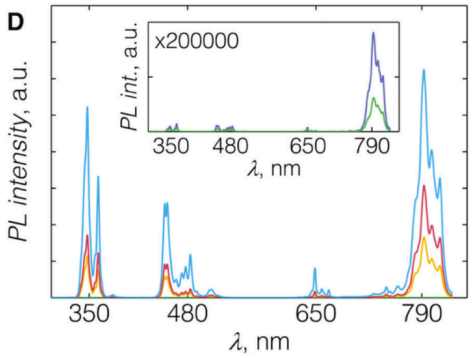

Fig 3.2: Emission spectra of $LiYbF_4$(25% Yb^{3+}, 0.5% Tm^{3+}) at the different sizes (respective colours) shown in Figure 3.2.

The inset figure shows the emission spectra of the smallest (green and then indigo) UCNPs synthesised demonstrating their inability to upconvert efficiently (from Cheng et al., 2018).

3.2. Stabilisation Synthesis of UCNPs

The first step in order to alleviate any sort of quenching effect in UCNPs is shelling them. Shells have proven time and time again to dramatically increase the upconversion emission spectra of UCNPs due to their shielding effect from external quenchers, which in this case would be the solvent the UCNPs are dispersed in. A shell prevents the detrimental effects of surface defects states and quenching due to ligand and solvent molecule interactions with the surface of the UCNP (Würth et al., 2018). Furthermore, changing the host lattice from $LiYF_4$ to a pure $LiYbF_4$ also increases the Upconversion emission due to more Yb^{3+} ions for light harvesting, in theory, capable of transferring more energy to the Tm^{3+} ions. This was a curious observation since earlier studies expressed severe emission quenching from Yb doping percentages higher than 25%, but recent studies since 2017 have demonstrated that as long as a passive shell coats an active core, the cation host lattice of the core can be composed purely of sensitiser ions (Zou et al., 2017). Utilising this method entails maximum light harvesting, and minimal surface quenching, ideally leading to brighter upconversion intensities. Thicker shells often leads to higher emissions as well, however large shell thicknesses means larger overall particles, so it is important that the thickness of the shell is another parameter which researchers need to control when tailoring the use of these UCNPs in biomedical applications.

It was soon discovered however that controllable shelling of the sub-10 nm cores synthesised by FN synthesis would be challenging due to an unforeseen problem. Various different methods were investigated in this paper using $LiYF_4$ as the shelling precursor: injecting 1) shelling precursor dissolved into OA/OM/ODE into FN cores, 2) shelling precursors dissolved into OA/ODE into FN cores, and 3) shelling precursors dissolved into OA/ODE into OA/ODE cores. In all these cases, the shell growth was unexpected, random, and erratic. The thickness of the shells

did not correspond to the theoretical thickness which can be approximated beforehand due to the amount of shelling precursor used in the actual injection procedure. The thickness can be estimated with the assumption that the cation intermixing at the interface between the $LiYbF_4$ core and the $LiYF_4$ shell is negligible. From Figure 3.3, below, it can be observed that the shell thickness varied drastically between the theoretical calculations versus the practical results, especially as the amount of shelling precursor used increased. From the figure, the researchers derived that there is a correlation between the unexpected size increase and the amount of OA present in the reaction mixture. Other important conclusions included the following: The presence of OM inhibits shell growth and actually promotes the nucleation and subsequent formation of more ultra-small UCNPs as can be seen from Figure 3.4 C), below, and the addition of shelling precursors dissolved in OA and injected in a solution of UCNP cores leads to the coarsening and coalescence of these cores thus resulting in varied size differences.

	Core (0.1 mmol)	Shell (+0.1 mmol)	Shell (+0.2 mmol)	Shell (+0.3 mmol)	Shell (+0.4 mmol)
Expected size (nm)	-	7.6	8.7	9.6	10.3
Actual size (nm) via approach A[1]	6 ± 0.5	8.4 ± 0.8	17 ± 1	21 ± 1	24 ± 2
Actual size (nm) via approach B[2]	6 ± 0.5	12 ± 1	15 ± 1	16 ± 1	21 ± 2
Actual size (nm) via approach C[3]	6 ± 0.5	6.2 ± 0.9			

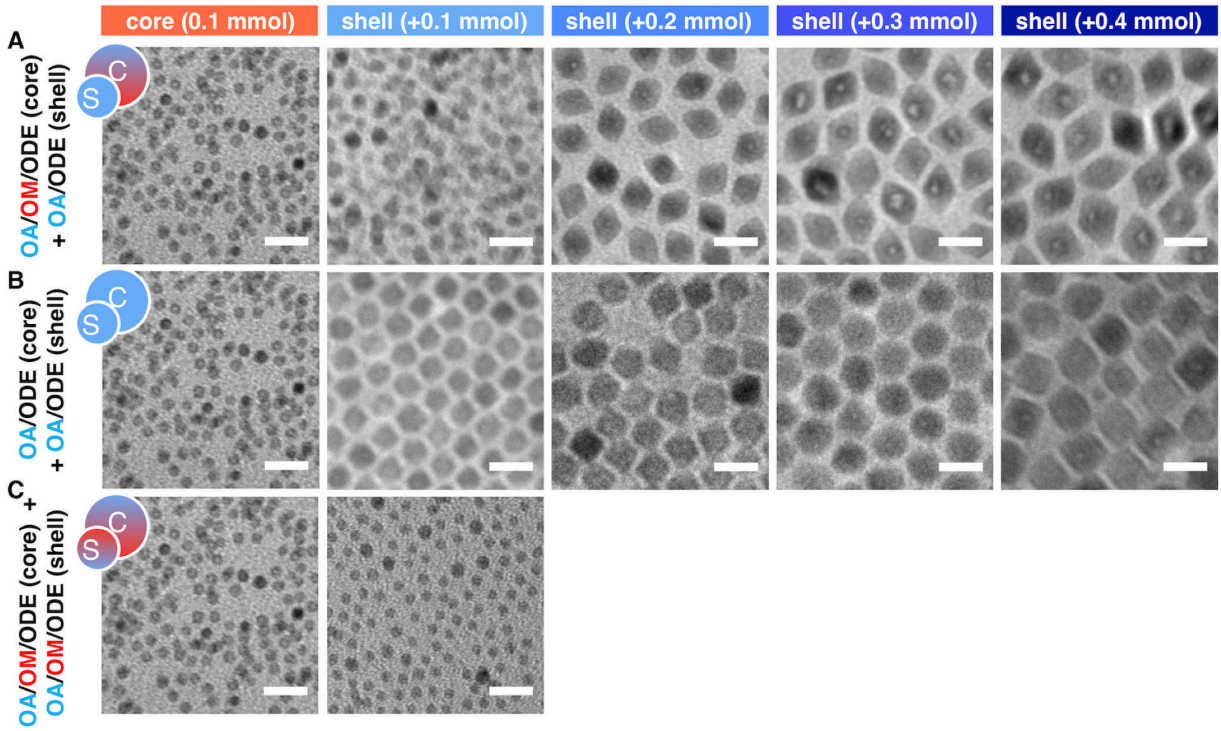

Fig 3.3 (top): Table cataloguing the expected vs actual sizes of the UCNPs once shelling precursors are injected into the solution of UCNP cores synthesised by FN synthesis.

Approach A is shell precursors in OA/ODE injected into cores in OA/OM/ODE, Approach B is shell precursors in OA/ODE injected into cores in OA/ODE, and Approach C is shell precursors in OA/OM/ODE injected into cores in OA/OM/ODE (from Cheng et al., 2018).

Fig 3.4 (bottom): Corresponding TEM images of the shell growth process under the approaches highlighted in Figure 3.3.

Notice that only at the second injection step in Approach A is the sudden increase in size observed, vs the sudden increase in size in Approach B after the first injection. This is because in solution A, the 'critical' OA volume is achieved only after the second injection when more shelling precursors are added into the solution, as opposed to in Approach B where OA is the dominating and only coordinating ligand. The TEM scale bar is 20 nm (Cheng et al., 2018).

From these observations, certain conclusions were drawn including the most important one in that the cores formed in the FN synthesis which were between 5-10 nm in diameter were thermodynamically unstable. The subsequent addition (or injection) of a ligand with a stronger coordinating capability like OA into a solution containing OM can refocus the cores to become

slightly larger but thermodynamically stable. Thus, it is imperative to 'stabilise' all cores formed by FN synthesis to make them malleable for shelling and surface modifications. This thermodynamic instability may also result in the weaker emission spectra observed in Figure 3.2. The stabilisation procedure entails the injection and/or addition of fresh OA/ODE containing no precursor shelling material into the FN cores (which are dispersed in OA/OM/ODE). Following this procedure increases the size of the FN cores from approximately 5 nm to approximately 10 nm - in the case of this study from 5.8 nm to 9.4 nm, which can be observed from Figure 3.5A) and B), below. These stabilised particles assumed their bipyramidal shape, characteristic of larger UCNPs. XRD information from Figure 3.5C) also show their improved crystallinity and increased size. At the time of its publication these were the smallest reported $LiYbF_4(Tm^{3+})$ particles and even now, First Nuclei Synthesis continues to be the principal synthesis method employed when making tuneable Li-based UCNPs.

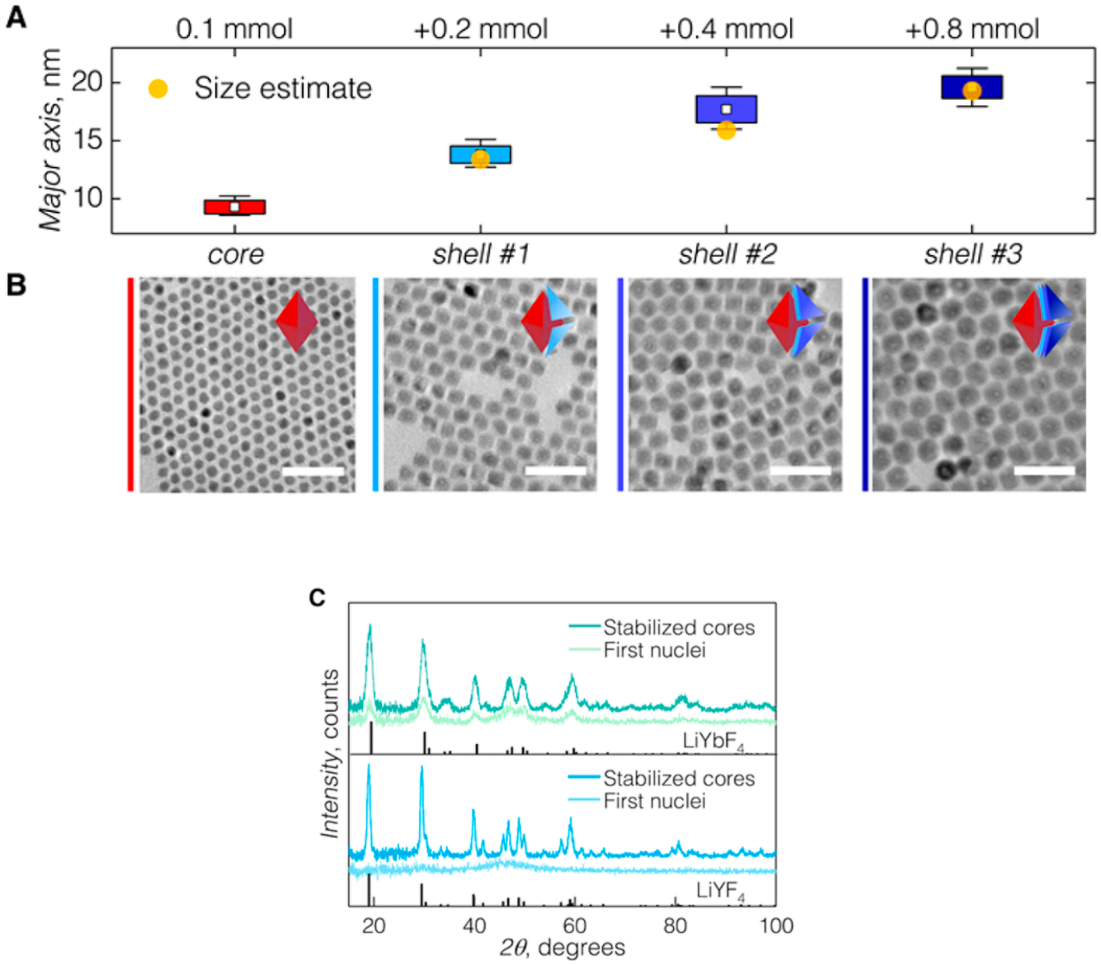

Fig 3.5: A) Size distribution of stabilised cores, B) TEM images of stabilised cores, C) XRD data comparing stabilised cores and FN cores (from Cheng et al., 2018).

3.3. Bright $LiYbF_4(Tm^{3+})$ UCNPs

The final step in increasing the brightness of these small particles was of course to shell them in order to prevent any quenching effects at the surface. As mentioned previously, thicker shells lead to brighter emissions - this paper investigated three different shell thicknesses, 2 nm, 4 nm, and 5 nm, and their corresponding upconversion emission spectra which can be seen in Figure 3.6, below. All three shells thicknesses drastically increased the intensities of the stabilised particles with the 5 nm shell being concluded as the most optimal one due to the relatively small change in intensity between the 4 nm and 5 nm shells. The size of the final particles grew, due to the shells, from 9.4 nm to 13.8 nm, 17.7 nm, and 19.6 nm respectively which are well within the sizes indicated for biological applications. Further studies on the lifetimes of the excited states, specifically the $^1I_6$ excited state at 347 nm, also increased in these shelled particles, indicating the suppression of energy losses from non-radiative decays related to surface, ligand, and solvent problems, responsible for upconversion emission quenching.

In conclusion, this paper reported on a synthesis technique in order to create small nanoparticles capable of upconverting in the UV and blue range effectively. The problem of thermodynamic instability arising from the method of synthesis was also resolved in order to ensure that these particles could later be modified for water dispersibility. Furthermore, the comparison between the then classical $LiYF_4(Yb^{3+}, Tm^{3+})$ and the $LiYbF_4(Tm^{3+})$ was also explored in detail, with the latter arising to the needs of biological applications being both malleable for FN synthesis and also brighter than its predecessor. In this thesis, the control particle will this very $LiYbF_4$(0.5% Tm^{3+})@$LiYF_4$ particle as an attempt is made to inject a middle shell in between the core and the outer shell in order to make them even brighter than it already is.

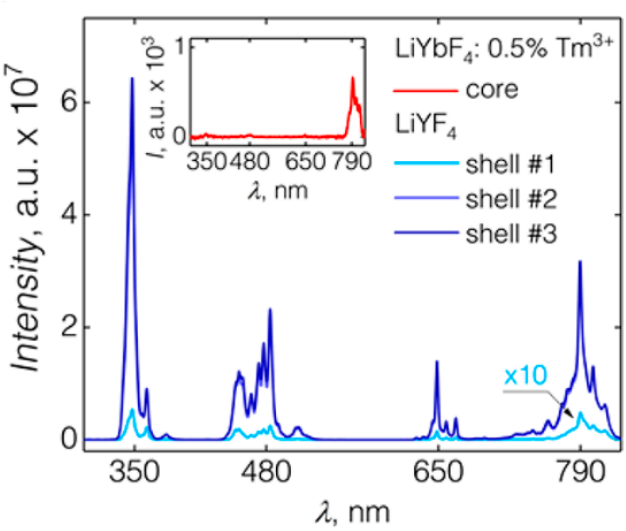

Fig 3.6: Upconversion Emission spectra of $LiYbF_4$ (0.5%Tm^{3+})@$LiYF_4$. Comparing shells of different thicknesses (shell 1: 2 nm, shell 2: 4 nm, shell 3: 5 nm) (from Cheng et al., 2018).

3.4. Multilayered Core-Shell UCNPs

While most UCNPs including the one mentioned in the previous paper are considered bright, they can, in theory, still be brighter. UCNP brightness depends on dopant concentrations, amongst other things, in that higher sensitiser and activator percentages within the host lattice will increase the amount of light harvested and then subsequently transferred to the light activating ions. However, as has been explained, high doping percentages of laser active ions leads to concentration quenching and detrimental cross-relation between neighbouring dopant ions (Wen et al., 2018). One such way to avoid the adverse effects of concentration quenching is by irradiating the UCNPs under high irradiance excitation (Zhao et al., 2013). However a side effect of employing such a method is the consequential effect that a high irradiance may have on human tissue. One way to avert the energy losses associated with cross-relaxation which is prevalent in all UCNPs as it is an intrinsic phenomenon, is by synthesising a multilayered UCNPs which employs the usage of energy migration and energy transfer at the interface between the layers. The use of energy mediating shells to increase Upconversion Luminescence has become popular in modern UCNP research as a way to enhance the emissions of the higher energy light, especially in the lower ranges, such as in the green, blue, and UV. Another attractive byproduct of utilising these middle shells is the ability to switch between the emission colours by using a single lanthanoid ion (Xu et al., 2022).

To design such a particle requires understanding of its specific optical functions and as a consequence its applications. In general, apart from a singular passive outer shell which

prevents surface quenching, at least one if not more middle shells are needed to manipulate the upconversion dynamics. In general, three different types of multi-layer-core-shell (MLCS) structures are possible and highlighted in Figure 3.7, below. In Scheme I, two different luminescent layers are separated by an optically inert layer. The point of this inert middle layer is to prevent any unwanted interactions of the laser active ions between the two active layers. Benefit of this structure is that it can emit different colours depending on the excitation wavelength, and thus is considered colour-tuneable (Deng et al., 2015; Wu et al., 2019). In Scheme II, the active layers are connected by an energy channel which acts an energy migratory lattice that can be used to manipulate the luminescent intensities (Zhou et al., 2020). Finally Scheme III shows a luminescent region which is constricted between two layers, either active, or inactive, as a way to confine the spectral manipulation - doing so can maybe enhance the upconversion emission spectra by averting deleterious energy migration between sensitiser ions.

These design schemes grant MLCS nanostructures enhanced freedom and flexibility in controlling excitation/emission dynamics and energy transport pathways, leading to the desired luminescence properties. Additionally, they create opportunities for integrating multiple functions at the single nanoparticle level. The thoughtful design of MLCS nanostructures not only facilitates precise energy flux control, but also aids in gaining a deeper understanding of ionic interactions and the fundamental principles of upconversion dynamics (Liu et al., 2022).

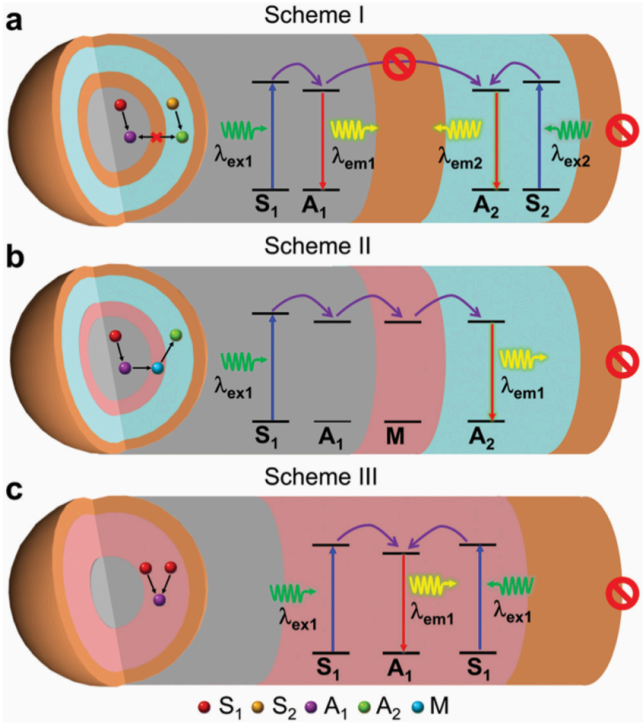

Fig 3.7: 3 Separate schemes describing the 3 distinct types of ways MLCS UCNPs can be designed. Scheme 1 a) shows two active layers separated by an inert layer, Scheme 2 b) shows an energy channel layer separating two active layers, Scheme 3 c) shows a luminescence confined layer (from Liu et al., 2022).

3.5. Nanoscale Interactions

The double-edged detrimental yet beneficial mechanisms such as energy transfer, energy migration, and cross-relaxation arise from the very prevalent ionic interactions within these UCNPs. The ionic interactions between lanthanoid ions can be extremely complex due to their random spatial distribution within the 3D matrix and the existence of many different processes owning to their rich and discrete energy levels (Zhou et al., 2020). Understanding these processes and interactions requires precise control over the position of these lanthanoid ions within the host matrix. However, whether in bulk materials or in nanomaterials, control over this factor is difficult as the lanthanoid dopants are randomly speckled within the host lattice making it difficult to identify the position of a specific ion or target a specific process (Liu et al., 2022; Lingeshwar et al., 2018). However MLCS UCNPs presents an ideal solution for achieving this control. By strategically designing nanostructures and carefully managing energy transfer pathways, as can be seen from Figure 3.8 below, it is possible for researchers to identify detailed interactions between the ions themselves.

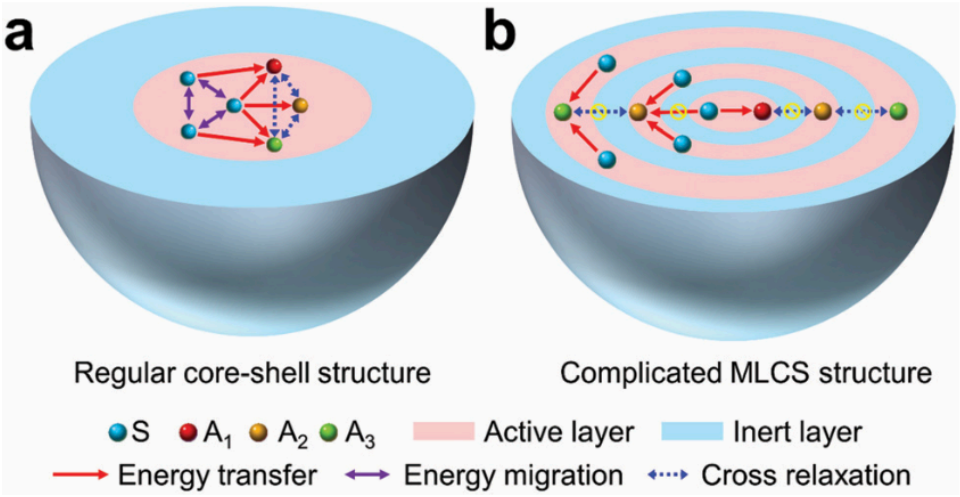

Fig 3.8: Comparison between the ionic interactions between lanthanoid ions within the UCNP between a) a classical core-shell structure, and b) a complex multi-shelled UCNP with different types of active and inert shells (from Liu et al., 2022).

In all UCNPs, it is no surprise, that the sensitiser-activator interaction is a key process when it comes to upconversion, and it depends sensitively on the distance between those ions according to the Dexter theory. This theory describes when an electron is transferred from one molecule (donor) to another (acceptor) via a non-radiative path, which means a phonon is released instead of a photon - usually this occurs at very short distances at around 1 nm or 10 Å (Wu et al., 2024). Since it is non-radiative, there is a quenching of the overall emission spectra. Utilising the technique presented with MLCS and the ability to control shell thickness via syntheses methods, researchers can look to further understand the affect of separation distance between the donor-acceptor on their corresponding intensities. This experiment can be conducted by separating active shells with inert shells, and observing the emission behaviour of the outermost luminescent shell. Experiments conducted on $NaYF_4$ MLCS UCNPs, from Figure 3.9 below, showed a two fold decrease in emission intensities when the interlayer (the layer that separates the sensitiser and activator active layers) thickness was in the range of 1.6 nm - 2.1 nm [70].

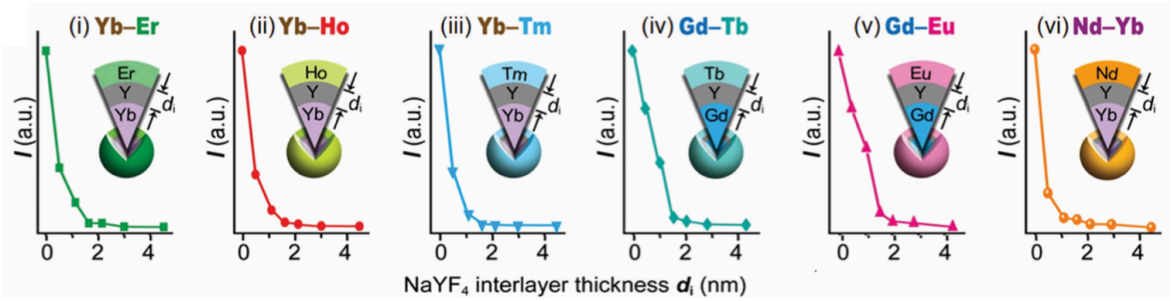

Fig 3.9: Emission intensities from the outermost layer of different $NaYF_4$ doped UCNPs as a function of the thickness of the interlayer (from Liu et al., 2022).

Energy migration is another significant and fascinating process that plays a key role in the interactions between lanthanide ions. Due to the inherent spectral overlap between the absorption and emission transitions of the same lanthanoid ion in the energy migratory state, energy migration can occur readily under appropriate conditions. One of the main benefits of energy migration is its ability to transfer energy over long distances. This phenomenon however was difficult to study since it usually occurs alongside other interactive upconversion processes, such as the various forms of energy transfer, in lanthanoid doped systems (Chen et al., 2016; Han et al., 2014). In a simple system the energy migratory ion can be activated by nearby ions rather than the excitation wavelength, making it difficult to identify the excitation sources. Therefore, energy migration, in typical lanthanoid systems such as the ones mentioned in this thesis so far, is difficult to single-out and harness. MLCS UCNPs however can aid in isolating these energy migratory systems. In detail, the energy migratory ions are doped within an intermediary shell which transfers energy between the outer shell and the inner core - usually the sensitisers and activators are separated, and the energy is transferred via this channel. Interfacial energy transfer (IET) plays a crucial role in such a system as energy is transferred between the several layers of an MLCS nanostructure (Liu et al., 2022).

Research on UCNPs such as $NaYF_4(Gd^{3+}, Tm^{3+})@NaYF_4(Tb^{3+})@NaYF_4(Eu^{3+})$ shows that the energy migration can be isolated and studied. In such a particle, the energy migratory ion, Tb^{3+} is activated by the Gd^{3+} ion in the core through IET, which is then followed by an energy transfer from the now activated Tb^{3+} to the Eu^{3+} ions in the outermost shell, leading to upconversion. Investigation has revealed that the intensities of the emission spectra of Eu^{3+} in the outer layer are highly dependant on the concentration of Tb^{3+} doping in the energy migrating layer. The intensities are weak at low Tb^{3+} doping concentration, until it reaches an optimal maximum at a 70% doping concentration. The emissions from the Tb^{3+} ion was also recorded in the emission

spectra meaning that, there was a competition of the Tb^{3+} ion's role: whether to emit radiatively (leading to its own emission) or to transfer energy to the Eu^{3+} ion. Research done on Na-based Yb-Er systems, where Yb^{3+} acted as the energy migratory ion revealed that Yb^{3+} demonstrated efficient energy migratory properties at low concentrations - most likely due to its simple electronic configuration as can be seen from Figure 1.5 (Yb^{3+} has only two energy levels: $^2F_{5/2}$ and $^2F_{7/2}$). Figure 3.10 below shows this interesting observation.

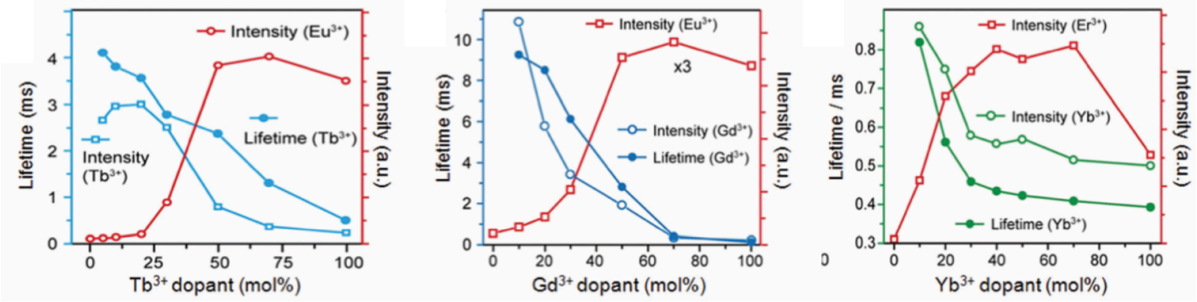

Fig 3.10: Lifetime versus Dopant concentration of 3 separate migratory ion dopants in the middle shell. The optimal Tb^{3+} and Gb^{3+} concentration in the middle shell was approximately 70% for both of them while Yb^{3+} reached a very high peak at only 40%. Also observe that the concentrations of Tb^{3+} and Gb^{3+} needed to be approximately 30% before any noticeable intensity spike was recorded, while only 10% Yb^{3+} was needed to notice a change in intensity (from Liu et al., 2022).

3.6. Energy Migrating Shell

Yb-based upconversion systems use only a single shell, which is the inert Yttrium shell to prevent surface quenching. Ting Cheng et al.'s paper described how with the use of an inert shell, the host matrix could be completely Ytterbium doped leading to higher light harvesting. However, energy migration between the sensitisers themselves is seldom understood and/or investigated. Since energy migration is strongly influenced by the size of the sensitiser sub-lattice, restricting the movement of energy-migrating ions to a confined area should effectively reduce energy migration between sensitisers, thereby improving upconversion emission intensities. Recently a paper investigated this effect by sandwiching a $NaYbF_4(Er^{3+})$ between two $NaYF_4$ shells, essentially reducing the total area covered by the Ytterbium host. This lead to an overall increase in upconversion emission intensity in the green region (Zhou et al., 2020).

In 2020, a paper published by Bin Zhou et al. reported on the creation of a multi-shelled Na-based Yb-Er UCNP which's emission intensities were increased 100-fold from the classical green-emitting UCNPs used in literature. They managed to suppress the cross-relaxation by separating the location of the activator and sensitiser ions - the activating Er^{3+} ions were doped within the core, and the sensitising Yb^{3+} ions were doped in the middle shell. Thus, the particle they proposed which could achieve this great jump in intensity was:

$NaYF_4(Er^{3+})@NaYbF_4@NaYF_4$ - by utilising a middle shell, they shortened the distance between the two ion types and rely on efficient IET to enhance the upconversion spectra.

Classical $NaYF_4(20\%Yb^{3+}, 2\%Er^{3+})@NaYF_4$ generate intense green emissions, $^2H_{11/2}$, $^4S_{3/2} \rightarrow {}^4I_{15/2}$, relatively strong red emissions, $^4F_{9/2} \rightarrow {}^4I_{15/2}$, and weak violet emissions, $^2H_{9/2} \rightarrow {}^4I_{15/2}$, under 980 nm excitation, as can be seen from Figure 2.4. Once the aforementioned MLCS UCNP was developed, with a 10% doping of Er^{3+} in the core, an immediate 100-fold increase in intensity was observed especially in the violet region at ~ 407 nm as can be seen from Figure 3.11, below. Another stark increase can also be seen in the red region, while the green emissions, although more intense, did not become as intense as the other peaks. The green emission only increased by 5-fold. This interesting discovery may indicate population saturation in the $^2H_{11/2}$, $^4S_{3/2}$ stark levels, unlike the levels responsible for emitting red and violet light. Furthermore, the other types of core-shell-shell and core-shell structures which are also indicated on the Figure, which were developed an investigated did not have intensities as intense as the one present in the reigning structure, despite their particle size and shell sizes being nearly the same. This means that a more efficient energy transfer upconversion occurs in this core-shell-shell structure as compared to the others, indicating the importance of energy migration and IET energy transfer in the upconversion process.

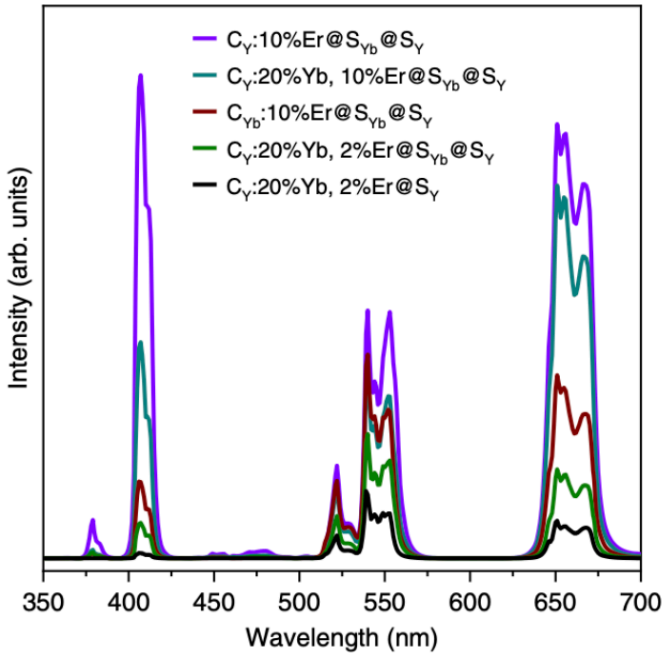

Fig 3.11: Upconversion emission spectra of different core-shell-shell Na-based Yb-Er particles. C_Y, C_{Yb}, S_{Yb}, S_Y are used to designate $NaYF_4$ core, $NaYbF_4$ core, $NaYbF_4$, and $NaYF_4$ shell respectively (from Zhou et al., 2020).

The paper also highlighted that the excitation energy enhancement is observed not only with a fully doped Yb^{3+} middle shell but also with an increase in the thickness of this sensitising shell. It was found that as the middle shell thickness (d_{SYb}) was progressively increased, the emission spectra of the particle also improved until an optimal thickness of 8.3 nm, beyond which the spectra were quenched. This trend was similar to that seen in the normal particle shown in Figure 3.11, where the shell thickness had a greater effect on enhancing the violet and red emissions compared to the green emission. Similarly, when the inert outer shell thickness (d_{SY}) reached around 2 nm, the emission intensity seemed to stabilise, with minimal impact on the overall spectral intensity. This is likely because a 2 nm thick shell is sufficient to protect the Yb^{3+} ions from solvent quenching, with any residual quenching possibly resulting from surface defects within the UCNP's internal structure.

Power dependence experiments conducted on the $C_{Y:}10\%Er@S_{Yb}@S_{Y}$ particles revealed that the 407-nm emission peak is formed by a 3-photon upconversion process while the 540-nm peak is 2-photon dependent. 2-photon emissions are often more efficient at lower excitation power densities, and since the power density of the laser used for the irradiation of these UCNP experiments was relatively high, the Er^{3+} green emitting levels were most likely saturated (Dong et al., 2017). On average, when the d_{SYb} was increased from 1.3 nm - 8.3 nm, there was a 22-fold increase in the number Yb^{3+} ions, with a corresponding 20-fold increase in the Er^{3+} ions. This finding indicates that the green-emitting intensities increase linearly with the increment of the Yb^{3+} ions. Even still, the overall intensities of the violet and red emissions increase by 440 and 180 times, significantly out performing the meagre increase in intensity of the green emission. This is indicative of the fact that the population of the $^4F_{9/2}$ and $^2H_{9/2}$ levels may be the result of triphotonic transitions (Figure 3.12, below). This would coincide with the hypothesis that at higher laser powers, the red and violet emissions will dominate over the green emission. However, this is only true up to a certain middle shell thickness: 8.3 nm, after which the peak intensities reach a maximum after which, any thicker shell leads to intensity decays of the red and green emissions, and a saturation of the violet peak. This phenomenon implies that the population of the $^4F_{9/2}$ state, the state responsible for red emission, may be hindered once a thicker fully-Yb doped middle shell is applied.

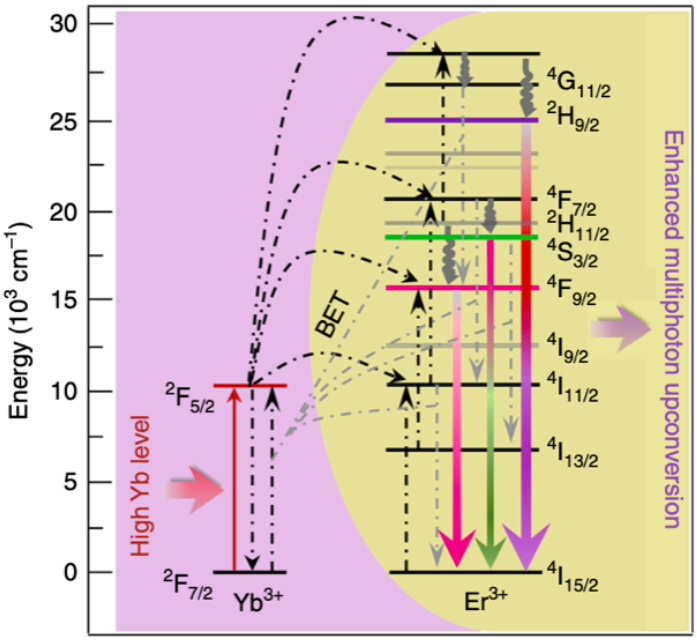

Fig 3.12: Simplified energy level diagram showing multiphoton upconversion from Yb^{3+} to Er^{3+} (from Zhou et al., 2020).

In order to fully understand the energy transfer which is occurring between the sensitiser, Yb^{3+}, and the activator, Er^{3+}, in these core-shell-shell particles, lifetime experiments were conducted. In separating the two ions from each other, the energy transfer from the Yb^{3+} to the Er^{3+} was obviously slowed, and thus the decay time for the $^2F_{5/2}$ state of the Yb^{3+} was increased, meaning it remained in it excited state longer. As a consequence, the rise and decay times for the Er^{3+} emissions are also prolonged since Er^{3+} received energy from the Yb^{3+} ions from the middle shell closest to the core, while within the migratory layer Yb^{3+} transferred energies between other Yb^{3+} ions. Furthermore, as more sensitisers are added, ie by increasing d_{SYb} up to 8.3 nm, all the rise and decay times for the red, green, and violet emissions also increase. This was proof that there is an energy migration happening within the middle shell in that the outermost Yb^{3+} ions absorb most of the incident excitation wavelength, and then transfer the energy along the width of the shell from one sensitiser to another until it reaches the core-shell interface.

This raises the question whether something like this can be conducted in other types of UCNPs. NaF_4-based particles are difficult to synthesis, and their sizes are difficult to manipulate since FN synthesis is only applicable for LiF_4-based. Furthermore, while Erbium UCNPs emit in the violet and green regions, Thulium UCNPs can emit in the UV and blue regions which are more energetic in nature. Thus a core-shell-shell particle was proposed to determine whether using IET and energy migration can be utilised to increase the the intensities of the upconversion emission spectra of LiF_4-based UCNPs.

The core would act as the light emitting section, and would comprise of the particles mentioned in Ting Cheng et al.'s paper: $LiYbF_4(0.5\%Tm^{3+})$. The middle shell would be the migratory layer: $LiYF_4(20\%Yb^{3+})$. The outer shell, was determined to be completely light absorbing in order to harvest as much incident excitation energy as possible: $LiYbF_4$.

The final particle proposed was thus: $LiYbF_4(0.5\%Tm^{3+})@LiYF_4(20\%Yb^{3+})@LiYbF_4$.

3.7. Methodology and Procedure

In order to create double shelled particles, four distinct synthesis steps are required - in order, they are: FN core synthesis, stabilisation, first shell synthesis, second shell synthesis. Each of these steps were modified to suit the need of the particles being made after several trial and error syntheses using the basic theory described in the paper published by Ting Cheng et al.. Furthermore, it is important to note that since absolute intensities would be compared, all the final particles made needed to adhere to two following restrictions: they all need to be of similar sizes, and the thickness of the each shell need to be the same across all particles. As can be seen from earlier, shell thickness can change the upconversion emission intensities, and therefore it is imperative that each synthesis step is executed as perfectly as possible to avoid any possible room for errors. The only particle which would be smaller than the rest is the control particle: $LiYbF_4$ (0.5% Tm^{3+}) since this particle is a single shelled particle as compared to the other particles mentioned. All precursors were derived from lanthanoid oxides, and the synthesis technique used for the core and shelling synthesis was hot injection synthesis, and one pot synthesis was used for the stabilisation.

Precursor preparation:

In a 50 mL 3-nozzle flask lanthanoid oxides of different masses depending on doping concentration were weighed and added. For calculations of each particle made and their corresponding precursor mass please look below. 5mL of distilled (DI) water and 5 mL of Trifluoroacetic Acid (TFAA) was added into the 3-nozzle flask with the lanthanoid oxides and then reacted at 80^0C overnight under constant stirring. This was achieved by submerging the 3-nozzle flask into an oil bath with a clamp holding it in place around it's middle neck. The two side necks of the 3-nozzle flask were capped, and a reflux tube was inserted into the middle neck with cold water running through the reflux system. This ensures that all vaporising liquids condense back into the flask.

After a full night of reacting, the solution will turn colourless (if it hasn't yet, it means that the reaction is not complete and requires a few more hours of reaction. This can happen if the stir bar wasn't stirring fast enough or if the temperature was too low). If the solution is colourless, the

precursors need to be dried: All caps and the reflux tube were removed, the stir bar was stopped, the water running through the reflux system was stopped, and the temperature was lowered to 70^0C. The drying procedure also takes the duration of an entire night, which means the precursors would be ready the day after they are set for drying.

The masses of the amount of each lanthanoid oxide needed for each section of the particle (ie, core or shell) was calculated stoichiometrically using the formula I created below:

For any particle $LiRE^1F_4(X\%\ RE^2,\ Y\%\ RE^3)$, where RE stands for "Rare Earth" - the oxide from which they are derived, for every *Z mmol* prepared the masses of the RE oxides are as follows:

$$RE^1{}_2O_3 = (Z/2)[(100\text{-}X\text{-}Y)/100](\text{Molar Mass of } RE^1{}_2O_3)$$
$$RE^2{}_2O_3 = (Z/2)(X/100)(\text{Molar Mass of } RE^2{}_2O_3)$$
$$RE^3{}_2O_3 = (Z/2)(Y/100)(\text{Molar mass } RE^3{}_2O_3)$$

Once dried, the precursors turn from a colourless liquid to a white powder - to know if they have fully dried, one must smell them: if they smell like vinegar (which is the scent of TFAA) then they still have not yet dried even if they look like a white powder. In this case, turn the temperature back up to 80^0C and keep checking every 30 mins to see if they have dried. Once fully dried, the precursors are ready for use in synthesis.

Core Synthesis:

The core for all the particles of interest was the same, it was the $LiYbF_4$ (0.5% Tm^{3+}) core which was used and tested by Ting Cheng et al., and it was also prepared by FN synthesis.

Before the experiment started, a syringe, piston, straight needle, and a curved needle were placed into a drying oven and the temperature was set to any point between 120^0C and 130^0C.

In a clean 100 mL 3-nozzle flask sealed on the two side necks by two septa, 7 mL of OA and 7 mL of OM were added as well as 14 mL of ODE. Here the OM and OA volumes are exactly the same leading to the creation of the smallest possible Li-based UCNPs of around 5 nm. The OM+OA volume must equal the volume of the ODE added. This solution was then degassed at 110^0C for 30 mins. This was done by clamping the flask on top of a heating mantle and attaching a vacuuming system to the middle neck of the flask. This part is imperative as it gets rid of any residual moisture (water) in the solution, as water can hinder the nucleation of the nanoparticles and cause issues in the synthesis later on. Furthermore, oxygen can oxidise the two oils (OA and OM) used and thus make them futile for synthesis. A good indicator that the solution remains unaffected by water or oxygen is it's colour: Initially, the solution may be colourless to a

light yellow in colour as these are the natural colours of the aforementioned surfactants and solvents. As the reaction progresses the yellow colour may darken to a honey-like yellowish-orange. Up to this point, the solution remains fine, however should it darken even further a become brown or black, it means that oxygen has infiltrated the system and has caused severe oxidisation of the solution and it is likely that the particles are no longer viable.

While the solution, now referred to as the 'reaction' solution (React Sol'n) was degassing, the second solution containing the precursors needed to be prepared. After drying, the dried precursors in the 50 mL 3-nozzle flask contained only the lanthanoid fluorides due to the TFAA added to the oxides. 299.9 (rounded up to 300) mg of Lithium Trifluoroacetate already in its solid powder form (purchased from a vendor) was weighed and added into this dry solution flask, together forming all the precursors necessary to make the FN UCNPs. The mass of the Lithium Trifluoroacetate was calculated depending on how much in mmol of core solution was being prepared, in most cases this is 2.5 mmol. Thus, similarly to how the masses of the lanthanoid oxides were calculated, the mass of the Lithium Trifluoroacetate was simply: 2.5 mmol x 119.96 mg (molar mass of Lithium Trifluoroacetate). Now, into this dry solution, 3 mL of OA and 6 mL of ODE was added for a total of 9 mL of liquid solution. This flask, will be referred to as the 'precursor' solution (Prec Sol'n).

Once the React Sol'n was close to finishing its degassing, the Prec Sol'n was hoisted up onto a clamp and submerged into an oil bath, adjacent to the React Sol'n, which was preheated to 65^0C. Caps were placed into the two side necks of the 3-nozzle flask. A needle pumping Argon gas was injected into the React Sol'n through one of the septa while the middle nozzle was replaced from the vacuuming system with to a back flow distillation tube which lead into a silicone oil bath. The point of this back flow tube was to release the pressure of the argon being pumped into the flask, into the silicone oil bath by the visual form of bubbles. The rate of formation of bubbles would give information about the rate at which the argon is being pumped in. Ideally, one would like to see one bubble per second. If the Argon pumping rate is too high, the solution of OA/OM/ODE may evaporate and be lost into a receptacle flask which was attached to the distillation tube. The vacuuming system was then placed into the middle nozzle of the Prec Sol'n flask and the Prec Sol'n was then degassed for 30 mins at 125^0C. In the meantime, the temperature of the React Sol'n was increased from 110^0C to 330^0C.

Mid-way through the degassing of the Prec Sol'n at around 10-15 mins, the degassing was stopped momentarily, and one of the caps was removed and 3 mL of OM was poured in. The cap was then placed back in, and the degassing was recommenced. This entire section of the experiment must be done as quickly as possible to avoid as little contaminants and/or moisture

getting into the solution. This is also a very important step: Initially only OA and ODE were added into the flask, but an equal volume of OM to the OA was missing - this is because the precursors as they exist take a very long time to dissolve in OM. For this reason it is imperative that the dried powdered precursors first dissolve in the OA and ODE before the OM is added into the solution. The total volume of this solution would now become 12 mL. Together with the React Sol'n which's volume was 28 mL, the expected volume of the total Sol'n would be 40 mL.

After the remaining time left for the degassing of the Prec Sol'n was done, it was time to transfer the Prec Sol'n into the React Sol'n via injection hence the name hot injection synthesis. The Prec Sol'n was extracted via the hot syringe, piston, and straight needle and then placed onto a pump. The straight needle was then replaced by the curve needle which sat in the oil bath of 125^0C. The pump was set to injection the solution at a rate of 1.5 mL/min, which was the rate used to create the 5 nm particles. In theory, increasing the pumping rate creates larger particles, and lowering it creates smaller particles. After the injection was completed and all of the Prec Sol'n was now in the React Sol'n, the solution was left to react for 1 hour at 330^0C. After the solution finished reacting, it was left to cool until the internal temperature of the solution was between 80 - 90^0C at which point it was transferred into a centrifuge tube was storing. During the cooling process it is natural for the solution to darken: a pale yellow to a honey colour is what one is looking for as a preliminary test to see if the UCNPs cores might be good for use.

This concludes the steps of FN synthesis - the key part of this type of hot injection as compared to a classical hot injection synthesis is the addition of OM with a volume equal to that of OA, which was of course mentioned

Stabilisation Synthesis:

After the FN synthesis is complete, stabilisation needed to occur in order to make the cores malleable for the shelling syntheses which follow. If the stabilisation was not done immediately after the core synthesis the solution of OA/OM/ODE in which the particles are suspended would solidify overnight and turn into a wax-like substance. If that occurred, the centrifuge tube was held under hot water until the entire solid transforms back into a liquid, at which point sonicating and vortexing was required to re-disperse the UCNPs equally in the solution.

Only half the entire solution could be stabilised at a time, which means that knowing the volume of the solution was important. This means that of the 2.5 mmol of UCNP cores created, only 1.25 mmol would become stabilised. After half the solution was extracted and poured into a 100 mL 3-nozzle flask with septa on the two side nozzles, equal amounts of OA and ODE were poured to reach a volume of 50 mL. So essentially:

Volume of OA and ODE = $(50 - X)/2$ where X is half the volume of the liquid obtained at the end of the core synthesis

Due to some evaporation which may have occurred during the reaction of the FN core synthesis, especially since ODE's boiling point is 315^{0}C, the final volume of the liquid was not always exactly 40 mL, but could vary between 34 - 37 mL.

Once the ODE and OA have been added, the solution was first degassed for 30 mins at 110^{0}C. During this process, it is vital that the degassing be observed for the first 5 - 10 mins. Due to residual water and moisture, there was a lot of effervescence. These bubbles can rise past the neck of the 3-nozzle flask and back flow into the receptacle flask - if this happens a lot of the liquid and subsequently UCNPs will be lost. If the bubbles started to near neck of the flask, the stir-bar was stopped until the bubbles diminished. After degassing, Argon was pumped in via a needle, like during the core synthesis, and the solution was left to react at 315^{0}C for 1 hour. Once the reaction was done, it was cooled to 80 - 90^{0}C and then transferred over into a centrifuge tube for storage. It's volume once again was not exactly 50 mL, and tended to be between 45 - 48 mL.

Shelling Synthesis:

Shelling synthesis requires the creation of shelling precursors first. These are made in the same way as the core precursors were made.

The overall procedure for shelling synthesis closely resembles that of core synthesis, as both are variations of hot injection synthesis. However, unlike the shelling method described in the paper by Ting Cheng et al., a different approach was developed and followed for all the shelling syntheses in this thesis. This alternative method proved to be more efficient, requiring less time and effort, while yielding results comparable to those in the aforementioned paper. Specifically, the core to shell precursor ratio, in mmol, was set at 0.5:2. The React flask contained the cores, while the Prec flask held the shelling precursors, which were later injected into the cores at a rate of 0.75 mL/min. The cores were extracted from the stabilised solution, and the extracted volume of cores needed to be:

$(0.5/1.25)(Y)$ where Y is the volume of the stabilised core solution

in most cases, the volume of cores to be extracted would be approximately 18 to 20 mL. If the extracted volume falls within this range, the solution volume can be rounded up to 20 mL. However, if the volume is less than 18 mL, OA and ODE should be added in equal amounts to reach a total volume of 20 mL. Unlike the cores, which are often prepared to create one batch of

UCNPs, the shelling precursors were always prepared in batches of 4 mmol. This would mean that a singular batch of shelling precursors could be used for two separate shelling syntheses. Once the shelling precursors had dried, 479.84 mg (rounded to 480 mg) of Lithium Trifluoroacetate was added and dissolved in 10 mL of OA and 10 mL of ODE under vacuum at 125^0C for 30 mins. This would act as our shelling precursor, and for each shelling to follow, 10 mL (half of the solution and thus only 2 mmol of precursors) would be extracted and injected into the cores at an injection rate of 0.75 mL/min. Unlike the FN synthesis in which the reaction temperature was 330^0C, the reaction temperature for all the shelling syntheses were 315^0C.

For double shelled particles after the first batch of shelling, that new solution contains 0.5 mmol of particles, since it was initially 0.5 mmol of cores which were shelled with 2 mmol of shelling precursors. This means that the total volume of liquid obtained after the first shell is around 30 mL, while the total volume of liquid obtained after the second shell is 40 mL, since 10 mL more of shelling precursors is added.

Post-synthesis modifications:

After all the syntheses are complete, the particles need to be washed before they can be used for any sort of characterisation. The washing step is crucial as it allows for the UCNPs to be dispersed in a more stable liquid, which in this case was hexane.

In order to wash the UCNPs, they are centrifuged at 7500 rpm for 10 mins with different organic solvents. The amount of UCNPs to be washed is completely up to the researcher as long as the key ratio between the hexane:ethanol is maintained at 1:3.

For TEM samples, which do not require large amounts of particles, a few drops of UCNP solution can be poured into an eppendorf tube after synthesis - ethanol is added to the 1.5 mL mark, and the tube is then centrifuged for 2 mins. After centrifuging, the supernatant is disposed off, and usually a small white pellet can be seen along the bottom side of the eppendorf tube. These are the particles. If it is not visible, that is also okay. A few drops of hexane is then added, and the tube is then sonicated for 10 seconds to re-disperse the particles in the hexane. Ethanol is added back up to the 1.5 mL mark, before the tube is centrifuged again for 2 mins. This process is repeated a total of three times after which 1 mL of hexane in which the UCNPs are dispersed.

For most spectral measurements, 5 mL of UCNPs were extracted from the OA/ODE solution in which were synthesised - the solution was first dispersed, by sonicating and vortexing, to ensure that the particles were dissipated equally within the liquid before extraction. This is an important step as will be explained later. Then, ethanol was added to the 15 mL mark (10 mL ethanol), and

the solution was centrifuged with the aforementioned the parameters. The supernatant was then disposed off, after which 5 mL of hexane was added into the tube and then sonicated. Vortexing the solution may also aid in re-dispersing the nanoparticles which often appear as visible a white pellet along the bottom side of the tube. Proper re-dispersion is key - the white pellet should disappear, and the hexane should turn from colourless to cloudy. At this point, 15 mL of ethanol was added, so the total volume of liquid in the tube was 20 mL. It was then centrifuged, and these steps were repeated thrice before 10 mL of hexane was added, constituting the last step.

If all the aforementioned steps are followed correctly from the start of the first core synthesis to the washing, the concentration of the 10 mL hexane solution should be between 10 - 13 mg/mL. In essence, approximately 10 mg of UCNPs are dispersed within 10 mL of hexane solution, which if it were used dried, would correspond to 100 mg of UCNPs. The concentration of the solutions prepared are extremely important since the point of this thesis is to increase the intensities of the emission spectra. If the concentration of a solution is too high then it would result in more intense spectra since there are more particles upconverting - therefore, in order to have a controlled experiment the concentrations of all the spectral vials have to be the same.
In order to measure the concentration of each solution, the weight of an empty eppendorf tube is measured. Then 1 mL of the 10 mL hexane solution in which the UCNPs are dispersed is extracted using a pipette and poured into the eppendorf tube. The solution is left to dry with the cap of the tube open - this usually takes one whole day. The eppendorf tube's weight is measured again and the difference in weight of the two tubes is the amount of UCNPs in mg that was extracted in 1 mL of that solution.

3.8. TEM Results of First Iteration of Double Shelled Particles

As is customary, TEM analysis is required after each synthesis step to quickly assess the quality of the UCNPs produced. As previously mentioned, visual inspection alone cannot reliably determine if the nanoparticles are suitable for use. TEM results provide valuable information on whether the nanoparticles are mono-disperse and if their sizes are uniform, which is crucial for ensuring a controlled experiment. As explained earlier, the size of the UCNPs significantly impacts upconversion emission efficiencies - larger UCNP cores cause the Yb and Tm ions to be farther apart, increasing the distance energy must travel from the sensitiser to the activator before upconversion occurs. Conversely, UCNPs that are too small can also reduce upconversion emission intensity

The goal for the size of the cores of the double shelled UCNPs after stabilisation was no larger than 15 nm. Utilising FN synthesis allows for this control, since the FN cores are significant small, reaching only 5 nm in size, and the subsequent stabilisation allows them to grow to sizes

between 9-13 nm according to the paper published by Ting Cheng et al. The extra 2 nm is a buffer size the UCNPs can reach after stabilisation which has been observed through other projects conducted during the duration of this thesis.

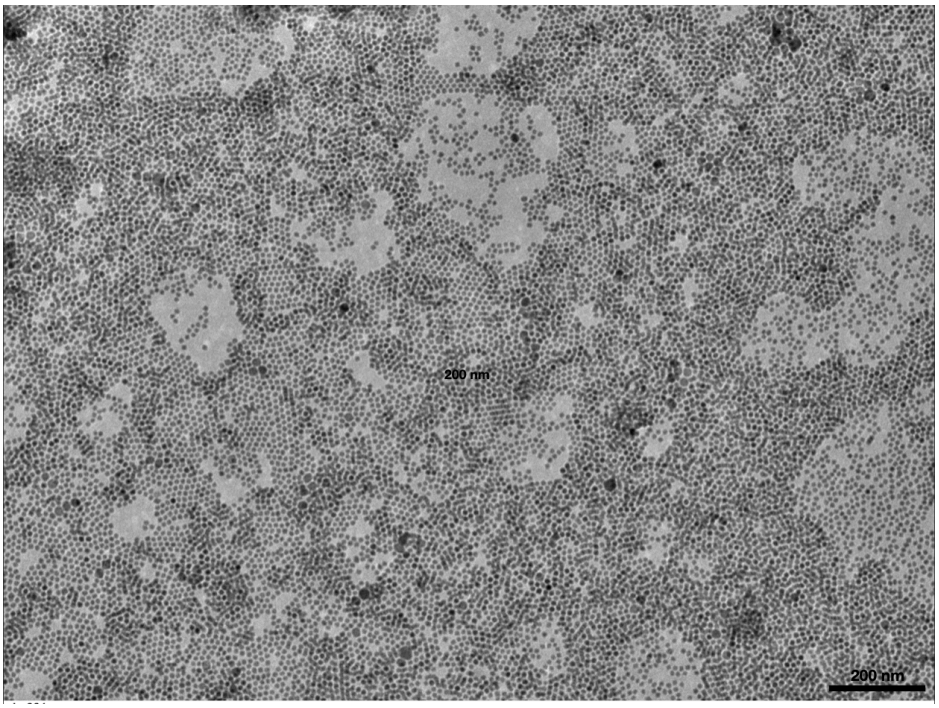

Fig 3.13: TEM image of $LiYbF_4(0.5\%Tm^{3+})$ Stabilised Core. The scale bar is 200 nm.

Figure 3.13 above is the TEM image of the stabilised $LiYbF_4(0.5\%Tm^{3+})$ cores. The first observation which can be made is its mosaic nature in that the particles are all of similar sizes, and mono disperse. Another thing to note is that they are not agglomerating together, which is also another key consideration. If the particles clump together, there is a higher chance that the intensities may get quenched. Clumping in TEM photos may not necessarily be because of particle agglomeration, but can be caused by creating a TEM grid which is too concentration (ie, dipping the grid into a solution which is very concentrated). Figure 3.14 below is a size distribution curve of the cores. The mean size of these stabilised nanoparticles is 9.98 nm, which is well within the expected range of sizes. As these are unshelled, raw cores, their spectral data was not recorded since they would essentially be non-upconverting due to serious quenching effects at their surface. Save for a few abnormal large particles, which can be seen as black ‘dots’ in the TEM picture above, the sizes of majority of them did not exceed more than 12 nm as can be seen from the histogram below.

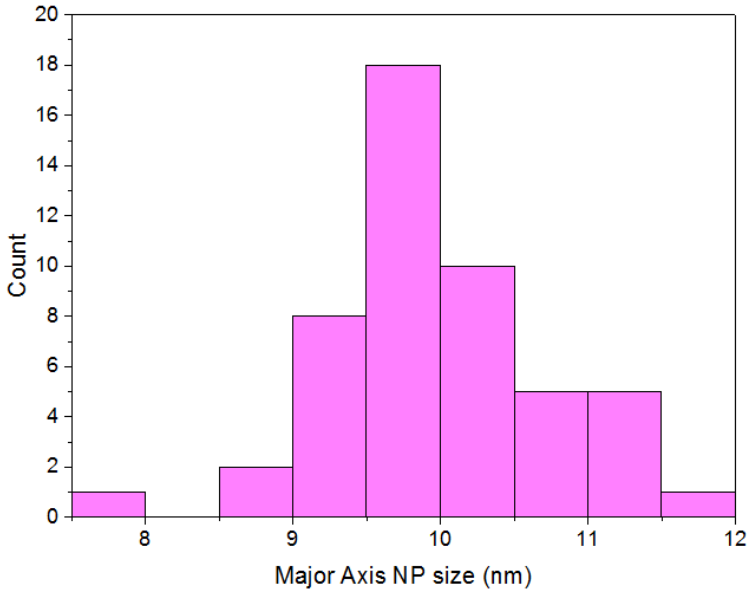

Fig 3.14: Size distribution histogram of stabilised cores.

The cores were then coated with the first $LiYF_4(20\%Yb^{3+})$ shell at an adjusted injection rate of 1.5 mL/min, which is double the typical injection rate of 0.75 mL/min used to create the standard particles. The higher injection rate was intended to produce a thinner shell. According to Bin Zhou et Al., if the shell becomes too thick, it leads to quenching of the intensities, while shells that are too thin fail to address concentration quenching. Previous experiments indicated that an injection rate of 1.5 mL/min results in shells thicknesses of approximately 3 nm. The TEM images and particle size distribution of these newly shelled particles are shown in Figure 3.15 below, with the same 200 nm scale bar as in Figure 3.13. It's clear that the particles are noticeably larger. From the histogram, the particle size increased from an average of 9.98 nm to 17.80 nm, with a larger standard deviation, which is outcome typical of shelling. The shell thickness was roughly 4 nm, just 1 nm thicker than expected, which falls within the experimental parameters. The particles also remained mono-disperse and were of similar sizes.

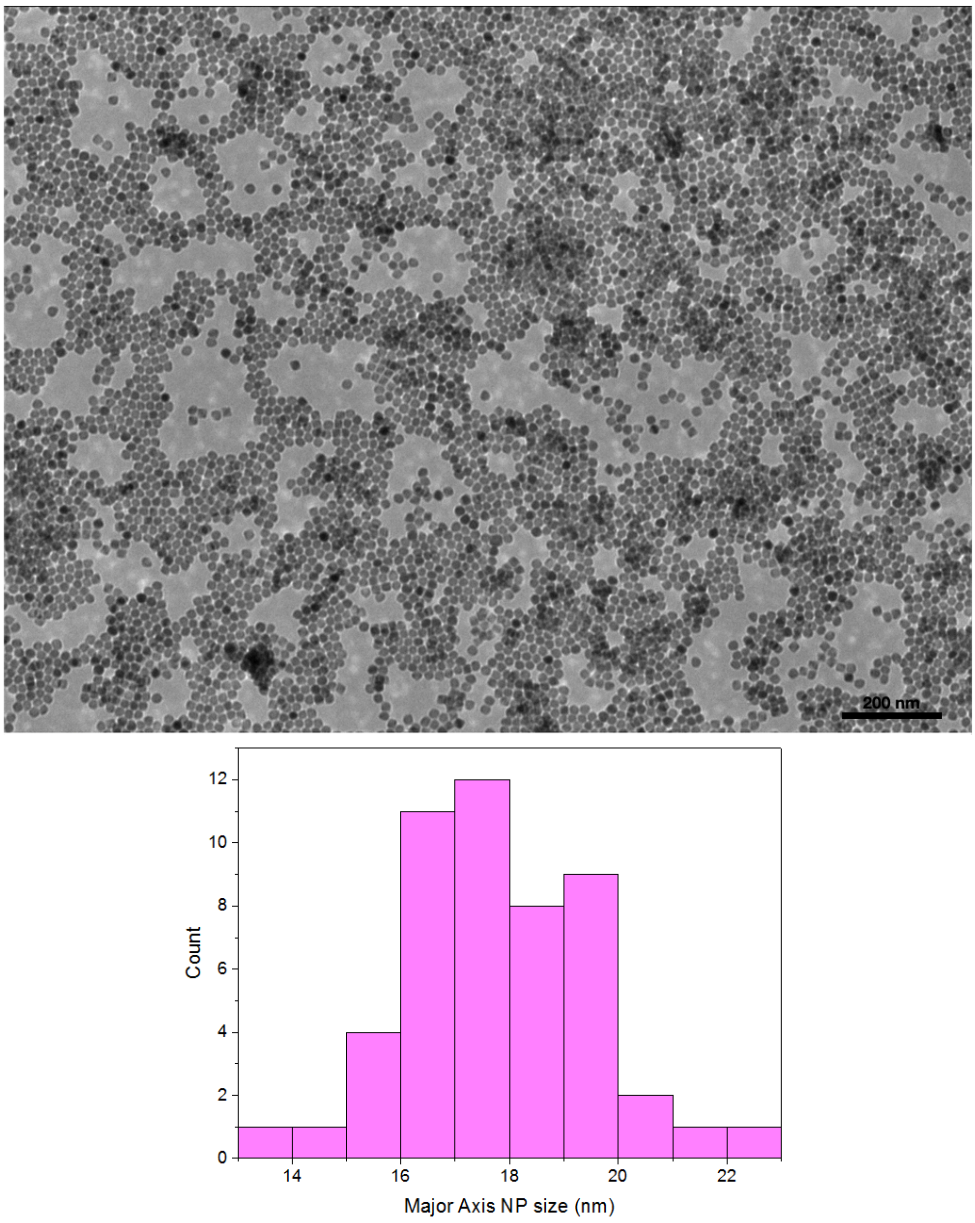

Fig 3.15: TEM images and size distribution histogram of $LiYbF_4(0.5\%Tm^{3+})@LiYF_4(20\%Yb^{3+})$. The scale bar is 200 nm.

After confirming successful shelling of the cores, the entire solution of these newly shelled particles were once again subjected to a shelling synthesis with an injection rate of 1.5 mL/min. They were shelled with $LiYbF_4$, which was meant to be the light absorbing shell since it is fully doped with sensitiser ions. 3 separate iterations of this particle were made to obtain a proof of concept - all 3 fully double shelled particles can be seen in the TEM images in Figure 3.16 below.

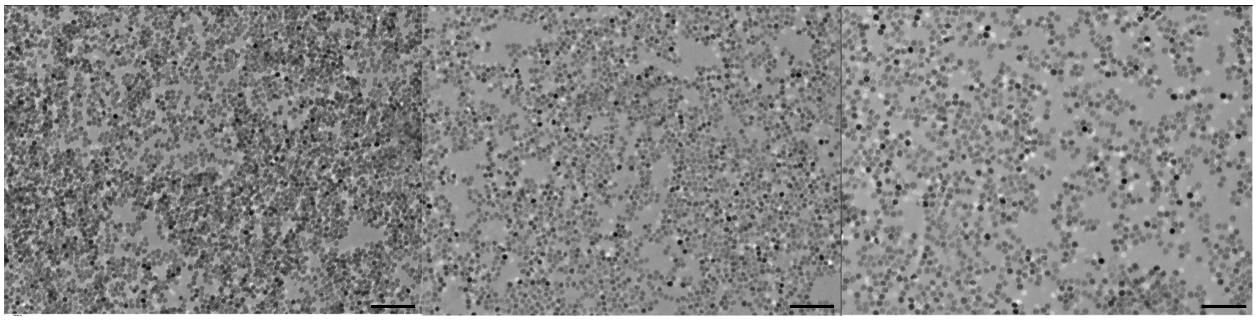

Fig 3.16: TEM images of $LiYbF_4(0.5\%Tm^{3+})@LiYF_4(20\%Yb^{3+})@LiYbF_4$.
From left to right: Iteration 1, Iteration 2, Iteration 3. The scale bar is 200 nm.

The average sizes of these particles from left to right were 25.30, 24.99, 24.75 nm respectively. Meaning that they grew from 17.80 nm to approximately 25 nm. The average shell thickness of the outermost shell was then approximately 3.60 nm, which coincides with the previous shell thickness of the middle shell. Thus the total particle size was 25 nm which is well within the experimental parameter range for applications in the biomedical field. Cellular matter in the human body tends to be in the micrometer range (Hatton et al., 2023), meaning that particles as small as these have improved cellular intake (Zhang et al., 2022; Mitchell et al., 2020). Particles which exceed 100 nm, which would be the case if other syntheses methods which have limited control over the size of the particles were employed, are less likely to be taken into cells due to their largeness in size. Hot injection excels at being able to control and manipulate particle size through the pump injection rate. In fact, nanoparticles up to 50 nm in size are still within range of both the EPR effect as mentioned previously and the cellular uptake effect, which means that even with this double shelled particle, there is still room for the growth of several more shells.

The TEM images also reveal the fact that the particles are mono disperse. In general, if the cores look good, then the shells will also most likely be good as well if the synthesis procedure is followed through correctly and with precision. The size distribution histograms in Figure 3.17 below reveal that there is a wide spread between the sizes of the particles, but they are all still of similar enough sizes and within a small deviation of each other, not being greater than 2.01, 2.41, and 2.02 nm for the first, second, and third iterations respectively. The largest particles recorded were 29.50, 31.35, and 27.99 nm, which are also all of similar sizes meaning that the maximum particle size when following the synthesis steps described before was approximately 30 nm. These particles would have a shell of thickness 6.10 nm. An outer shell thickness does not technically affect the intensity of the UCNPs since it acts as a shield against external quenchers, however as was observed from the previous papers, after a certain shell thickness, the intensities would plateau, meaning that the outer shell has obtained a thickness which is

enough to prevent any energy losses at the surface. A shell thickness of 6.10 nm is within range of this effect, and thus should not adversely affect the experimental results.

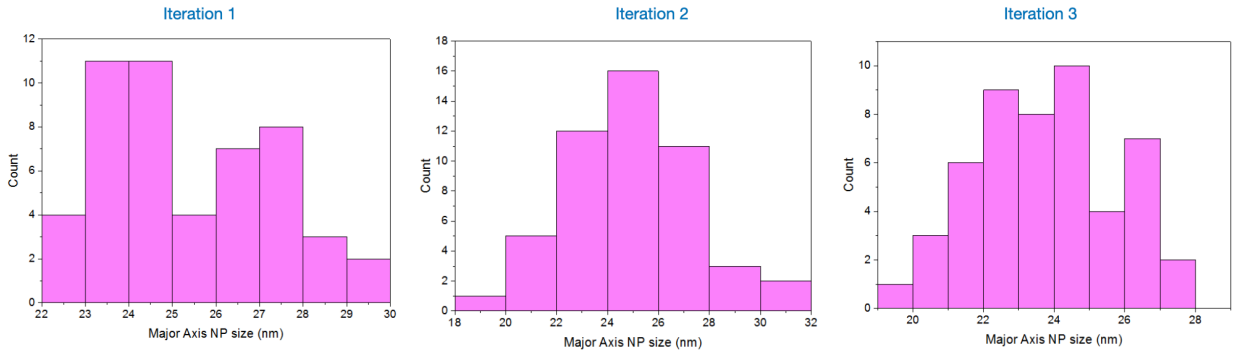

Fig 3.17: Size distribution histograms of the TEM samples in Figure 3.16. From left to right: Iteration 1, Iteration 2, and Iteration 3.

From the size distribution histograms it is clear that Iteration 2 had the best dispersion of particles with a clear average, however it also had the largest range of particle sizes, from 18 nm to 32 nm. This is representative of the fact that regardless of how carefully the syntheses steps are followed through, creating UCNPs is still a tricky and capricious task. Since these particles form in the nanoscale, impurities at the nanoscale can cause issues in the nucleation of these particles. Thus, proper and vigorous cleaning of the apparatus used in the synthesis of these particles is vital to their disparity and size consistency. Regardless, from the TEM images in Figure 3.16 as well as the acceptable range of values in Figure 3.17, all iterations were valid for spectral measurements.

The final step before spectral data collection was the creation of the classical shelled particle, which is essentially $LiYbF_4(0.5\%Tm^{3+})@LiYF_4$. This is a regular shelled particle where all the upconversion mechanisms and energy transfers occur within the core itself. The outer shell serves as an inert boundary, so the typical shelling procedure was followed, which involved an injection rate of 0.75 mL/min. This resulted in the formation of classical UCNPs with a mean size of 22.53 nm. The stabilised cores from which they were derived were slightly larger than the ones used to create double-shelled particles - they had a size of 12.63 nm. Consequently, the shell thickness was 4.95 nm, which is larger than the shells produced when the injection rate was doubled. Figure 3.18 below depicts the stabilised core and the shell of these classical, control particles.

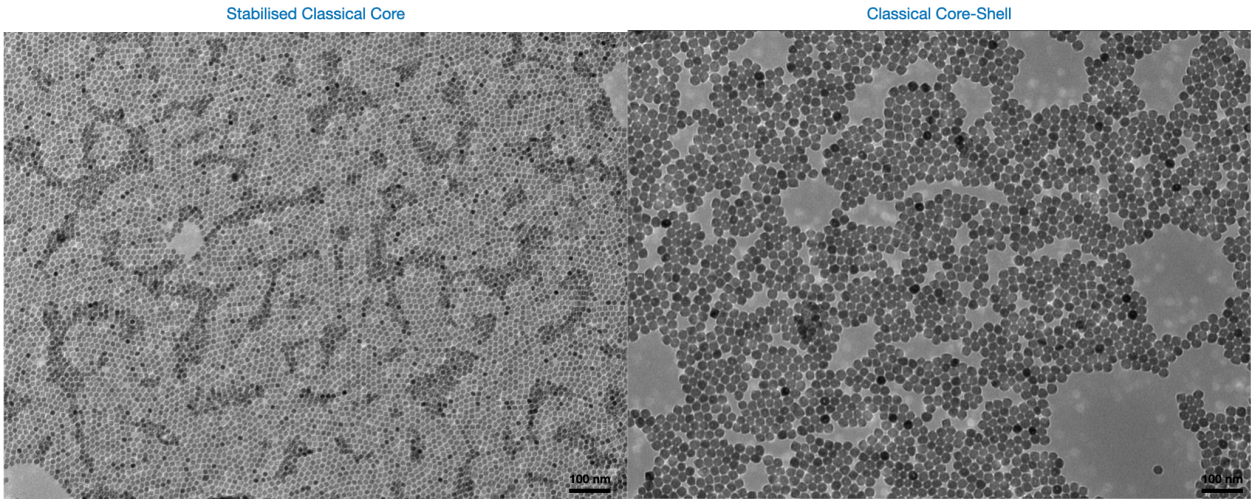

Fig 3.18: Stabilised $LiYbF_4$(0.5%Tm^{3+}) cores and Shelled $LiYbF_4$(0.5%Tm^{3+})@$LiYF_4$. The scale bar is 100 nm.

The histogram below, Figure 3.19, for the classical particles, also illustrate the mono disparity of the shells produced. The primary objective of the TEM analysis is to ensure that all the particles synthesised were of similar sizes, as size disparities can influence the emission intensities. It can observed that all the particles were of the same size, and the shell thicknesses were maintained at a consistent and steady value. Table 3.1 below provides a summary of the average sizes of all the particles, and the shells.

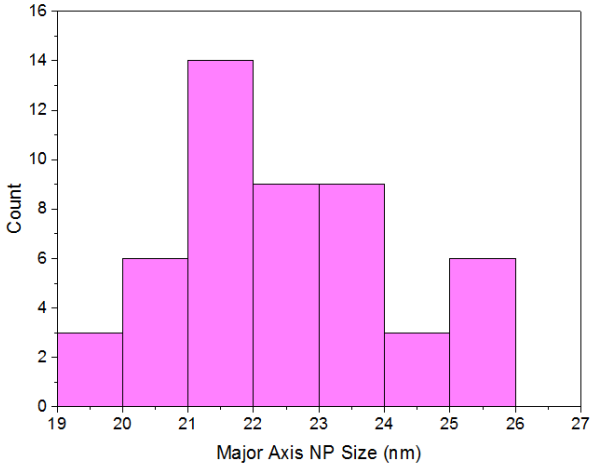

Fig 3.19: Size distribution histogram of $LiYbF_4$(0.5%Tm^{3+})@$LiYF_4$.

Table 3.1: Catalogue of all UCNPs synthesised with details as to shell thicknesses and total UCNP size. The Thicknesses and Sizes are in nm.

UCNP	1st Shell Thickness	2nd Shell Thickness	Total UCNP Size
$LiYbF_4(0.5\%Tm^{3+})$ Cores for Double Shelled Particles			9.98
$LiYbF_4(0.5\%Tm^{3+})@LiYF_4(20\%Yb^{3+})$	3.91		17.80
$LiYbF_4(0.5\%Tm^{3+})@LiYF_4(20\%Yb^{3+})@LiYbF_4$ Iteration 1	3.91	3.75	25.30
$LiYbF_4(0.5\%Tm^{3+})@LiYF_4(20\%Yb^{3+})@LiYbF_4$ Iteration 2	3.91	3.60	24.99
$LiYbF_4(0.5\%Tm^{3+})@LiYF_4(20\%Yb^{3+})@LiYbF_4$ Iteration 3	3.91	3.48	24.75
$LiYbF_4(0.5\%Tm^{3+})$ Cores for Classical Particles			12.63
$LiYbF_4(0.5\%Tm^{3+})@LiYF_4$	4.95		22.53

3.9. Spectral Results of First Iteration of Double Shelled Particles

Now that the particle morphologies were confirmed through TEM images and their size distributions analysed to ensure that the spectral data wouldn't be influenced by their structure and size, the next step was to measure the concentrations of each sample to ensure they were almost, if not exactly, the same. As previously mentioned, if the hexane solution in which the particles are dispersed is too concentrated, the intensities would be very high, and vice versa. After following the steps outlined in section 3.6, the concentrations of the samples to be measured are presented in table 3.2 below. As can be seen, the concentrations of each solution was close enough to each other as to not influence the absolute intensities. They were 7.2 mg/mL, 6.6 mg/mL, 7.5 mg/mL, and 6.9 mg/mL for the Classical particles, and then Iterations 1, 2, and 3, respectively.

Table 3.2: Concentration measurements of Classical, Iteration 1, Iteration 2, and Iteration 3 particles. The weights are in mg.

UCNP	Weight of Empty Eppendorf Tube	Weight of Dried Eppendorf Tube	Concentration (mg/mL)
Classical	959.7	966.9	7.2
Iteration 1	954.9	961.4	6.6
Iteration 2	1092.8	1100.3	7.5
Iteration 3	967.1	974.0	6.9

Note that since Iterations 1, 2, and 3 are all the same particle, even if one of them is less concentrated than the other, like Iteration 1 for example, it would not influence the overall measurements since there are other iterations which's concentrations are similar to that of the Classical particle, such as Iteration 2. As mentioned previously, hexane solution concentrations are very difficult to control in UCNP synthesis. It is a problem that has yet to be addressed in any literature review or research. This is a consequence of the way the particles act during the synthesis procedure and the subsequent washing procedures. UCNPs prepared via thermal decomposition tend to 'clump' together and are generally resistant to dispersion in any sort of solution, in that after several minutes, they will sink to the bottom of the canteen. This means, that in order to utilise them for experiments or analysis they require several minutes to hours of proper sonication and vortexing in order for them to return to their natural concentration. Even then, it is difficult to tell whether the particles have re-dispersed themselves within the liquid in an orderly manner or whether a larger concentration of them still exists towards the bottom of the liquid since they are significantly heavier than the liquid they are kept in (whether it is the solution of OA/ODE/(OM) or any organic solvent). Toluene has been shown to be a better dispersion agent than hexane, however is significantly more toxic when inhaled and is also subject to faster evaporation, for which reason it is not used for analysis experiments (Jiang et al.,).

On the topic of concentration measurements, there is another factor which can skew the concentration values when calculated using the method outlined in section 3.6. The double shelled particles are evidently more heavy than the single shelled particles due to the existence of an extra shell. $LiYbF_4(0.5\%Tm^{3+})@LiYF_4$ has a total molecular weight of approximately 426.86 grams per mole, while $LiYbF_4(0.5\%Tm^{3+})@LiYF_4(20\%Yb^{3+})@LiYbF_4$ has a molecular weight of approximately 699.67 grams per mole, which is about 272.81 mg heavier than the classical particle. Therefore, technically, even if the weight of the powder left behind in the eppendorf tubes of Iterations 1-3 are similar to that of the weight of the powder left behind by the classical particles there are overall fewer double shelled particles than there are classical particles. Furthermore, due to the nature of the synthesis technique, theoretically, the concentration of the hexane solution containing the double shelled particles should be a slightly less concentrated. This is because, in order to create the second shell, the entire solution of the first shells is required - the ratio between core to shell (in mmol) must remain 0.5:2. During the first shelling synthesis, 0.5 mmol of cores are extracted from a stabilised solution (approximately 20 mL), and 10 mL of shelling precursors are injected to create a total solution volume of 30 mL. This means that 0.5 mmol of shelled particles are dispersed in 30 mL of solution - this is the case in a classical shelling which are just single shelled particles. However, in order to shell these particles again, the entire 30 mL of solution is used in the next shelling synthesis, into

which a further 10 mL of shelling precursors are injected. This means that the volume of solution in which the 0.5 mmol of double shelled particles are dispersed in is 40 mL. So, the concentration of the OA/ODE solution in which the classical particles are dispersed in is approximately 0.5 mmol/30 mL as opposed to the 0.5 mmol/40 mL which is the concentration of the double shelled particles.

These are just some comments that need to be stated before the spectral data analysis was conducted in order to ensure that the reader is aware of potential errors in the intensities and what they may be caused by, and to highlight the fact that controlling the concentrations of these solutions are practically beyond the control of the researcher due to several minuscule factors.

After the concentrations were measured, 1 mL of each solution was extracted and pipetted into a cuvette. The cuvette was then placed into a cuvette holder on a rail 47 centimetres away from the laser. A detector was attached to the cuvette holder at a 90-degree angle. This arrangement makes it so that approximately only 25% of the total luminescence from all the particles is detected. This is because only the light entering the detector quadrant is recorded while all the other rays splayed out in the other directions are not. Figure 3.20 below presents the characteristic upconversion emission spectra of the $LiYbF_4(0.5\%Tm^{3+})@LiYF_4$ particles synthesised in Figure 3.18. The peaks precisely match previous upconversion data related to the Yb-Tm ion pair emissions, which can be observed in figures like the one in Figure 3.6.

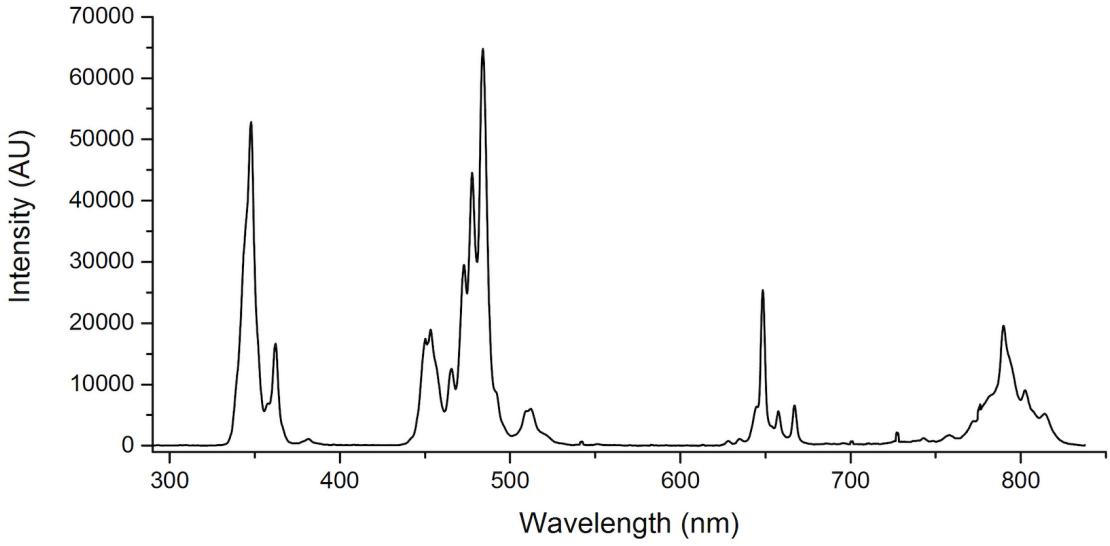

Fig 3.20: Characteristic Upconversion Emission Spectra of $LiYbF_4(0.5\%Tm^{3+})@LiYF_4$.

Apart from the peak locations, the intensities of the peaks also correspond with the intensities observed in Figure 3.6. Furthermore, the identity of the peaks can be matched with the

corresponding energy level transitions from Dieke's Diagram from Figure 1.5. This would give the following information as catalogued in Table 3.3.

Table 3.3: Emissions peak locations (wavelength in nm) and corresponding energy level transitions of typical upconverting Yb-Tm ion pair.

Peak Location (Approximate Wavelength in nm)	Transition
347.83	$^1I_6 \rightarrow {}^3F_4$
362.24	$^1D_2 \rightarrow {}^3H_6$
453.28	$^1D_2 \rightarrow {}^3F_4$
484.06	$^1G_4 \rightarrow {}^3H_6$
648.51	$^1G_4 \rightarrow {}^3F_4$
790.28	$^3H_4 \rightarrow {}^3H_6$

Since all the particles created in this thesis utilise the Yb-Tm ion pair as the upconverting source, all the spectra, regardless of the shells - how many there are, or how thick they are - will produce the exact same spectra as the one in Figure 3.20, meaning that the same energy level transitions will take place. The only observable difference that would be analysed is just the intensities of the peaks - by maintaining good size control of the cores and shells between all the particles, as well as maintaining similar concentrations for spectral experiments, absolute intensities can be measured and compared with little error.

The spectra of Iterations 1 - 3 were also measured in the same manner, and are shown below in Figure 3.21.

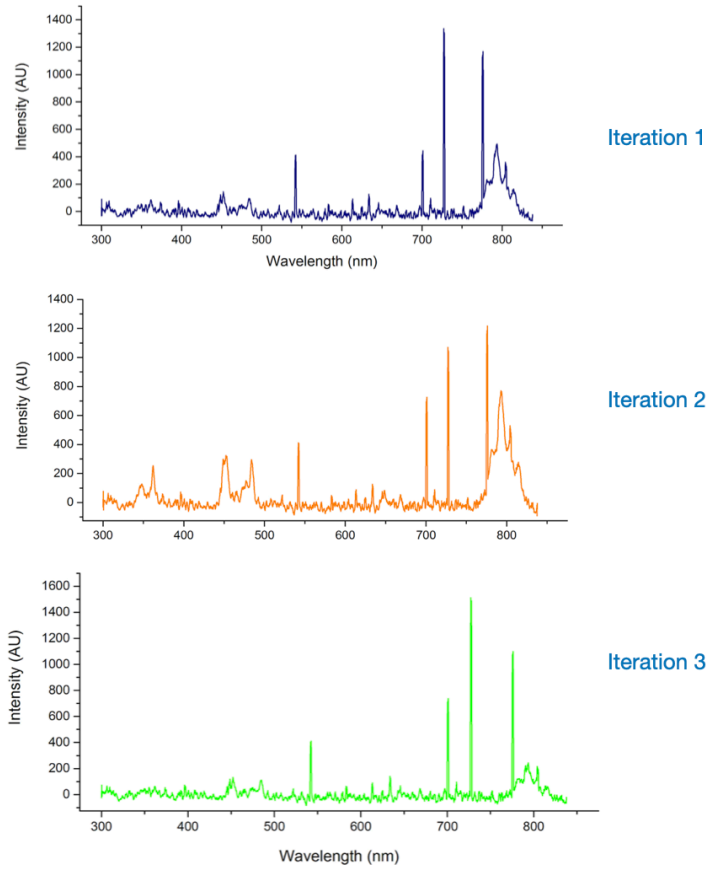

Fig 3.21: Upconversion Emission spectra of Iteration 1 - 3 double shelled particles.

The sharp, thin peaks in Figure 3.21 are the background peaks, the same ones visible at ~ 725 and 775 nm in Figure 3.20. It is clear that the classical spectrum dwarfs the spectrum of these double shelled particles. While the intensities of the emission peaks of the classical spectrum were in the tens of thousands, the intensities of the double shelled particles barely breached 1500 AU as can be seen from the Y-axis values. This is not to say that the double shelled particles did not upconvert - the peak at 790 nm is still visible in all three iterations quite clearly although it is very quenched. The peaks at 453 nm and 484 nm, ie the $^1D_2 \rightarrow {}^3F_4$ and $^1G_4 \rightarrow {}^3H_6$ are also still present even though they are less intense than the background radiation. This means that these double shelled particles were unable to amplify the emission spectra intensities as was intended, and in fact simply quenched the intensities to some insignificant values.

The reason for this lay in the structure of the particle and the intentions of each shell. When UCNPs are shelled, each shell is meant to serve a purpose, which means the smaller we make

the core, the more shells we can grow on the UCNP before it reaches a size unable to be utilised for biomedical applications. In these first three iterations of double shelled particles, $LiYbF_4(0.5\%Tm^{3+})@LiYF_4(20\%Yb^{3+})@LiYbF_4$, the core served as the light emitting source, the middle shell served as the energy mediator, and the outer shell served as the light absorbing source. However, upon closer inspection of these nanoparticles, the sheer amount of Yb present in this structure dominates the activator ion, Tm. There is nearly 100% of Yb in the core, 20% in the middle shell, and 100% in the outer shell. This could lead to a lot of back transfer of energy between the Yb ions themselves rather than an excitation of the Tm ion. This meant that the energy which was lost for upconversion may have been released in the downshifting region, ie in the 1000+ nm region (IR) or even as heat. However, since nanothermometry is beyond the scope of this thesis, these particles have been stored in the fridge for further heat analyses at a later time.

For now, another problem with the structure of the double shelled particles was resolved: The outer shell being completely light absorbing does not actually do anything for the particle. The amount of energy present at the outer edge of the $LiYF_4(20\%Yb^{3+})$ shell will always be nearly 100% whether there is a completely light absorbing shell, like $LiYbF_4$, present or not. This also highlights the fact the energy transfers within the structure may also have been lost to the solvent (hexane) during the spectral measurements, since there is no inert shell to shield the core and middle shell. So the structure of these double shelled particles were adjusted, and this new particle was made in order to test this hypothesis: $LiYbF_4(0.5\%Tm^{3+})@LiYF_4(20\%Yb^{3+})@LiYF_4$. The outer shell was swapped with an inert, LiYF4 shell to provide shielding from solvent quenching, as well as removing the excess Yb present in the previous structure.

3.10. TEM and Spectral Results of $LiYbF_4(0.5\%Tm^{3+})@LiYF_4(20\%Yb^{3+})@LiYF_4$

Following the same synthesis procedure as with the first 3 iterations of double shelled particles, this new particle was made. Essentially, the particle itself is just a mimic of the original particle, just with a classical outer shell. The only difference between this particle, and the classical particle published in Ting Cheng et al.'s paper is the insertion of an inert middle shell doped with 20% Yb^{3+}. Figure 3.22 below is the TEM images of the core, core-shell, and core-shell-shell, along with the corresponding size distribution histograms.

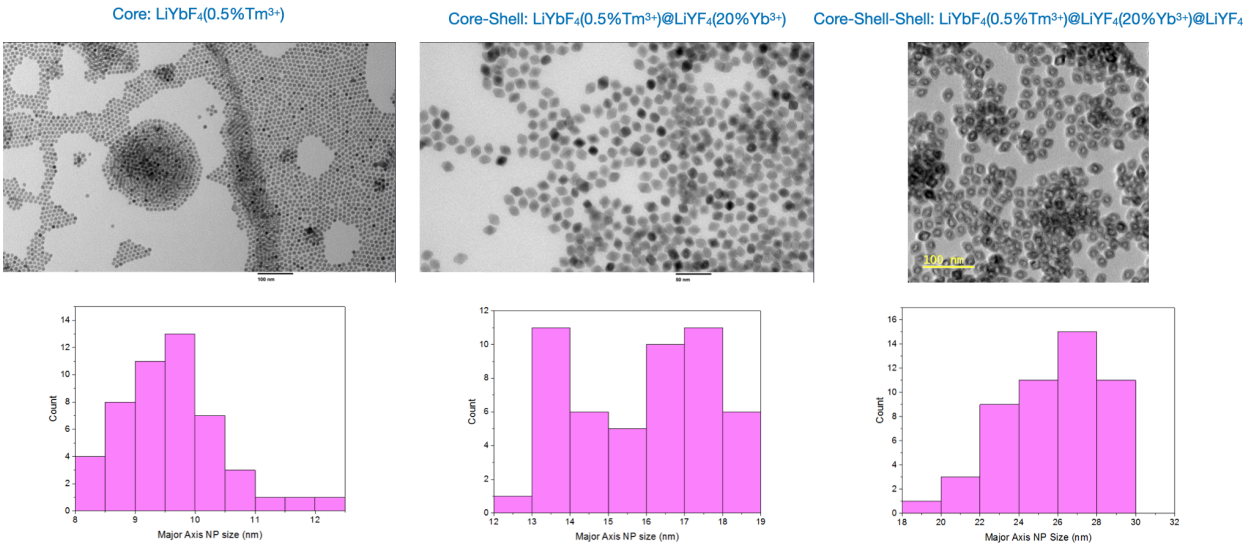

Fig 3.22: TEM images and Size distribution histograms of rectified Core-shell-shell $LiYbF_4(0.5\%Tm^{3+})@LiYF_4(20\%Yb^{3+})@LiYF_4$. The scale bar for the core is 100 nm, for the core-shell is 50 nm, and for the core-shell-shell is 100 nm.

Once again, the mono disparity of the particles can be observed immediately upon looking at the TEM images. The TEM of the core does not look like a normal TEM photo (ie, like a mosaic) just because of the way it was prepared, however the particles themselves are of similar size. The following two shells also displays the consistent similarity in particle size from just visual inspection. The average sizes of the cores was 9.58 nm, almost the exact same as the ones prepared for the previous set of experiments. The average sizes of the core-shell, and the core-shell-shell particles were, 15.85 nm and 25.78 nm respectively. The sizes of the shells themselves were 3.13 nm, and 4.96 (5) nm respectively. The middle shell was slightly thinner than expected, by approximately 1 nm, however this small error can be neglected since a shell thickness of above approximately 2 nm still managed to enhance the intensities of the upconverting spectra according to the research published by Bin Zhou et Al. It is worth mentioning that the injection rate for the outermost shell was not 1.5 mL/min anymore, as was the case with the previous double shelled particles - instead the normal injection rate of 0.75 mL/min for the outermost shell was employed. This choice was made due to the fact that the outermost shell now served no purpose beyond acting as a shield against surface quenching, so the traditional shelling procedure as outlined by Ting Cheng et al.. was followed.

After confirming the sizes and the disparity of the UCNPs through TEM analysis, the spectral data was measured in the same manner as outlined before. The concentration of these particles once dispersed in hexane was around 6.7 mg/mL (the weight of the empty eppendorf tube was

982.4 mg and the weight of the dried eppendorf tube was 989.1 mg), meaning it was slightly less concentrated than the classical particles. However, it was still within a similar range, a difference of less than 2 mg/mL between the two concentrations, which should not affect the overall intensities of the peaks by such a significant margin that they would no longer be comparable. The spectrum of this double shelled particle is shown in Figure 3.23 below.

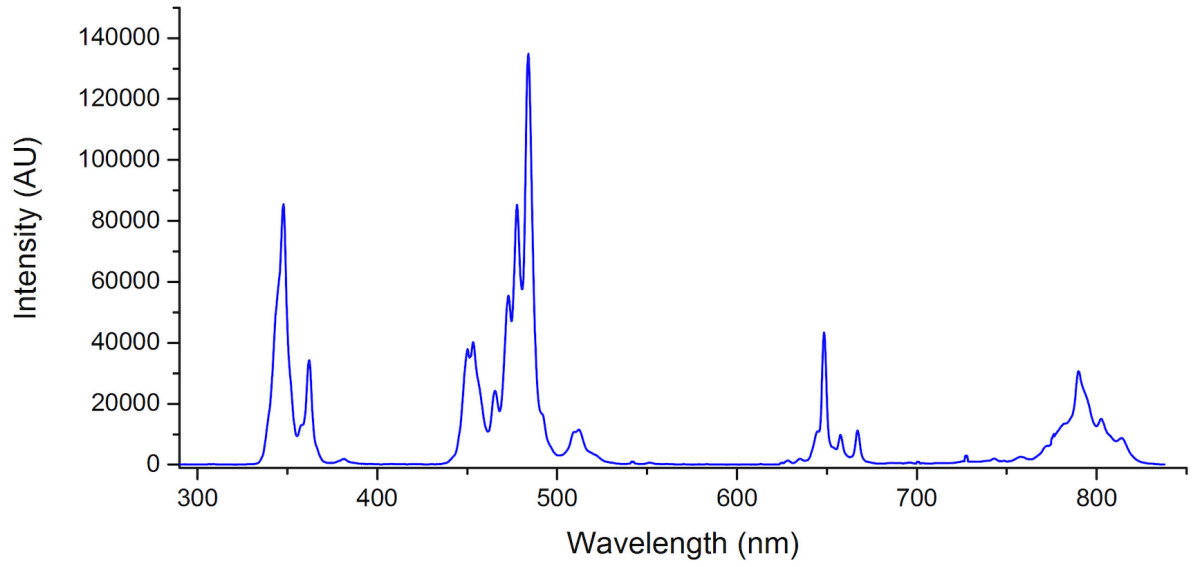

Fig 3.23: Upconversion Emission Spectra of $LiYbF_4(0.5\%Tm^{3+})@LiYF_4(20\%Yb^{3+})@LiYF_4$.

The spectrum above is a clear and distinct characteristic Tm^{3+} emission spectrum, with all the appropriate and accurate emission peaks, and can be directly compared to the classical emission spectrum in Figure 3.20. Furthermore, just by looking at the Y-axis values, it is clear that there is a significantly observable increase in the intensities of the peaks in the UV and blue region. For example, the intensity value of the 347.83 nm peak, ie the $^1I_6 \rightarrow {}^3F_4$ transition, for the black (classical) spectrum in Figure 3.20 is 52,818, while the intensity value of this same peak for the blue (20% Yb3+ middle shell doped double shell particle) spectrum is 85,442. The intensity of the 347.83 nm peak of the double shelled particle is 1.62 times the classical peak. This is proof that such a particle with a mediator ion doped into a central shell between the light absorbing region (the outer shell) and the light emitting inner core, with an inert shielding shell, can in fact enhance the emission spectrum of classical sensitiser-activator doped UCNPs. The next step was to explore the effects of the doping concentrations in the central shell - for the purposes of this thesis, only two separate doping concentrations was tried and test, 10% and 25%, to determine viability. In essence, will reducing the doping percent still increase the upconversion intensities, and if so by how much, and vice versa, will increasing the doping percent continue to increase the upconversion or will they plateau.

3.11. TEM and Spectral results of $LiYbF_4(0.5\%Tm^{3+})@LiYF_4(25\%Yb^{3+})@LiYF_4$ and $LiYbF_4(0.5\%Tm^{3+})@LiYF_4(10\%Yb^{3+})@LiYF_4$

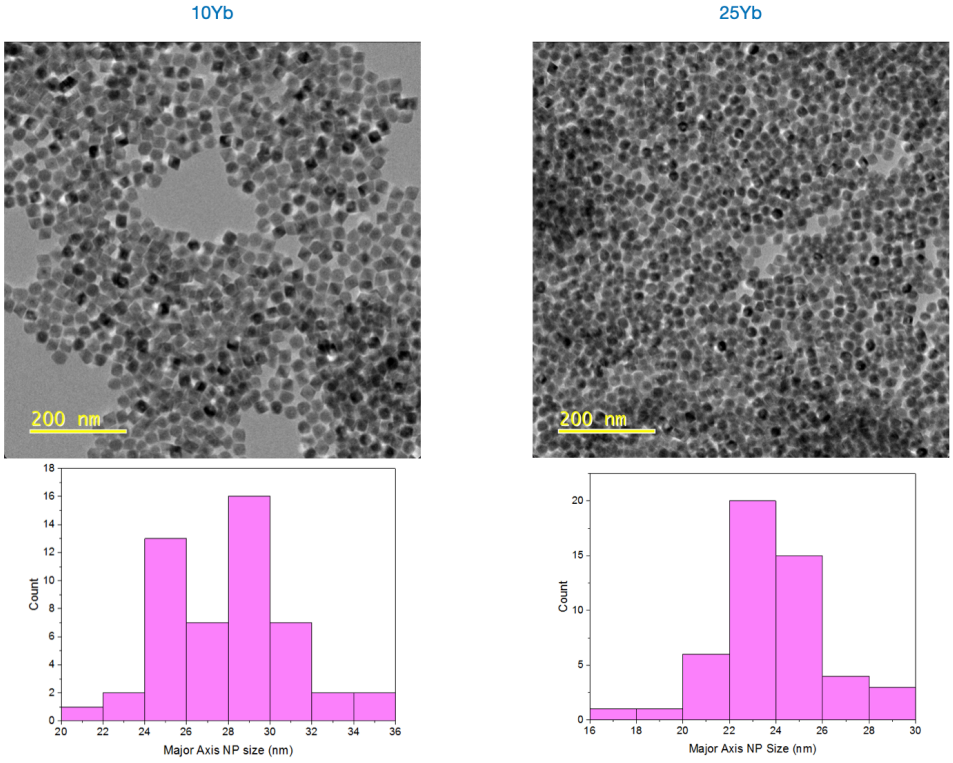

Fig 3.24: TEM images of $LiYbF_4(0.5\%Tm^{3+})@LiYF_4(10\%Yb^{3+})@LiYF_4$, 10Yb, and $LiYbF_4(0.5\%Tm^{3+})@LiYF_4(25\%Yb^{3+})@LiYF_4$, 25Yb, and their corresponding size distribution histograms.

Both these particles, hence forth referred to as 10Yb and 25Yb, were prepared in the same way as the 20Yb particle. This means that the outer shell thickness is closer to that of the classical particle's first shell (ie, its outer shell), and the middle shell's thickness was approximated to 3.13 nm. The TEM images below show the final double shelled particles in question. Their mono disparity can be seen as well as their similarity in sizes. The average size of the entire particle was 26.87 nm, and 24.82 nm for 10Yb and 25Yb respectively. While the 25Yb particle was close in size to the other particles made in this thesis, the 10Yb particle was a little bit larger than expected, and was in fact larger than most of the particles made in the first double shelled set of experiments, and of the second set. There is no definitive way to determine what exactly caused these particles to grow to such a size especially due to the minutiae of errors that could occur during the shelling syntheses, such as slow stirring, slow argon rate, tiny temperature

differences during the injection procedure. As mentioned before, synthesising UCNPs via thermal decomposition is quite a challenging task, as they are very susceptible to the slightest of environmental changes. However, with that being said, the outer shell thickness, as written in literature, does not have a very distinct effect on the upconversion intensities, and thus should not affect the final spectral results. The outer shell thickness for both these particles were then approximately: 5.51 nm for the 10Yb particle, and 4.48 nm for the 25Yb particle.

The concentration of the hexane solution into which these particles were dispersed was 8.4 mg/mL for the 10Yb particle, and 7.0 for the 25Yb particle. It is worth noting here that for all three particles, 10Yb, 20Yb, and 25Yb, the overall weight of these particles is heavier than the classical by the weight of $LiYF_4(20\%Yb^{3+})$ - the middle shell, which's weight is approximately: 188.62 mg/mol. The spectral data is compiled below for the 10Yb and the 25Yb particles from Figure 3.24.

From just visual inspection of the spectral data it is clear that the 10Yb particle definitely did not enhance the UV peaks, and with slight analysis (complied in Table 4, below), did not enhance the blue peaks either, ie the 484.06 nm peak. The intensity value of the 484.06 nm peak for the 10Yb particle was 62,828, while it was 64,765 for the classical particle - the values themselves are very close, which makes for an interesting observation. The value of the intensity of the UV peak, 347.83 nm, for the 10Yb particle was 38,890, and 52,818 for the classical particle. From this it means that the addition of the middle shell, when doped sparsely with a mediating ion, did not seem to affect the blue emissions as much as it did the UV emissions. Without further experiments it is difficult to determine what causes this, but it can be stated that a lower doping percent seemed to enhance the population of the I^1_6 band, and less so the, $^1G_4$ band. In order to test and confirm this hypothesis, an even more sparsely populated middle shell, ie 8% or 5% Yb^{3+} doping percent, would needed to have been made and measured.

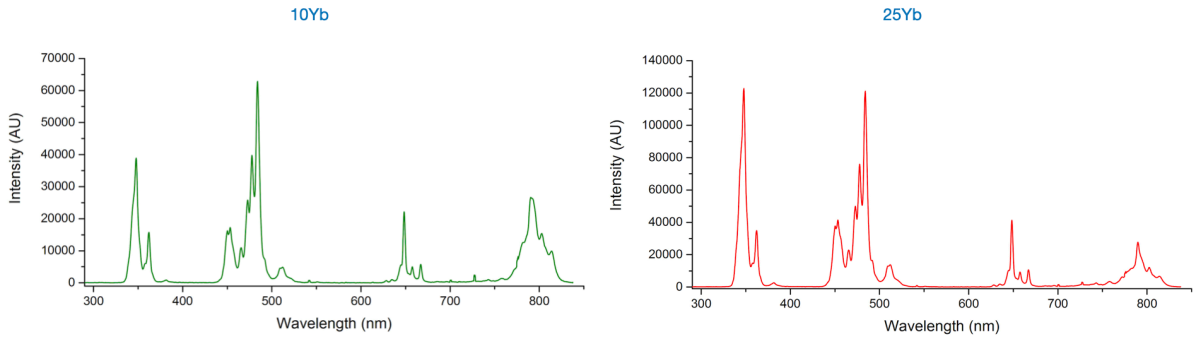

Fig 3.25: Upconversion Emission Spectra of $LiYbF_4(0.5\%Tm^{3+})@LiYF_4(10\%Yb^{3+})@LiYF_4$, 10Yb, and $LiYbF_4(0.5\%Tm^{3+})@LiYF_4(25\%Yb^{3+})@LiYF_4$, 25Yb.

However, while the 10Yb particle failed to demonstrate any viability in enhancing the spectra of the classical particles, the 25Yb particle did the complete opposite. The peak intensities values skyrocketed especially on the UV and Blue region side. The values of all the peaks of all four particles, classical, 10Yb, 20Yb, and 25Yb have been complied into table 4 below for easier analysis.

Table 3.4: Peak values of all 4 particles.

Wavelength	Classical Peak Intensity Values	10Yb Peak Intensity Values	20Yb Peak Intensity Values	25Yb Peak Intensity Values
347.83 nm	52,818	38,890	85,442	122,738
362.24 nm	16,631	15,720	34,170	34,865
453.28 nm	18,900	17,241	40,203	41,386
484.06 nm	64,765	62,828	134,847	121,087
648.51 nm	25,369	22,144	43,369	41,193
790.28 nm	19,425	26,476	30,579	27,250

The highlighted cells from the table above indicate the highest value amongst the 4 particles. From table 4, it is clearly evident that a higher doping concentration seems to increase the intensities of the peaks in the UV and blue region. The values of the 362.24 nm and 453.28 nm peaks of the 20Yb and 25Yb particles are close enough to each other that they can be neglected for comparison. During the spectral measurements, maybe the 25Yb particles sank to the bottom of the hexane in the cuvette, leading to a slightly more intense 362.24 and 453.28 nm peak. However, the UV peak of the 25Yb particle is more than double (2.32 times to be exact) that of the classical UV peak, and is also significantly stronger than the 20Yb UV peak (1.43 times stronger). While these values are not the 100-fold increase which was presented by Bin Zhou et Al, it is still a serious increase in intensities for just an small insertion of an extra shell. Furthermore, in the paper published by Bin Zhou et Al, the doping concentrations of the middle shell were not really explored, mostly the shell thickness. Another major difference between that paper and the experiments conduced in this thesis, was that they used a Sodium Fluoride based particle, while here a Lithium Fluoride particle is explored. Niche consequences of the different structures may also cause quenching of the peaks (however, Yb-Tm ion systems tend to only work in Lithium based systems anyway). Another difference was that in Bin Zhou et Al's paper, they separated the activator and sensitisers in two separate shells, however one of the core factors of these particles is that the activators are in the classical core, meaning they are also surrounded by the sensitising ions.

The largest 484.06 nm peak was found in the 20Yb particle, at a value of 134,847 compared to the meagre 64,765 of the classical blue peak - increased by a factor of 2.08. The 25Yb value of this wavelength was 121,087, which is lower than 134,847 but still in the 100,000. The issue herein lies in the jump of doping concentration. In hindsight, changing the doping concentration of the middle shell from 20% to 25% isn't that significant of a jump for these two particles to be compared to each other. They can individually be compared to the classical particle, which lacks this middle shell, however to debate which one of these two is better is difficult due to the very small doping percent increase. A true comparison for the 20Yb particle would be a 40% middle shell doped particle and a 30% middle shell doped particle - these are larger increases in doping percentages which would possibly lead to higher emissions. If it can be assumed that the values of the peaks of wavelengths larger than 484.06 nm (ie blue to red) are close enough to each other for the 20Yb and 25Yb particle, then it can be concluded that over all, the 25Yb particle is better simply due to the significant increase in intensity of the 347.83 nm (UV) peak. This is the most compelling indication that 25% doping is not the most optimal doping percent for the middle shell and that maybe larger percentages may in fact lead to stronger intensities.

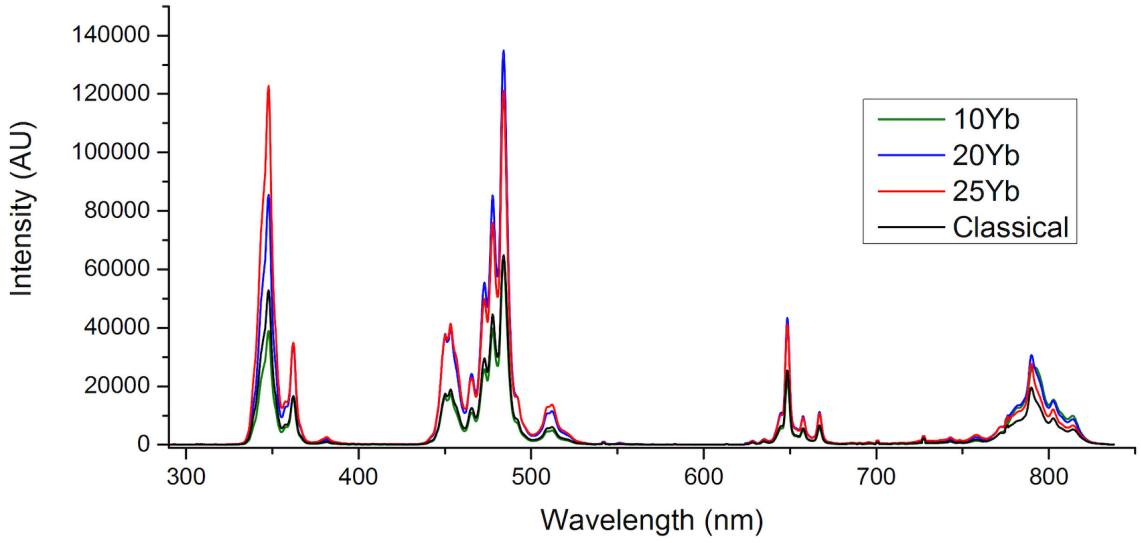

Fig 3.26: Upconversion Emission spectra overlayed on top of each other for all 4 particles of interest.

However, the goal of this thesis was achieved. From Figure 3.26, above, it can clearly be seen that the insertion of a middle shell with a mediator doping percent of between 20-25% drastically increases the intensities of the classical, $LiYbF_4(0.5\%Tm^{3+})@LiYF_4$ particle, especially in the region which is of most interest: UV - blue.

5. CONCLUSION

Upconversion is the process in which multiple low-energy photons are absorbed sequentially to emit a higher-energy photon. This results in the emission of light of a shorter wavelength and higher energy than the excitation light, such as the conversion of Near Infrared (NIR) light into visible or ultraviolet (UV) light.

The Stokes Shift occurs when the emitted photon has lower energy than the absorbed photons which is a common phenomenon in fluorescence and Raman spectroscopy. It happens due to vibrational relaxations or energy loss to the surrounding environment. In contrast, the Anti-Stokes Shift happens in upconversion, where the emitted photon has higher energy than the absorbed one. This extra energy gain can come from mechanisms like thermal dissipation or triplet-triplet annihilation.

While organic molecules can upconvert, this paper discusses the inorganic nanoparticles which are derived from lanthanoids, which have been shown to excel in this field. Research on lanthanoids is essential to improve their upconversion efficiency.

Two-photon absorption and second harmonic generation also involve the emission of higher-energy photons, but they differ in their mechanisms from upconversion. Upconversion can occur through various mechanisms, and today, five have been identified: ESA, PA, ETU, EMU, and CU. These mechanisms work in materials like lanthanoid-based macrostructures that contain ions capable of upconversion.

ESA, is a multistep process where photons are absorbed sequentially to excite an ion from the ground state to an excited state. Initially, a photon excites an ion from the ground state to an intermediate state, and further photons excite it to higher energy levels. Phonons may assist in these energy transfers. Importantly, ESA is a single ion process, meaning the upconverting ion concentration in the material does not affect the pumping rates. Furthermore in ESA, there are two separate laser powers which work together in order to excite an ion to its highest excited state.

Cross-Relaxation refers to ion-ion interactions in upconverting crystals, where energy is transferred between two ions. In this process, ion 2 transfers some of its excited energy to ion 1, particularly when the excited state of ion 2 interacts with the ground state of ion 1. The process

depends on the dopant concentrations in the crystals, and high doping levels can lead to weaker photoluminescence due to concentration quenching. However, Cross-Relaxation can still be used intentionally to control the colour output or enhance photon avalanche upconversion. The ions involved can be of the same type, and not necessarily be different upconverting ions.

PA is a complex process involving three key steps: transmission, emission, and rise time, with a critical pump threshold tied to pump power intensity. In a four-energy system (E0, E1, E2, and E), the process begins with an electron absorbing energy from an excitation wavelength. This energy may not perfectly match the intermediate states like E2, but cross-relaxation allows the electron to move to E2. Energy transfer occurs between the E2 electron and one in the ground state (E0), forming two electrons in the E1 state. Under continuous radiation, one of these electrons gains energy and enters the upper excited state, interacting with electrons in the ground state to produce more electrons in the E1 state. As the radiation resonates with the transition from E1 to E, the process repeats itself, forming a feedback loop.

ETU is an efficient mechanism in lanthanoids, involving two or more lanthanoid ions doped into a crystal lattice to achieve upconversion. It operates independently of pump power and occurs when the sensitiser and activator ions are close enough in the lattice, allowing energy transfer from the sensitiser to the activator. This transfer can also happen through phonon-assisted non-radiative processes if there is an energy mismatch between the sensitiser and the activator. Designing these materials requires careful doping concentrations, though efficient ETU can still occur with a single lanthanoid ion acting as both the donor and receiver.

UCNPs are nanoparticles capable of upconversion, in that they absorb IR photons and emit visible or UV photons, depending on dopants like Tm^{3+} and Er^{3+}. UCNPs provide a more detailed understanding of upconversion compared to bulk crystals due to their diverse applications. The upconversion process requires metastable states that allow for the sequential photon absorption, which is facilitated by the complex electronic structures of lanthanoids, capitalising on their 4f orbitals.

When doped into a nano crystalline host lattice, these 4f orbitals split to form intermediate states essential for upconversion. The non-bonding nature of the 4f orbitals, coupled with shielding from the 5s and 5p shells, results in weak coupling to the surrounding lattice, which leads to long excited-state lifetimes and sharp optical features.

UCNPs exhibit surface and size-related effects, unlike bulk crystals, which can influence their performance. Issues arise from energy dissipation through radiative and non-radiative relaxation,

where radiative transitions involve photon absorption or emission, while non-radiative transitions involve energy transfer or dissipation. Phonon density of states plays a crucial role in energy transfer, as phonons can help excited electrons reach intermediate states. However, the competing effects of non-radiative relaxation and phonon assistance affect the energy transfer efficiency and the lifetime of excited states in UCNPs.

The structure and chemical composition of UCNPs significantly impact their upconversion efficiency. The choice of host lattice is crucial for determining spectral characteristics, as it mediates energy conduction and transfer between ions. Key factors in selecting a host lattice include low phonon energy, high chemical stability, and low lattice symmetry. Low phonon energy minimises non-radiative phonon quenching, while high chemical stability ensures the lanthanoid ions remain non-bonding and the UCNPs remain neutral and non-reactive.

The Laporte Selection Rule suggests that UCNPs with low symmetry lattices, such as tetrahedral crystals, exhibit brighter emission spectra due to less restrictive electronic transitions. Initially, oxides were used for their stability, but their high phonon energies resulted in low brightness. Halogen ions like chlorine and bromine offer low phonon energies but are chemically unstable. Fluoride ions (F^-) provide a better balance of stability and low phonon energy, making them ideal for UCNP synthesis, with common cations like Lithium and Sodium, which bond easily with F^- and match the size of lanthanoid ions.

Choosing appropriate ion pairs is also critical, as the energy level differences between the ground, intermediate, and excited states of activator ions must align to facilitate smooth energy transfer and minimise non-radiative losses. The Ytterbium ion, Yb^{3+}, is a common sensitiser due to its large absorption cross-section for NIR light and compatible energy levels with activator ions like Er^{3+} and Tm^{3+}, enabling efficient energy transfer. Concentration of ions is important, as high concentrations can lead to cross-relaxation and weaker emission.

Dieke's Diagram, developed in the 1950s and 1960s, catalogs the energy levels of lanthanoids and helps identify appropriate sensitiser and activator pairs for upconversion. The diagram also illustrates the splitting of energy levels and the term symbols associated with them, which are important for understanding energy transitions and selecting ion pairs for efficient upconversion.

UCNPs are highly versatile and malleable, making them suitable for a range of fields, from semiconductors to biomedical engineering, due to their chemical stability, small size, and ease of post-synthesis modification. However, during their synthesis, UCNPs are initially capped with organic ligands, which make them dispersible only in organic solvents. For biomedical

applications, UCNPs need to be made water-dispersible through a ligand exchange process, replacing hydrophobic ligands with hydrophilic ones like PEG or Polyacrylic Acid PAA.

This exchange process, though essential, is challenging and can cause aggregation of the particles, leading to a loss of their intense emission spectra. Despite efforts with reagents like Hydrochloric Acid (HCl) and Nitrosonium Tetrafluoroborate ($NOBF_4$), aggregation remains a problem, and improper preparation can introduce toxic residues, making them unsuitable for biomedical use.

Nevertheless, the ability to modify UCNP surfaces to generate localised high energy light, and achieve tuneable emissions makes them attractive for biomedical applications such as drug release, bioimaging, biosensing, and temperature detection, where they leverage the unique phenomenon of upconversion to interact with the complex functions of the human body.

The rise of nanotechnology has opened up new, non-invasive, and precise methods for treating diseases, but it also raised concerns about safety, synthesis of medicines, and potential risks to human health, animals, and the environment. These concerns led to the need for toxicological analyses and regulations, even for UCNPs, which are largely considered safe for biomedical use. Key challenges before UCNPs can be applied in clinical trials include reproducible synthesis, size and shape control, biocompatible surface chemistry, in-vivo detection, and theranostic applications.

Theranostics, a technique in Personalised Medicine, combines diagnostic and therapeutic functions, such as in nuclear medicine, in which agents like iodine-131 were used for thyroid cancer. However, theranostics faces challenges, including safety, efficacy, cost, and precise targeting. UCNPs show promise in theranostics due to their biocompatibility, broad emission spectra, and the ability to be activated with simple lasers, reducing costs and the need for specialised equipment. However, their synthesis remains costly due to the high price of the rare earth materials used.

The development of novel bottom-up synthesis methods for lanthanoid-doped Nanomaterials has enabled the production of well-defined UCNPs with tuneable sizes, making them increasingly used in nanotechnology and biomedicine. Their ability to mimic the size of natural biological systems, such as cells and proteins, enhances their biocompatibility and reduces the probability to invoke an adverse immune response.

A key factor in their effectiveness, especially in cancer treatment, is their ability to take advantage of the Enhanced Permeability and Retention (EPR) effect, where nanoparticles are

more likely to accumulate in solid tumours than in normal tissues. Controlling the size of UCNPs is crucial for targeting cancer cells, and recent studies have shown promise in using sodium-based Yb-Er UCNPs to treat liver cancer.

Unlike traditional fluorescent labels, which can damage tissues with high-energy light, UCNPs operate in the NIR spectral region, avoiding harmful effects and reducing light scattering. This makes them ideal for applications like cellular nanothermometry. Additionally, UCNPs can emit light across various wavelengths depending on their dopant composition, allowing for tailored emission properties. For example, UCNPs emitting UV light can be used for deep tissue therapies, offering the energy needed for photochemical reactions.

To optimise UCNPs for biomedical applications, specific design parameters need to be considered. The Yb-Er pair is commonly used because when irradiated with 980 nm light, the Er^{3+} ion emits green light (520-550 nm), which is useful for applications like photocleaving polymers to release drugs or triggering photochemical reactions. However, while green light is more energetic than IR, NIR, or red light, it often performs its task slowly in drug release applications. This is because the emitted light's intensity is significantly reduced in vivo due to the surrounding water, which absorbs 980 nm light, leading to an overall energy loss.

The water absorbance causes a quenching effect, where a large portion of the light is absorbed by the water molecules instead of the UCNPs, reducing the intensity of emitted light in biological settings compared to lab conditions. Despite this, UCNPs must remain water-dispersible for effective biological applications, making this a key consideration when designing them for use in living tissues.

To improve the efficiency of drug release using UCNPs, it is crucial to make them brighter, as low emission intensities often limit drug release rates. Brighter UCNPs will emit higher intensities when irradiated, enhancing their effectiveness. UCNPs should also be small to ensure they adhere to the EPR effect, which allows them to target tumours effectively. Smaller particles are also less likely to cause immune responses and have longer blood half-times, making them more effective when delivered intravenously.

Regarding the excitation wavelength, 808 nm light is preferred over 980 nm light due to its deeper tissue penetration. Although 808 nm light excites the Nd^{3+} ion, which has high quantum efficiency, it results in weaker upconversion luminescence due to energy back transfer. Therefore, the Ytterbium ion is chosen as the sensitiser, with Tm^{3+} as the activator, as it emits UV and blue light. Blue light is more energetic than green light, and UV light can be used locally

to induce the production of reactive oxygen species (ROS), which can help destroy cancer tissue without harming surrounding healthy tissue.

Using the research developed in Ting Cheng et al's paper as a basis, the particle of interest became $LiYbF_4(0.5\%Tm^{3+})$. While Sodium-based UCNPs are often employed for use in biomedical applications, $LiYF_4$-based upconversion nanoparticles (UCNPs) are also efficient in generating sharp and intense emission peaks, particularly in the UV/Blue range, and sometimes preferred over Sodium counterparts. The study introduces a method to tune the size of these UCNPs, which were previously too large (80 nm) for cell internalisation applications. It also addresses the issue of enhancing upconversion intensities by modifying the size of the cores, which would allow for more surface modifications and shelling.

The paper focuses on the $LiYF_4(Yb^{3+}, Tm^{3+})$ UCNPs, which while able to. Emit in the UV range, still mainly emitted NIR light. The authors aimed to increase UV emission from these particles. By adjusting the synthesis method, particularly the ratios of Oleylamine (OM) and Oleic Acid (OA), the size of the UCNPs was controlled, ranging from 5 to 90 nm. The paper also reported that UCNPs below 10 nm emitted more NIR light and were unstable, making them difficult to modify. To overcome this, the study introduced a new technique to create stable UCNP cores around 10 nm, suitable for shelling and further surface modifications.

First Nuclei synthesis was introduced in Ting Cheng et al's paper and revolutionised the synthesis of Lithium-based UCNPs. After several iterations of experiments and trials, the authors found that in having an OA and OM ratio of 1:1, with both acting as coordinating ligands in the nucleation process, induced the production of extremely smalls nanoparticles, around 5 nm in diameter. These nanoparticles however were unsuitable for any sort of post-synthesis modification, such as shelling, and were very weakly emitting. In order to overcome this problem, Ting Cheng et al created a stabilisation procedure in which these newly formed super small UCNPs were grown to a size of approximately 8-10 nm in diameter in the presence of the more stable of the two coordinating ligands, OA. These stable and still extremely small cores became of great interest as, once shelled by an inert shell, they emitted greatly in the UV and blue range, ie, with energies capable of causing cellular destruction.

The brightness of UCNPs can theoretically be improved by adjusting dopant concentrations, as higher sensitiser and activator levels increase light harvesting and transfer to activating ions. However, high doping levels can cause concentration quenching and detrimental cross-relaxation between neighbouring ions. One way to overcome this is by using high irradiance excitation, although it may have harmful effects on human tissue. To avoid energy losses from cross-relaxation, multilayered UCNPs with energy-migrating shells are used. These shells

enhance upconversion luminescence, particularly in the green, blue, and UV ranges, and can also allow emission colour switching using a single lanthanoid ion.

Designing UCNPs with a goal to increase their emissions requires understanding their optical functions and applications. In addition to a passive outer shell to prevent surface quenching, at least one or more middle shells are necessary to manipulate upconversion dynamics. Three types of multi-layer-core-shell (MLCS) structures to date have been discussed to date: First, two luminescent layers are separated by an inert layer to prevent unwanted interactions between laser-active ions. This structure is colour-tuneable and emits different colours depending on the excitation wavelength. Second, active layers are connected by an energy migratory lattice that manipulates luminescent intensities. And finally third, a luminescent region is confined between two layers (active or inactive) to enhance upconversion emission spectra by reducing harmful energy migration between sensitiser ions.

With the cosmopolitan research being conducted around the usage of multi-shelled UCNPs in improving their functions, a multi-shell UCNP with $LiYF_4(Yb^{3+}, Tm^{3+})$ as the core, was synthesised and researched. A paper, published in 2020, by Bin Zhou et al, reported on a 100-fold increase in intensity of Sodium-based Yb-Er UCNPs with an energy mediating middle shell, in essence employing the science of the third MLCS structure. Whether such an increase would be possible in the already strong-UV-and-blue-emitting UCNPs reported by Ting Cheng et al, became the basis of this thesis. And thus, the first proposed particle became $LiYbF_4(0.5\%Tm^{3+})@LiYF_4(20\%Yb^{3+})@LiYbF_4$. The idea was to have an energy mediating middle shell doped with a small percentage of the sensitiser, and a completely light absorbing outer shell.

The first three iterations of this MLCS UCNP failed in its function. They were prepared with a protocol modified from the one published by Ting Cheng et al, however still were of an acceptable size. The cores were around 10 nm, and the double shelled particles were between 24-25 nm with a middle shell thickness of approximately 4 nm. With these parameters, the particle was hypothesised to have increased the the intensities of characteristic Yb-Tm spectrum. However, all the peaks were quenched and were completely incomparable to the classical emission spectra. This was not to say that they did not upconvert - although the peaks were severely quenched and barely more intense than the background peaks, the spectra did show slight deviations in the red range which indicated that some form of red light was still being emitting, and hence these particles were upconverting.

The issue herein lay in the in fact that these iterations lacked any sort of shielding from the solvent. This was rectified by changing the completely light absorbing outer shell with an inert

$LiYF_4$ shell. In essence, this would not change the function of the UCNP. Whether there is a completely doped Yb shell or not on the outermost surface does not matter since at the outer edge of the nanoparticle, the amount of light available will always be 100%. In fact, the addition of this passivating shell, should in theory increase the intensities of the unconverted emission spectra. And they did.

The new $LiYbF_4(0.5\%Tm^{3+})@LiYF_4(20\%Yb^{3+})@LiYF_4$ particle in fact increased the intensity of the UV peak by at least double, 2.19 to be exact. The intensities of all the other peaks were also increased drastically. This was by no means close to a 100-fold increase, however was still a visually and quantitatively significant increase. With the proof of concept proved, two more particles were made in a similar fashion with adjustments to the doping concentration of the middle shell which were adjusted to 10% and 25%. Spectral experiments conducted on these new particles revealed that lowering the concentration of the Yb in the middle shell to 10% actually quenched the peaks to values lower than the classical peak except for the red peak which was still stronger than its classical counterpart. However, increasing the doping concentration by just 5% drastically enhance the UV peak, while the value of the blue peak remained somewhat the same. This was indicative of the fact that there may be doping percentages of Yb in the middle shell higher than 20-25% that would yield in a greater increase of upconverting intensities.

4.1. Future Prospects

With this information in mind, a lot of future experiments can yet be conducted. Firstly, changing the doping concentrations to more observable intensity changes than what was observed with just a 5% increase needs to be done. With just a small concentration change, the peak intensity values increased, which means that at larger values they may increase more. So, optimisation of the doping concentration of the middle shell is something that needs to be tested: having a concentration of 10%, 20%, 40%, 50%, and 70% of Yb^{3+} may show at which point the doping percentage begins to plateau or quench the peaks. On this note, the middle shell thickness remained (somewhat) constant between all iterations, however as was reported by Bin Zhou et al, and others conducting experiments on MLCS UCNPs, the shell thickness also plays a crucial part in manipulating the intensities.

For future, apart from just optimising the doping concentration values of the Yb^{3+}, the middle shell's thickness must also be varied to determine its optimal thickness. This is an easily adjustable experiment since, with hot injection synthesis, the thickness of the middle shell can be manipulated in a variety of different ways, including the injection rate, as well as core-shell ratio. The thickness of the outer shell does not matter as much, since the inert shell's existence

is only to prevent quenching at the surface, so as long as it is thick enough to stop energy losses to the solvents at the surface, it can remain at a constant value. From previous experiments and papers, this value varies between 5-8 nm.

Finally, and most crucially: these UCNPs were made with the goal of applying them in biomedical research, primarily in cancer treatment. The entire point of making them super bright was to ensure that even with a little excitation light, they are still able to upconvert efficiently enough to produce enough energy to perform their functions, whether that is to create ROS, photo cleave, or trigger photochemical reactions. This is because, 980 nm light, the wavelength of excitation, is absorbed by the water surrounding the tissue, therefore most of it does not actually excite the UCNPs. After optimising the shell thickness and the doping concentration of the middle shell, the very final experiment must be to strip the UCNPs of their organic ligands at the surface, and make them water dispersible. Then spectra must be measured in the same fashion, ie, dispersed in 1 mL of water rather than hexane, in order to determine by what margin are they quenched. This will give a holistic and accurate result to their actual performance in vivo. At this point, this project may be concluded.

Since these nanoparticles were already quite bright in their nature and are within the range of the EPR effect, if the experiments in water reveal that they remain bright(er) than their classical counterparts then they can be used directly for cancer treatment experiments. The focus of this thesis was to capitalise off the FN synthesis method developed by Ting Cheng et al., to create small and even brighter UCNPs in order to leave plenty of space for surface modifications. This was achieved, and in doing so, since the particles did not exceed 25 nm in diameter, leaves upwards of 50-70 nm to work with in terms of conjugating the surface of these particles with biological molecules for biological treatments.

With all that being said, there is no doubt that the insertion of an appropriate middle shell does increase the overall intensities of the classical $LiYbF_4(0.5\%Tm^{3+})@LiYF_4$ particle, which was the entire goal of this thesis. In doing so, there is a step forward in utilising such a particle for the treatment of cancerous tumours. Not only are these particles bright, but also their sizes and other parameters, such as doping concentrations, are easily changeable to suit the need of their function.

6. BIBLIOGRAPHIE

D. E. Achatz, R. J. Meier, L. H. Fischer, and O. S. Wolfbeis, “Luminescent Sensing of Oxygen Using a Quenchable Probe and Upconverting Nanoparticles,” *Angewandte Chemie*, vol. 50, no. 1, pp. 260–263, Oct. 2010, doi: https://doi.org/10.1002/anie.201004902 [Last Accessed 13 Feb 2025]

R. Arppe *et al.*, “Quenching of the upconversion luminescence of NaYF4:Yb3+,Er3+and NaYF4:Yb3+,Tm3+nanophosphors by water: the role of the sensitizer Yb3+in non-radiative relaxation,” *Nanoscale*, vol. 7, no. 27, pp. 11746–11757, 2015, doi: https://doi.org/10.1039/c5nr02100f [Last Accessed 13 Feb 2025]

F. Auzel, “Upconversion and Anti-Stokes Processes with f and d Ions in Solids,” *Chemical Reviews*, vol. 104, no. 1, pp. 139–174, Jan. 2004, doi: https://doi.org/10.1021/cr020357g [Last Accessed 13 Feb 2025]

S. Barua and S. Mitragotri, “Challenges associated with Penetration of Nanoparticles across Cell and Tissue Barriers: A Review of Current Status and Future Prospects,” *Nano today*, vol. 9, no. 2, pp. 223–243, Apr. 2014, doi: https://doi.org/10.1016/j.nantod.2014.04.008 [Last Accessed 13 Feb 2025]

J.-C. G. Bünzli and V. K. Pecharsky, *Handbook on the Physics and Chemistry of Rare Earths*. Elsevier, 2011

Y. Cao *et al.*, “Assessing the activity of antibodies conjugated to upconversion nanoparticles for immunolabeling,” *Analytica chimica acta*, vol. 1209, p. 339863, 2022, doi: https://doi.org/10.1016/j.aca.2022.339863 [Last Accessed 13 Feb 2025]

X. Chen *et al.*, “Confining energy migration in upconversion nanoparticles towards deep ultraviolet lasing,” *Nature Communications*, vol. 7, no. 1, Jan. 2016, doi: https://doi.org/10.1038/ncomms10304 [Last Accessed 13 Feb 2025]

G. Chen, H. Ågren, T. Y. Ohulchanskyy, and P. N. Prasad, “Light upconverting core–shell nanostructures: nanophotonic control for emerging applications,” *Chemical Society Reviews*, vol. 44, no. 6, pp. 1680–1713, 2015, doi: https://doi.org/10.1039/c4cs00170b [Last Accessed 13 Feb 2025]

G. Chen, H. Qiu, P. N. Prasad, and X. Chen, “Upconversion Nanoparticles: Design, Nanochemistry, and Applications in Theranostics,” *Chemical Reviews*, vol. 114, no. 10, pp. 5161–5214, Mar. 2014, doi: https://doi.org/10.1021/cr400425h [Last Accessed 13 Feb, 2025]

J. Chen and J. X. Zhao, “Upconversion Nanomaterials: Synthesis, Mechanism, and Applications in Sensing,” *Sensors*, vol. 12, no. 3, pp. 2414–2435, Feb. 2012, doi: https://doi.org/10.3390/s120302414 [Last Accessed 13 Feb, 2025]

X. Cheng, J. Luo, and F. Rosei, “Photon upconversion tuning through energy migration in lanthanides sensitized nanoparticles,” *Nano Materials Science*, May 2024, doi: https://doi.org/10.1016/j.nanoms.2024.04.003 [Last Accessed 13 Feb 2025]

T. Cheng, R. Marin, A. Skripka, and F. Vetrone, “Small and Bright Lithium-Based Upconverting Nanoparticles,” *Journal of the American Chemical Society*, vol. 140, no. 40, pp. 12890–12899, Sep. 2018, doi: https://doi.org/10.1021/jacs.8b07086 [Last Accessed 13 Feb 2025]

L. Đačanin Far and M. D. Dramićanin, “Luminescence Thermometry with Nanoparticles: A Review,” *Nanomaterials*, vol. 13, no. 21, p. 2904, Jan. 2023, doi: https://doi.org/10.3390/nano13212904 [Last Accessed 13 Feb 2025]

R. Deng, F. Qin, R. Chen, W. Huang, M. Hong, and X. Liu, “Temporal full-colour tuning through non-steady-state upconversion,” *Nature Nanotechnology*, vol. 10, no. 3, pp. 237–242, Jan. 2015, doi: https://doi.org/10.1038/nnano.2014.317 [Last Accessed 13 Feb 2025]

H. Dong, L.-D. Sun, W. Feng, Y. Gu, F. Li, and C.-H. Yan, “Versatile Spectral and Lifetime Multiplexing Nanoplatform with Excitation Orthogonalized Upconversion Luminescence,” *ACS Nano*, vol. 11, no. 3, pp. 3289–3297, Feb. 2017, doi: https://doi.org/10.1021/acsnano.7b00559 [Last Accessed 13 Feb 2025]

N. Dubey and S. Chandra, “Upconversion nanoparticles: Recent strategies and mechanism based applications,” *Journal of Rare Earths*, Apr. 2022, doi: https://doi.org/10.1016/j.jre.2022.04.015 [Last Accessed 13 Feb, 2025]

Y. Feng *et al.*, “Internal OH− induced cascade quenching of upconversion luminescence in NaYF4:Yb/Er nanocrystals,” *Light: Science & Applications*, vol. 10, no. 1, May 2021, doi: https://doi.org/10.1038/s41377-021-00550-5 [Last Accessed 13 Feb 2025]

X. Fu *et al.*, “Excitation energy mediated cross-relaxation for tunable upconversion luminescence from a single lanthanide ion,” *Nature Communications*, vol. 13, no. 1, Aug. 2022, doi: https://doi.org/10.1038/s41467-022-32498-4 [Last Accessed 13 Feb 2025]

F. Ghasemi *et al.*, “Paper-based optical nanosensors – A review,” *Analytica Chimica Acta*, vol. 1238, p. 340640, Jan. 2023, doi: https://doi.org/10.1016/j.aca.2022.340640 [Last Accessed 13 Feb 2025]

J. F. Gomes Marin *et al.*, “Theranostics in Nuclear Medicine: Emerging and Re-emerging Integrated Imaging and Therapies in the Era of Precision Oncology,” *Radiographics: A Review Publication of the Radiological Society of North America, Inc*, vol. 40, no. 6, pp. 1715–1740, Oct. 2020, doi: https://doi.org/10.1148/rg.2020200021 [Last Accessed 13 Feb 2025]

M. Haase and H. Schäfer, “Upconverting Nanoparticles,” *Angewandte Chemie International Edition*, vol. 50, no. 26, pp. 5808–5829, May 2011, doi: https://doi.org/10.1002/anie.201005159 [Last Accessed 13 Feb 2025]

F. Han *et al.*, “Magnetic resonance imaging with upconversion nanoprobes capable of crossing the blood-cerebrospinal fluid barrier,” *Journal of Nanobiotechnology*, vol. 22, no. 1, Jan. 2024, doi: https://doi.org/10.1186/s12951-024-02301-1 [Last Accessed 13 Feb 2025]

S. Han, R. Deng, X. Xie, and X. Liu, “Enhancing Luminescence in Lanthanide-Doped Upconversion Nanoparticles,” *Angewandte Chemie International Edition*, vol. 53, no. 44, pp. 11702–11715, Sep. 2014, doi: https://doi.org/10.1002/anie.201403408 [Last Accessed 13 Feb 2025]

I. Hatton, E. D. Galbraith, Nono, T. P. Miettinen, B. M. Smith, and J. A. Shander, “The human cell count and size distribution,” *Proceedings of the National Academy of Sciences of the United States of America*, vol. 120, no. 39, Sep. 2023, doi: https://doi.org/10.1073/pnas.2303077120 [Last Accessed 13 Feb 2025]

A-Ra. Hong, S. Y. Kim, S.-H. Cho, K. Lee, and H. S. Jang, “Facile synthesis of multicolor tunable ultrasmall LiYF 4 :Yb,Tm,Er/LiGdF 4 core/shell upconversion nanophosphors with sub-10 nm size,” *Dyes and Pigments*, vol. 139, pp. 831–838, Apr. 2017, doi: https://doi.org/10.1016/j.dyepig.2016.12.048 [Last Accessed 13 Feb 2025]

T. L. de Jager, A. E. Cockrell, and S. S. Du Plessis, “Ultraviolet Light Induced Generation of Reactive Oxygen Species,” *Advances in Experimental Medicine and Biology*, vol. 996, pp. 15–23, 2017, doi: https://doi.org/10.1007/978-3-319-56017-5_2 [Last Accessed 13 Feb 2025]

D. Jaque *et al.*, “Nanoparticles for photothermal therapies,” *Nanoscale*, vol. 6, no. 16, pp. 9494–9530, 2014, doi: https://doi.org/10.1039/c4nr00708e [Last Accessed 2025]

W. Jiang, J. Yi, X. Li, F. He, N. Niu, and L. Chen, “A Comprehensive Review on Upconversion Nanomaterials-Based Fluorescent Sensor for Environment, Biology, Food and Medicine Applications,” *Biosensors*, vol. 12, no. 11, p. 1036, Nov. 2022, doi: https://doi.org/10.3390/bios12111036 [Last Accessed 13 Feb 2025]

Y. Jin *et al.*, “Harness the Power of Upconversion Nanoparticles for Spectral Computed Tomography Diagnosis of Osteosarcoma,” *Advanced Functional Materials*, vol. 28, no. 33, Jun. 2018, doi: https://doi.org/10.1002/adfm.201802656 [Last Accessed 13 Feb 2025]

M.-F. Joubert, “Photon avalanche upconversion in rare earth laser materials,” *Optical Materials*, vol. 11, no. 2–3, pp. 181–203, Jan. 1999, doi: https://doi.org/10.1016/s0925-3467(98)00043-3 [Last Accessed 13 Feb, 2025]

K. Lingeshwar Reddy, R. Balaji, A. Kumar, and V. Krishnan, “Lanthanide Doped Near Infrared Active Upconversion Nanophosphors: Fundamental Concepts, Synthesis Strategies, and Technological Applications,” *Small*, vol. 14, no. 37, p. 1801304, Jul. 2018, doi: https://doi.org/10.1002/smll.201801304 [Last Accessed 13 Feb 2025]

S. Liu, L. Yan, J. S. Huang, Q. Y. Zhang, and B. Zhou, “Controlling upconversion in emerging multilayer core–shell nanostructures: from fundamentals to frontier applications,” *Chemical Society Reviews*, vol. 51, no. 5, pp. 1729–1765, Jan. 2022, doi: https://doi.org/10.1039/d1cs00753j [Last Accessed 13 Feb 2025]

G. Liu, “Advances in the theoretical understanding of photon upconversion in rare-earth activated nanophosphors,” *Chemical Society Reviews*, vol. 44, no. 6, pp. 1635–1652, 2015, doi: https://doi.org/10.1039/c4cs00187g [Last Accessed 13 Feb 2025]

M. S. Meijer *et al.*, “NIR-Light-Driven Generation of Reactive Oxygen Species Using Ru(II)-Decorated Lipid-Encapsulated Upconverting Nanoparticles,” vol. 35, no. 37, pp. 12079–12090, Aug. 2019, doi: https://doi.org/10.1021/acs.langmuir.9b01318 [Last Accessed 13 Feb 2025]

E. M. Mettenbrink, W. Yang, and S. Wilhelm, “Bioimaging with Upconversion Nanoparticles,” *Advanced photonics research*, vol. 3, no. 12, Sep. 2022, doi: https://doi.org/10.1002/adpr.202200098 [Last Accessed 13 Feb 2025]

M. J. Mitchell, M. M. Billingsley, R. M. Haley, M. E. Wechsler, N. A. Peppas, and R. Langer, “Engineering precision nanoparticles for drug delivery,” *Nature Reviews Drug Discovery*, vol. 20, no. 1, pp. 1–24, Dec. 2020, doi: https://doi.org/10.1038/s41573-020-0090-8 [Last Accessed 13 Feb 2025]

V. Muhr, S. Wilhelm, T. Hirsch, and O. S. Wolfbeis, “Upconversion Nanoparticles: From Hydrophobic to Hydrophilic Surfaces,” *Accounts of Chemical Research*, vol. 47, no. 12, pp. 3481–3493, Oct. 2014, doi: https://doi.org/10.1021/ar500253g [Last Accessed 13 Feb 2025]

R. Naccache, Q. Yu, and J. A. Capobianco, “The Fluoride Host: Nucleation, Growth, and Upconversion of Lanthanide-Doped Nanoparticles,” *Advanced Optical Materials*, vol. 3, no. 4, pp. 482–509, Mar. 2015, doi: https://doi.org/10.1002/adom.201400628 [Last Accessed 13 Feb 2025]

O. D. Neikov and N. A. Yefimov, “Nanopowders,” *Handbook of Non-Ferrous Metal Powders*, pp. 271–311, 2019, doi: https://doi.org/10.1016/b978-0-08-100543-9.00009-9 [Last Accessed 13 Feb 2025]

M. Nomura *et al.*, “Review of thermal transport in phononic crystals,” *Materials Today Physics*, vol. 22, pp. 100613–100613, Jan. 2022, doi: https://doi.org/10.1016/j.mtphys.2022.100613 [Last Accessed 13 Feb, 2025]

S. Okamoto, T. Shiga, and N. Tamaki, “Clinical Perspectives of Theranostics,” *Molecules*, vol. 26, no. 8, p. 2232, Apr. 2021, doi: https://doi.org/10.3390/molecules26082232 [Last Accessed 13 Feb 2025]

H. Oliveira *et al.*, “Critical Considerations on the Clinical Translation of Upconversion Nanoparticles (UCNPs): Recommendations from the European Upconversion Network (COST Action CM1403),” *Advanced Healthcare Materials*, p. 1801233, Dec. 2018, doi: https://doi.org/10.1002/adhm.201801233 [Last Accessed 13 Feb 2025]

P. S. Peijzel, A. Meijerink, R. T. Wegh, M. F. Reid, and G. W. Burdick, “A complete energy level diagram for all trivalent lanthanide ions,” *Journal of Solid State Chemistry*, vol. 178, no. 2, pp. 448–453, Feb. 2005, doi: https://doi.org/10.1016/j.jssc.2004.07.046 [Last Accessed 13 Feb 2025]

Mihir Kumar Purkait, M. K. Sinha, P. Mondal, and R. Singh, “Biologically Responsive Membranes,” *Interface science and technology*, pp. 145–171, Jan. 2018, doi: https://doi.org/10.1016/b978-0-12-813961-5.00005-x [Last Accessed 13 Feb 2025]

Sylwia Ryszczyńska, I. R. Martín, and T. Grzyb, “Near-infrared optical nanothermometry via upconversion of Ho3+-sensitized nanoparticles,” *Scientific Reports*, vol. 13, no. 1, Sep. 2023, doi: https://doi.org/10.1038/s41598-023-42034-z [Last Accessed 13 Feb 2025]

H. L. Schläfer and Günter Gliemann, *Basic Principles of Ligand Field Theory*. John Wiley & Sons, 1969.

Artiom Skripka *et al.*, “A Generalized Approach to Photon Avalanche Upconversion in Luminescent Nanocrystals,” *Nano Letters*, vol. 23, no. 15, pp. 7100–7106, Jul. 2023, doi: https://doi.org/10.1021/acs.nanolett.3c01955 [Last Accessed 13 Feb 2025]

L. B. Solnes, M. Shokeen, and N. Pandit-Taskar, “Novel Agents and Future Perspectives on Theranostics,” *Seminars in Radiation Oncology*, vol. 31, no. 1, pp. 83–92, Jan. 2021, doi: https://doi.org/10.1016/j.semradonc.2020.07.010 [Last Accessed 13 Feb 2025]

Q. Su *et al.*, “The Effect of Surface Coating on Energy Migration-Mediated Upconversion,” *Journal of the American Chemical Society*, vol. 134, no. 51, pp. 20849–20857, Dec. 2012, doi: https://doi.org/10.1021/ja3111048 [Last Accessed 13 Feb 2025]

M. A. Subhan, S. S. K. Yalamarty, N. Filipczak, F. Parveen, and V. P. Torchilin, “Recent Advances in Tumor Targeting via EPR Effect for Cancer Treatment,” *Journal of Personalized Medicine*, vol. 11, no. 6, p. 571, Jun. 2021, doi: [Last Accessed 13 Feb 2025]

K. Suzuki, T. Kotani, and K. Sato, “First-principles method justifying the Dieke diagram and beyond,” *Physical Review Research*, vol. 5, no. 1, Feb. 2023, doi: https://doi.org/10.1103/physrevresearch.5.013111 [Last Accessed 13 Feb 2025]

P. Vilela, Afaf El-Sagheer, T. M. Millar, T. Brown, O. L. Muskens, and A. G. Kanaras, “Graphene Oxide-Upconversion Nanoparticle Based Optical Sensors for Targeted Detection of mRNA Biomarkers Present in Alzheimer’s Disease and Prostate Cancer,” *ACS Sensors*, vol. 2, no. 1, pp. 52–56, Dec. 2016, doi: https://doi.org/10.1021/acssensors.6b00651 [Last Accessed 13 Feb 2025]

S. Wang *et al.*, “Multifunctional Self-Oxygenating Ucnp–Chlorin E6–Cyanobacteria Nanoplatform: Nir-Triggered Photodynamic and Photothermal Therapy with Efficacy Against Periodontitis-Related Bacteria,” *Ssrn.com*, 2024. https://papers.ssrn.com/sol3/papers.cfm?abstract_id=4909255 [Last Accessed 13 Feb 2025]

Y. Wang, S. Zhou, P. Hu, W. Zhong, and J. Fu, “Temperature-sensitive lanthanide-doped core-multishell nanocrystals with excitation-wavelength-dependent bimodal luminescence thermo-behaviors and their application in dynamic anticounterfeiting,” *Journal of Alloys and Compounds*, vol. 938, p. 168442, Dec. 2022, doi: https://doi.org/10.1016/j.jallcom.2022.168442 [Last Accessed 13 Feb 2025]

C. Wang, H. Tao, L. Cheng, and Z. Liu, “Near-infrared light induced in vivo photodynamic therapy of cancer based on upconversion nanoparticles,” *Biomaterials*, vol. 32, no. 26, pp. 6145–6154, Sep. 2011, doi: https://doi.org/10.1016/j.biomaterials.2011.05.007 [Last Accessed 13 Feb 2025]

M. Wang, G. Abbineni, A. Clevenger, C. Mao, and S. Xu, “Upconversion nanoparticles: synthesis, surface modification and biological applications,” *Nanomedicine: Nanotechnology, Biology and Medicine*, vol. 7, no. 6, pp. 710–729, Dec. 2011, doi: https://doi.org/10.1016/j.nano.2011.02.013 [Last Accessed 13 Feb 2025]

S. Wen, J. Zhou, K. Zheng, A. Bednarkiewicz, X. Liu, and D. Jin, “Advances in highly doped upconversion nanoparticles,” *Nature Communications*, vol. 9, no. 1, Jun. 2018, doi: https://doi.org/10.1038/s41467-018-04813-5 [Last Accessed 13 Feb 2025]

J. Wu, J. Wu, W. Wei, Y. Zhang, and Q. Chen, “Upconversion Nanoparticles Based Sensing: From Design to Point-of-Care Testing,” *Small*, vol. 20, no. 29, Feb. 2024, doi: https://doi.org/10.1002/smll.202311729 [Last Accessed 13 Feb 2025]

J. Wu, “The Enhanced Permeability and Retention (EPR) Effect: The Significance of the Concept and Methods to Enhance Its Application,” *Journal of Personalized Medicine*, vol. 11, no. 8, p. 771, Aug. 2021, doi: https://doi.org/10.3390/jpm11080771 [Last Accessed 13 Feb 2025]

M. Wu, Y. Long, T. Wang, B. Zhou, and Q. Zhang, “Controlling Red Color–Based Multicolor Upconversion through Selective Photon Blocking,” *Advanced Functional Materials*, vol. 29, no. 25, Apr. 2019, doi: https://doi.org/10.1002/adfm.201804160 [Last Accessed 13 Feb 2025]

J. Wu, S. Du, and Y. Wang, “Photosensitizer coated upconversion nanoparticles for triggering reactive oxygen species under 980 nm near-infrared excitation,” *Journal of Materials Chemistry B*, vol. 7, no. 46, pp. 7306–7313, Jan. 2019, doi: https://doi.org/10.1039/c9tb01629e [Last Accessed 13 Feb 2025]

X. Wu, G. Chen, J. Shen, Z. Li, Y. Zhang, and G. Han, “Upconversion Nanoparticles: A Versatile Solution to Multiscale Biological Imaging,” *Bioconjugate Chemistry*, vol. 26, no. 2, pp. 166–175, Oct. 2014, doi: https://doi.org/10.1021/bc5003967 [Last Accessed 13 Feb 2025]

C. Würth, S. Fischer, B. Grauel, A. Paul Alivisatos, and U. Resch-Genger, “Quantum Yields, Surface Quenching, and Passivation Efficiency for Ultrasmall Core/Shell Upconverting Nanoparticles,” vol. 140, no. 14, pp. 4922–4928, Mar. 2018, doi: https://doi.org/10.1021/jacs.8b01458 [Last Accessed 13 Feb 2025]

H. Xu *et al.*, “Anomalous upconversion amplification induced by surface reconstruction in lanthanide sublattices,” *Nature Photonics*, vol. 15, no. 10, pp. 732–737, Sep. 2021, doi: https://doi.org/10.1038/s41566-021-00862-3 [Last Accessed 13 Feb 2025]

W. Zhang *et al.*, “Effects of morphology and size of nanoscale drug carriers on cellular uptake and internalization process: a review,” *RSC Advances*, vol. 13, no. 1, pp. 80–114, Dec. 2022, doi: https://doi.org/10.1039/D2RA06888E [Last Accessed 13 Feb 2025]

Y. Zhang *et al.*, “Ultrasmall-Superbright Neodymium-Upconversion Nanoparticles via Energy Migration Manipulation and Lattice Modification: 808 nm-Activated Drug Release,” *ACS Nano*, vol. 11, no. 3, pp. 2846–2857, Mar. 2017, doi: https://doi.org/10.1021/acsnano.6b07958 [Last Accessed 13 Feb 2025]

S. Zhao *et al.*, “UCNP–Bi2Se3 Upconverting Nanohybrid for Upconversion Luminescence and CT Imaging and Photothermal Therapy,” *Chemistry - A European Journal*, vol. 26, no. 5, pp. 1127–1135, Nov. 2019, doi: https://doi.org/10.1002/chem.201904586 [Last Accessed 13 Feb 2025]

J. Zhao *et al.*, “Single-nanocrystal sensitivity achieved by enhanced upconversion luminescence,” vol. 8, no. 10, pp. 729–734, Oct. 2013, doi: https://doi.org/10.1038/nnano.2013.171 [Last Accessed 13 Feb 2025]

B. Zhou, Q. Li, L. Yan, and Q. Zhang, “Controlling upconversion through interfacial energy transfer (IET): Fundamentals and applications,” *Journal of Rare Earths*, vol. 38, no. 5, pp. 474–482, Jan. 2020, doi: https://doi.org/10.1016/j.jre.2020.01.009 [Last Accessed 13 Feb 2025]

B. Zhou *et al.*, “Enhancing multiphoton upconversion through interfacial energy transfer in multilayered nanoparticles,” *Nature Communications*, vol. 11, no. 1, p. 1174, Mar. 2020, doi: https://doi.org/10.1038/s41467-020-14879-9 [Last Accessed 13 Feb 2025]

J. Zhou, Q. Liu, W. Feng, Y. Sun, and F. Li, “Upconversion Luminescent Materials: Advances and Applications,” *Chemical Reviews*, vol. 115, no. 1, pp. 395–465, Dec. 2014, doi: https://doi.org/10.1021/cr400478f [Last Accessed 13 Feb 2025]

X. Zhu *et al.*, “Near-Infrared Nano-Optogenetic Activation of Cancer Immunotherapy via Engineered Bacteria,” *Advanced Materials*, vol. 35, no. 8, Oct. 2022, doi: https://doi.org/10.1002/adma.202207198 [Last Accessed 13 Feb 2025]

X. Zhu, J. Li, X. Qiu, Y. Liu, W. Feng, and F. Li, “Upconversion nanocomposite for programming combination cancer therapy by precise control of microscopic temperature,” *Nature Communications*, vol. 9, no. 1, Jun. 2018, doi: https://doi.org/10.1038/s41467-018-04571-4 [Last Accessed 13 Feb 2025]

Q. Zou *et al.*, “Cooperative and non-cooperative sensitization upconversion in lanthanide-doped LiYbF4 nanoparticles,” *Nanoscale*, vol. 9, no. 19, pp. 6521–6528, Jan. 2017, doi: https://doi.org/10.1039/c7nr02124k [Last Accessed 13 Feb 2025]

“What is Upconversion? - Edinburgh Instruments,” *Edinburgh Instruments*, Jul. 13, 2021. https://www.edinst.com/resource/what-is-upconversion/ [Last Accessed 13 Feb 2025]